Interactions between Extracellular Vesicles, Nanoparticles and Cells in the Presence of a Protein Corona

Dissertation

for Attaining the Academic Degree of

“Doktor rerum naturalium (Dr. rer. Nat)“

of the Department:

10 – Biology

of the Johannes Gutenberg University Mainz

Laura Dietz

born in Schwalmstadt-Ziegenhain

Mainz, May 2024

First Reviewer: [redacted]

Second Reviewer: [redacted]

Day of the PhD defence: 26th of June 2024

I hereby declare that I wrote the dissertation submitted without any unauthorized external assistance and used only sources acknowledged in the work. All textual passages which are appropriated verbatim or paraphrased from published and unpublished tests as well as all information obtained from oral sources are duly indicated and listed in accordance with bibliographical rules. In carrying out this research, I complied with the rules of standard scientific practice as formulated in the statutes of Johannes Gutenberg University Mainz to insure standard scientific practice.

Abstract

Controlling the *in vivo* targeting of synthetic nanocarriers is one of the major obstacles impairing their clinical translation. This is mainly caused by the high level of complexity involved in the targeting, the dynamic change of the *in vivo* environment, and a lack of knowledge concerning the molecular determinants guiding this process. After injection of nanocarriers into the bloodstream a layer of biomolecules, mostly proteins, rapidly adsorb to the surface of the nanocarrier. This layer, called protein corona, adds another level of complexity as it is determined by the physicochemical properties of the carrier and in turn influences its behavior in the *in vivo* environment. Thus, when designing a nanocarrier, the influence on the protein corona composition needs to be considered as well. Here, PEGylation, which increases the hydrophilicity of the carrier surface, is often used to prolong the blood circulation time. This is accompanied by the reduction of unspecific uptake into immune cells, which is in favor of targeted delivery. As a next step in the targeting process, the nanocarriers need to accumulate at the target site, for example in the tumor tissue. To achieve this a plethora of targeting ligands for many different target sites have been developed. Finally, the nanocarrier must overcome several biological barriers such as tissue barriers, the cell membrane, or intracellular barriers, which led to the development of functional moieties that facilitate barrier crossing. One approach to designing a multi-functional nanocarrier is to use a modular building principle and attach several different functional moieties to the nanocarrier surface.

An alternative that does not require a rational design of the carrier surface is using biologically derived membranes as nanocarrier surface coating. Such membranes can be derived from cells but recently small vesicles, termed extracellular vesicles, became of interest as drug delivery vehicles. EVs serve as a transport system for biological cargo between distant cells. Therefore, it is hypothesized that they are naturally equipped with a variety of functionalities needed for navigating the *in vivo* environment. In this work, we aimed to explore different aspects of using EV membranes as a multi-functional surface coating for drug delivery nanocarriers.

Sections 3.1 and **3.2** focus on developing a strategy to package synthetic nanocarriers into EVs without impairing their membrane integrity as it is crucial to their functionality. Here, we developed a strategy to utilize the cellular EV biogenesis pathway to directly package the NPs during the biogenesis of EVs. We hypothesize that this prevents

damage to the EV membrane or the embedded proteins. While we used polystyrene NPs as model NPs for developing a general packaging protocol in **Section 3.1**, we used this protocol as a blueprint for packaging therapeutically relevant silica nanocapsules in **Section 3.2**. The purification protocol developed here is based on size exclusion chromatography, which is a commonly used gentle extracellular vesicle purification method. The success of our packaging strategy was confirmed by fluorescence cross-correlation spectroscopy, which identified a packaging rate of 3-7%.

Section 3.3 aimed to understand the influence of the protein corona on the exocytosis of silica NPs as exocytosis is a pre-requisite for harvesting NPs packaged in extracellular vesicles. Therefore, the presence or absence of a protein corona could be one parameter for optimization of the packaging protocol. Here, we found that the presence of a plasma protein corona enhances exocytosis in an NP diameter-dependent manner. The exocytosis of larger silica NPs (100 nm) was enhanced by the presence of a corona, whereas the exocytosis of smaller silica NPs (10 nm) was not affected. Aside from gaining insight into parameters relevant to the optimization of packaging, this section also contributes important insights into the relation between protein corona formation and NP exocytosis. This aspect has not yet been addressed by NP protein corona research.

In the last section, we aimed to investigate the protein corona composition of the extracellular vesicles used for packaging the NPs in **sections 3.1** and **3.2**. Here, we compared the protein corona of extracellular vesicles to liposomes as this is the synthetic nanocarrier type most similar to extracellular vesicles. We found that the protein corona of extracellular vesicles increased the uptake in immune cells similar to the effect observed for liposomes. *In vivo,* this is associated with rapid blood clearance and impairs efficient drug delivery to target cells. These findings have implications for using extracellular vesicles as surface coating and suggest that further modifications of the EV membrane might be needed. Beyond the usage of extracellular vesicles for drug delivery, these findings are valuable to understanding the basic biology of extracellular vesicles.

Zusammenfassung

Nanopartikel so zu gestalten, dass sie im menschlichen Körper an ihren Wirkort gelangen, ist immer noch eine große Herausforderung in der Nanomedizin. Die Hauptgründe hierfür sind das hohe Maß an Komplexität, die dynamischen Verhältnisse im menschlichen Körper und die immer noch bestehenden Wissenslücken der molekularen Details eines gezielten Wirkstofftransports. Nachdem die therapeutischen Nanopartikel in die Blutbahn des Patienten injiziert wurden, lagern sich verschiedenste Biomoleküle, hauptsächlich Proteine, an. Diese Proteinschicht wird als Protein Corona bezeichnet und bestimmt maßgeblich die Interaktion der Nanopartikel mit der biologischen Umgebung. Da die Zusammensetzung und Wirkung der Protein Corona durch die physikalisch-chemischen Eigenschaften des Nanopartikels bestimmt wird, muss diese beim Design der Partikeloberfläche mitbeachtet werden. Eine der meist verwandtesten Modifizierungen ist die PEGylierung, die die Hydrophobizität der Nanopartikeloberfläche verringert. Dies beeinflusst die Protein Corona, sodass sich die Blutzirkulationszeit der Nanopartikel erhöhet, indem die unspezifische Aufnahme durch verschiedene Immunzellen gehemmt wird. Insgesamt wird der gezielte Wirkstofftransport dadurch verbessert. Als weiteren Schritt müssen sich die therapeutischen Nanopartikel im Zielgewebe, wie zum Beispiel einem Tumor, anreichern. Hierzu wurden zahlreiche Liganden entwickelt, die zielgerichtet an bestimmte Zellen oder Gewebe binden. Als letzten Schritt müssen die Nanopartikel verschiedene biologische Barrieren überwinden, was ebenfalls zur Entwicklung funktionaler Liganden führte. Daraus ergibt sich die Möglichkeit die Nanopartikeloberfläche nach dem Baukastenprinzip mit verschiedenen funktionalen Liganden zu modifizieren.

Alternativ dazu können biologische Membranen für die Funktionalisierung von Nanopartikeln verwendet werden. Hierbei muss man nicht auf rationale Designprinzipien zurückgreifen, sondern kann eine Membran verwenden, die schon über die gewünschten Eigenschaften verfügt. Hierfür eignet sich besonders die Membran von Extrazellulären Vesikeln, da diese im menschlichen dafür zuständig sind Biomoleküle zwischen weit-entfernten Zellen zu transportieren. Man spekuliert, dass diese Vesikel deshalb über alle relevanten Eigenschaften für ein Wirkstofftransportsystem verfügen. In der vorliegenden Arbeit wollen wir deshalb die Möglichkeit untersuchen die Vesikelmembran für eine funktionale Beschichtung von Nanopartikeln zu verwenden.

Im ersten und zweiten Abschnitt beschäftigen wir uns damit eine Methode zu entwickeln, um die zelluläre Biogenese-Maschinerie für die Verpackung der Nanopartikel in Extrazelluläre Vesikel zu nutzen. Für die Etablierung eines vorläufigen Protokolls in **Abschnitt 3.1** haben wir zunächst Polystyrol-Nanopartikel benutzt. Die daraus gewonnen Erkenntnisse haben wir dann in **Abschnitt 3.2** für die Verpackung von kleineren, relevanteren Silika-Nanokapseln angewendet. Für die Isolierung der Vesikel haben wir Größenausschlusschromatographie angewendet, um die Vesikelmembran oder darin eingebettete Proteine nicht zu beschädigen. Den Erfolg der Verpackung von Silika-Nanokapseln konnten wir schließlich mit Hilfe von Fluoreszenz-Cross-Correlation-Spektroskopie nachweisen.

In **Abschnitt 3.3** haben wir den Einfluss der Protein Corona auf die Exocytose von Silika-Nanopartikeln untersucht, da die Exocytose eine Voraussetzung dafür ist, Nanopartikel aus dem Zellkulturüberstand isolieren zu können. Hierbei haben wir herausgefunden, dass die Anwesenheit einer Protein Corona für eine verstärkte Nanopartikel-Exocytose sorgt. Dieser Effekt war allerdings von dem Durchmesser der verwendeten Nanopartikel abhängig. Für große Nanopartikel (100 nm) war dieser Effekt besonders ausgeprägt, wohingegen die Exocytose von kleinen Nanopartikeln (10 nm) nicht durch die Protein Corona beeinflusst wurde. Diese Ergebnisse legen nahe, dass die Protein Corona ein möglicher Parameter ist, den man für die Optimierung des Verpackungsprotokolls anpassen könnte. Darüber hinaus sind die Ergebnisse auch von Interesse für die Protein Corona-Forschung. Hier wurde bislang der Einfluss der Protein Corona auf die Endozytose von Nanopartikeln untersucht. Dass diese auch die Exocytose beeinflusst, ist eine neue Erkenntnis.

Im letzten Abschnitt wurde die Zusammensetzung der Protein Corona von Extrazellulären Vesikeln untersucht und mit der von Liposomen verglichen. Liposome sind für diesen Vergleich besonders interessant, da sie diejenige Klasse synthetischer Wirkstofftransportsysteme sind, die den zellulären Vesikeln am ähnlichsten sind. Hier haben wir herausgefunden, die Protein Corona der Vesikel, sowie der Liposome, die Aufnahme in Immunzellen fördert. *In vivo* ist dies mit einer verkürzten Blutzirkulationszeit assoziert und reduziert den zielgerichteten Wirkstofftransport. Diese Erkenntnisse implizieren, dass weiter Modifizierungen der Extrazellulären Vesikel nötig sein könnten, um sie erfolgreich für eine funktionale Beschichtung von Nanopartikeln einsetzen zu

können. Darüber hinaus tragen diese Erkenntnisse zum grundlegenden Verständnis der Biologie der Extrazellulären Vesikel bei.

Table of Contents

1 Theoretical background

1.1 Synthetic NPs as drug delivery vehicles

1.1.1 Application of NPs for drug delivery

Using NPs (nanoparticles) as drug nanocarriers is a promising technology that opens fundamentally novel treatment opportunities. Until now, around 80 NP formulations have been approved by the Food and Drug Administration (FDA).[1] The first NP formulations were approved in the 1980s. The liposomal formulation Doxil® for the treatment of ovarian cancer and Kaposi's sarcoma was among the first FDA-approved drug nanocarriers.[2] During the coronavirus disease 2019 (COVID-19) pandemic, NP formulations have become widely known to the public due to the success of lipid nanoparticles (LNP)-based vaccine formulations.[3]

The major advantage of NP formulations over free drugs is the protection of the fragile cargo from biodegradation during systemic distribution.[4] In the case of Doxil®, the chemotherapeutic drug doxorubicin is encapsulated by liposomes. This drastically decreases the degradation of the drug and enhances therapeutic efficacy.[2] For the delivery of rapidly degradable RNA, a drug delivery system is even more pivotal to its therapeutic effect.[5,6] By increasing the circulation time of drug molecules, passive tumor targeting can be achieved. The vessels connecting the vasculature with the tumor tissue are often leaky, which allows enhanced extravasation of NPs. This effect is known as enhanced permeation and retention (EPR) effect.[7] The EPR effect contributes to the accumulation of Doxil® in the tumor and decreases toxicity by unspecific distribution.[8] Not all NP formulations have tumor cells as targets. Here, other targeting mechanisms need to be applied. LNP-based RNA vaccines for example target dendritic cells by fine-tuning the net charge of the LNP.[9] Precise targeting of NPs is a key factor for successful drug delivery. Aside from tuning the net charge or the NP surface properties, biologically inspired targeting moieties are extensively explored for targeting.[10]

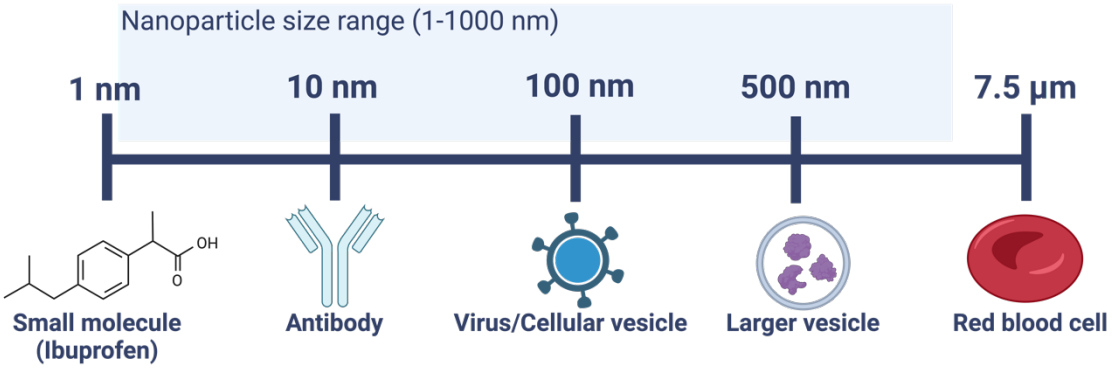

Figure 1.1.1: Length scale of NPs in comparison to medically relevant and biological molecules. This graphic was created with BioRender.com.

By definition, synthetic NPs have a diameter between a few nanometers to just below a micrometer (**Figure 1.1.1**). While a diameter of approx. 10 nm is similar to that of an antibody [11], a diameter of 900 nm is closer to the diameter of a red blood cell, which is 7.5 µm.[12] The typical NP is between 100 nm and 200 nm in diameter. This is approximately the size range of viruses or extracellular vesicles.[13] Due to their specific size range, NPs interact with living cells in a very specific manner. While small molecules passively permeate the cellular plasma membrane or enter cells by using protein channels or they are actively transported by transmembrane proteins, NPs undergo active, energy-dependent uptake by cells by engulfment into a lipid bilayer enclosed intracellular compartment.[14] This specific interaction with living cells also bears the risk of size-specific toxicity. It was reported that NPs can induce oxidative stress [15], inflammation [16,17], metabolic dysfunction [18], and genotoxicity.[16]

Synthetic NPs can be grouped according to the material they are composed of. There are three main classes, such as polymeric, inorganic, and lipid-based NPs as depicted in **Figure 1.1.2**. Furthermore, there are NPs that cannot be assigned to one of these classes, such as protein NPs or core-shell NPs. Depending on the different material properties, the NP type must be chosen based on the application.

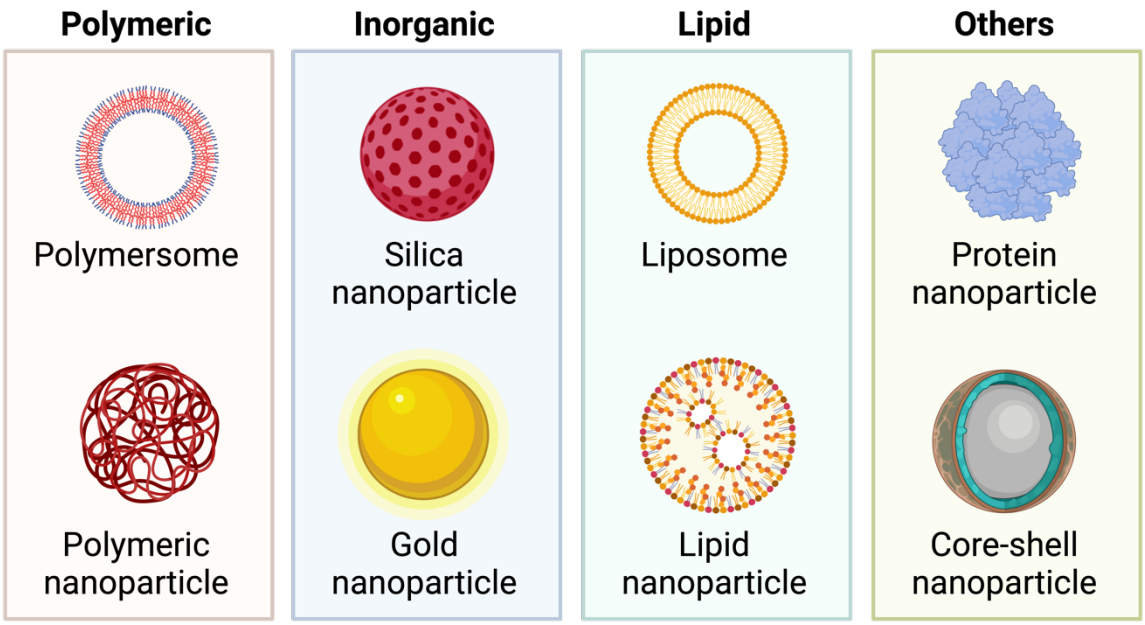

Figure 1.1.2: NP classes and prominent representatives for biomedical applications. This graphic was created with BioRender.com.

Polymeric NPs can be synthesized from a variety of different monomers and polymerization techniques, which can result in different sizes and physicochemical properties.[19] The drug cargo can either be loaded into the polymer matrix, chemically conjugated to the particle, or encapsulated in the hollow NP core.[19] Similar to liposomes, polymersomes consist of a membrane built from block copolymers that encloses an inner compartment.[20] Polymersomes can be used for drug delivery.[21]

Inorganic NPs have the advantage that they can be synthesized in various sizes and shapes.[10] Gold NPs are frequently used for various applications including drug delivery, imaging, and theranostics.[22] Another prominent representative used in drug delivery is silica NPs, which are made of silicon dioxide.[23] Mesoporous silica NPs can carry drug cargo inside the silica matrix [24] and showed a good safety record in clinical trials.[25]

Lipid-based NPs are most frequently used in clinical applications due to their high biocompatibility.[26] Liposomes are composed of a lipid bilayer, which encloses an aqueous compartment to carry hydrophilic cargo. Hydrophobic cargo can be carried in the membrane representing a suitable delivery system for various cargo.[27] Another lipid-based formulation is LNPs, which became popular as an RNA vaccine against COVID-19.[3] In this formulation, the negatively charged RNA molecule is complexed by positively charged lipids inside of a tightly packed lipid NP.[28]

There are some NPs that do not fit into this classification. Protein nanocapsules (NCs) are composed of naturally derived proteins such as bovine serum albumin (BSA) and are therefore highly biocompatible. Similar to liposomes, protein NCs can carry hydrophilic cargo inside their aqueous lumen.[29]

1.1.2 The protein corona and its implications for drug delivery

When synthetic NPs encounter biological fluids, a layer of proteins and other biological molecules rapidly adsorb to their surface. The adsorbed proteins are named protein corona.[30] As the protein corona crucially determines how synthetic NPs interact with biological matter, it is especially important for the medical application of nanomaterials.[31]

Vronman et al. were the first to describe the adsorption of proteins from blood plasma to surfaces in the 1960s.[32] Later, they found that proteins initially adsorbed to a surface due to their abundance are exchanged by proteins with a higher affinity for the surface.[33] This effect is described as the Vronman effect and applies also to NP surfaces. The exchange of proteins at the NP surface reaches an equilibrium state within a few minutes to several hours.[34-36] The resulting equilibrium state protein corona is highly stable and therefore, determines the interaction with tissue barriers and cells.[36] However, the equilibrium state protein corona composition can still change when facing a new biological environment with a different protein composition.[37,38] This was observed for NP trafficking through the endolysosomal system of cells. Here, the protein corona represented a fingerprint of different endolysosomal compartments, which allowed mapping of the trafficking route.[39] The protein corona can be divided into the hard corona, which is the inner layer of tightly bound proteins, and the soft corona, which is the outer layer of more rapidly exchanging proteins.[40] The protein adsorption process is mainly governed by hydrophobic interactions. Here, water molecules are released from the hydration layer around the NPs and contribute to an entropy increase.[41] This results in lowering the surface free energy of the NPs in the aqueous solution.[38] This process can cause (partial) unfolding of involved proteins to allow interaction with the hydrophobic patches buried inside the folded proteins. Proteins can also interact with the NP surface via hydrogen bonding or electrostatic forces.[42]

How the corona proteins interact with the NP surface and which proteins adsorb to the NP highly depends on the NP surface properties. Here, the NP material and respective

charge [43], biochemical modifications [44], the particle shape [45], the particle size, and resulting curvature [46] play a role. This results in distinct protein corona compositions for different NP systems.[47] Although the protein corona composition does not reflect the abundance of the plasma proteins [46], some plasma proteins were found frequently in the NP corona. Albumin, immunoglobulin G (IgG), and fibrinogen are highly abundant in the blood plasma and were often found in the NP protein corona.[34,48,49] The protein composition of the corona ultimately determines the NPs' fate during blood circulation in the human body. IgG and complement proteins are referred to as opsonizing proteins. This type of protein enhances the uptake of the NPs by the mononuclear phagocyte system (MPS), which accelerates their blood clearance. Accumulation of the NPs in the liver, spleen, lung, and lymph nodes is characteristic of the NP blood clearance by the MPS.[50] This phenomenon is a major obstacle to the application of NPs in drug delivery because it decreases the delivery efficiency.[51] It was found that increasing the hydrophilicity of NPs decreases their opsonization.[47] The most prominent modification to enhance the hydrophilicity of an NP is the covalent attachment of polyethylene glycol (PEG) to the NP surface. The so-called PEGylation has been used to enhance the blood circulation time of a variety of different NPs including liposomes [52], gold NPs [53], and polymeric NPs.[54,55] This effect is also referred to as the 'stealth effect'. It was found that PEGylated NPs adsorbed less total protein due to steric hindrance, which contributes to the stealth effect.[44] Further, Schöttler et al. demonstrated that the stealth effect was mediated by the enrichment of the corona with clusterin (apolipoprotein J).[56] Therefore, proteins that decrease uptake by the MPS are named stealth or dysopsonizing proteins. However, accumulation of PEG in the body [57], antibody-mediated clearance [58], and generation of hypersensitivities against it [59], raise the need for alternative stealth moieties.

1.1.3 Endocytosis of NPs in cells

NP endocytosis by target cells is essential for the delivery of drug cargo. Furthermore, the endocytosis pathway determines the intracellular fate of the nanocarrier, which also influences the delivery. Exocytosis is another, but often neglected, process that equally contributes to the net delivery rate. Depending on the NP size and surface properties, most NPs are taken up by the energy-dependent, active endocytosis process.[60] However, NPs smaller than 10 nm or positively charged NPs can pass the cell membrane

passively by diffusion.[61] Small molecule therapeutics also enter the cell by passive diffusion or by transporter-mediated entry.[62]

Endocytosis mechanisms can be divided into phagocytotic and pinocytotic uptake.[63] Phagocytosis is predominantly limited to phagocytic immune cells, which take up bacteria, other pathogens, or cell debris by this mechanism.[64] During phagocytosis, the particle is engulfed by membrane protrusions in an actin-dependent process.[65] After internalization, the particle is located in an endosomal vesicle called phagosome.[66] Phagocytes express multiple receptors to recognize pathogens and subsequently trigger phagocytosis. Some of these receptors recognize patterns like microbial sugars or phosphatidyl serine of apoptotic cells.[67,68] These pattern recognition receptors can also be involved in NP phagocytosis.[69] More relevant for NPs is the opsonin-mediated phagocytosis. Here, opsonizing proteins in the NP protein corona interact with Fc and complement receptors, triggering phagocytosis.[64] In the context of NP drug delivery, this can be an unwanted uptake that results in rapid blood clearance and a decrease in the therapeutic effect.[70] Micropinocytosis is related to phagocytosis but can occur in most eukaryotic cells as it is not specific to phagocytic cells.[71] It also requires actin-dependent protrusion of the cell membrane, by which extracellular fluids are engulfed.[72] This process is unspecific and NPs are taken up by chance if contained in the engulfed fluid.[73] In contrast, there are several receptor-mediated endocytosis pathways that internalize NPs upon interaction with cellular surface receptors. Receptor-mediated endocytosis is also the most common entry route for viruses, which are in the same size range as NPs.[74] Clathrin-mediated endocytosis (CME) is the best-understood receptor-mediated pathway. It requires a set of intracellular proteins, which facilitate the inward budding of the plasma membrane, endosomal vesicle stabilization, and membrane scission. The characteristic of this endocytic pathway is the protein clathrin forming a regular coat on the endosomal vesicle.[75] Aside from receptor activation, CME depends on the particle size, and particles that are larger than 200 nm are not taken up by this pathway.[76] In addition to CME, there is caveolae-dependent and clathrin/caveolae-independent endocytosis, which both rely on membrane invagination assisted by a multi-protein machinery.[14]

1.1.4 Intracellular trafficking and exocytosis of NPs

The uptake mechanism crucially influences the further processing of NPs inside the cell and in consequence the success of drug delivery. The success of the delivery also depends on the final localization to the site of action of the therapeutic compound. With a few exceptions, the site of action usually is the cytosol or the nucleus.[77] Endocytic uptake routes deliver the NPs to the endolysosomal system.[78] This is a highly dynamic system of various vesicles and tubular compartments that fuse and separate to deliver their endocytic payload to its target compartment.[79] Endolysosomal trafficking can result in lysosomal degradation or storage, recycling to the plasma membrane, transcytosis, or endosomal escape which results in translocation to the cytosol. Recycling to the cell membrane, lysosomal degradation or storage are mostly unwanted processes as they abrogate the therapeutic effect of the cargo.[80] Transcytosis describes the process of traversing NPs through the cell. This process can facilitate the crossing of tissue barriers like the blood-brain barrier.[81] For cytosolic delivery, NPs must escape the endosome. Thus, endosomal escape is considered a rate-limiting step to cargo delivery.[82]

Once being translocated to the cytosol, exosomes can associate with the exosome machinery at the multivesicular bodies (MVB). Inward budding into the MVB lumen eventually results in the packaging of the NPs in exosomes, which constitutes a potential exocytosis route.[83,84] Further, outward budding of the plasma membrane can result in microvesicle-associated exocytosis. Another NP exocytosis route is the endosomal recycling of the NPs to the plasma membrane.[85] Upon trafficking to the lysosome, NPs can also be exocytosed by lysosomal exocytosis.[86]

Autophagy can also be involved in the intracellular processing of nanoparticles.[87] During autophagy, the phagophore engulfs cytosolic material or cellular organelles, which results in the formation of an autophagosome.[88] Subsequently, the autophagosome can fuse with late endosomes or MVBs.[89] This stage is named amphisome. The autophagosome and the amphisome can both fuse with the lysosome to facilitate degradation of the engulfed material.[88] In theory, it is thinkable that nanoparticles either enter the autophagy pathway by being engulfed by the phagophore or via fusion of autophagosomes with nanoparticle-containing endosomes or MVBs. Autophagy of nanoparticles is not only a process that can abrogates the therapeutic efficacy but can also be the cause of nanoparticle-related toxicity.[87]

1.1.5 Functionalization and coating of NPs

A major obstacle to the clinical translation of NPs still is the lack of highly specific *in vivo* targeting strategies. This involves active targeting of the desired site and a decrease in unspecific uptake by the MPS. Both problems can be addressed by engineering the NP surface. By altering the physicochemical properties of the surface, uptake by the MPS can be drastically reduced. The most applied method to prolong the blood circulation time of nanocarriers is attaching PEG or PEG alternatives such as polyethyl ethylene phosphate (PEEP) to the NP surface. This increases the NP hydrophilicity and decreases protein corona-mediated uptake by the MPS.[56] Fine-tuning the NP surface charge can facilitate targeting dendritic cells in lymphatic organs.[9] Further, a combination of poly(β-amino esters) and PEG grafted on LNPs was capable of delivering mRNA to the lungs of mice with higher efficiency due to reduced opsonization and MPS uptake.[90] The molecular mechanism behind targeting through tuning the physicochemical properties of an NP remains elusive. Since synthetic surfaces interact with biological structures through mediation by a rapid formation of a protein corona, targeting is likely achieved by adsorbing a specific set of proteins. Therefore, another surface modification strategy is the pre-coating of NPs with certain proteins.[91] The NP pre-coating with clusterin (apolipoprotein J), which contributed to the stealth effect of PEG-coated NPs, resulted in a reduced unspecific uptake.[92] Simon et al. demonstrated that pre-coating of NPs with targeting antibodies also facilitated specific targeting irrespective of an additional protein corona.[93] Antibodies are among the most frequently used targeting moieties and a variety of different conjugation strategies are used for NP conjugation.[94] To reduce unspecific immune cell uptake via the Fc part of the antibody [95], nanobodies, which consist only of the antigen-binding domain and are much smaller, are used alternatively.[96] Another alternative for targeting specific cell structures is the generation of affinity peptides via library selection.[97] The usage of antibodies and other affinity ligands as targeting moieties allows for the design of highly rational targeting strategies. However, this also requires the identification of cell surface structures that are unique to the target cell population. An alternative to raising affinity ligands against specific cell structures is the usage of biological ligands. Carbohydrate molecules are often involved in the cell specificity of viruses for their target cells and can also facilitate specific targeting.[98] Mannose-decorated poly lactic-co-glycolic acid

(PLGA) NPs were reported to specifically target macrophages.[99] This targeting strategy exploits the high expression of mannose receptors such as lectins on macrophages.[100,101] In addition to carbohydrate molecules, there are many naturally derived targeting ligands that have high affinities for cellular receptors. Transferrin is a protein that transports iron through blood and is specifically taken up by cellular transferrin receptors.[102] As transferrin receptors are overexpressed on tumor cells, it was used to target PLGA NPs to MCF-7 cells.[103] Another example is folate, which is a small molecule with a high affinity for the folate receptor and is overexpressed on various tumor cells.[104] Folate-conjugated NPs were used for the successful delivery of doxorubicin to ovarian tumors *in vivo*.[105] Often, it is not specific enough to target a single structure present on the target cells. Therefore, dual targeting strategies were employed.[106] NPs functionalized with hyaluronic acid and folate were used to target ovarian tumors *in vivo*.[105]

However, *in vivo,* targeting is a highly complex multi-step process. A single targeting moiety or dual targeting strategies are eventually not sufficient to navigate through this dynamic environment. Additionally, multiple biological barriers need to be overcome. This might require the NP surface to exert different functionalities. Aside from the difficulty of generating such a multi-functional NP, there is a lack of understanding of all relevant processes. An approach to mastering this complexity without knowledge of all molecular details is the use of biomembranes for NP coating. Biomembranes are hypothesized to include all necessary features to cope with the complexity of an *in vivo* environment and facilitate targeted drug delivery.

The first cell membrane that was transferred to NPs was derived from red blood cells (RBCs).[107] The RBC membrane was cloaked onto NPs by extrusion and increased their blood circulation time compared to naked NPs.[108] The RBC membrane is especially suited for NP stealth coating as it displays multiple self-signals that prevent phagocytosis. Therefore, RBCs have a prolonged blood circulation time of up to 3 months in the human body.[109] CD47 was identified to be one of the mediators of the prolonged blood circulation time and is known as the “don’t eat me” signal.[109] Leukocytes were also used for NP coating due to their ability to move in the direction of inflammation and thus, target tumor tissues.[110] Another strategy is to coat NPs with cancer cell membranes. Cancer cell membrane-coated NPs showed immune evasion as well as targeting tumor tissues.[111] As an alternative to transferring cell membranes to NPs, EV

membranes were used for coating.[84,112] EVs are vesicles that are secreted by multiple cell types and function as cell-to-cell communication system in most organisms including humans.[113] Therefore, the hypothesis is that the EV membrane contains a diverse set of proteins and other factors that allow navigating the complex *in vivo* environment. Further EVs bear the potential to target specific organs based on their cellular origin.[113]

1.2 Extracellular vesicles as drug delivery vehicles

1.2.1 Biology of extracellular vesicles

Extracellular vesicles (EVs) are lipid bilayer-confined nanovesicles that are equipped with a set of transmembrane proteins and contain a mixture of proteins, nucleic acids, and small molecules in their aqueous lumen (**Figure 1.2.1**). Based on their biogenesis pathway, EVs can be divided into three subclasses, which are exosomes [114], microvesicles [114], and apoptotic bodies [115]. Besides their cellular origin, the different subclasses differ in size and composition. Exosomes are generated by inward budding of the membrane of multivesicular bodies and have a size range between approx. 40-120 nm. Microvesicles bud from the plasma membrane and have a size range between approx. 50-1000 nm.[116] While exosomes and microvesicles are secreted during cell homeostasis, apoptotic bodies are characteristically released during cell apoptosis.[116] Exosomes and microvesicles are difficult to separate due to their overlap in particle size and surface receptor profile.[117] Therefore, the mixture of exosomes and microvesicles is often referred to as extracellular vesicles (EVs).[116] The most common EV markers are the tetraspanins CD9, CD63, and CD81 which play a role in membrane organization and cargo sorting.[118,119] Furthermore, EVs contain integrins, which are involved in cellular adhesion and EV tropism.[120,121] Associated with the EV membrane are RAB GTPases and annexins.[122,123] The aqueous lumen contains a mixture of different biomolecules. There are proteins like ALG-2 interacting protein X (ALIX), tumor susceptibility gene 101 protein (TSG101), and glycolytic enzyme glyceraldehyde-3-phosphate dehydrogenase (GAPDH), which were derived from the endosomal sorting complex required for transport (ESCRT) machinery or during EV assembly.[124,125] Further, heat shock proteins (HSP) 70 and 90 are frequently found in EV preparations.[126,127] Aside from soluble proteins, the EV lumen also contains different nucleic acids, such as microRNAs (miRNAs), mRNAs, non-coding RNAs [128], and DNA.[129,130]

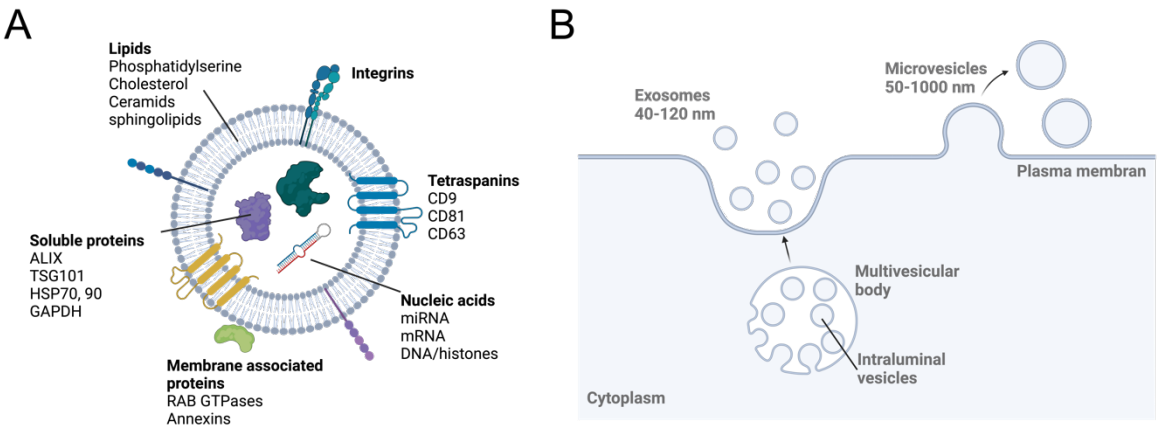

Figure 1.2.1: Schematic depiction of EV composition and biogenesis. A. EV composition and structure. B. Biogenesis of exosomes and microvesicles. This graphic was created with BioRender.com.

After secretion, EVs can either affect the parent cell [119], neighboring cells, and distal cells or reach distant tissues and organs through systemic distribution.[131] The recipient cell can either be affected by signal transduction via EV surface binding [132] or by internalization and cargo release.[128] EVs were reported to be internalized by clathrin-mediated and clathrin-independent endocytosis, micropinocytosis [133,134], lipid raft-mediated endocytosis [135], and direct fusion with the plasma membrane.[136] The regulation of the uptake route by the EV and the recipient cell, as well as subsequent intracellular trafficking routes, remains poorly understood.[137] However, it is known that EVs are capable of delivering their cargo to the cytosol [128,138], which either requires direct fusion of the EVs with the plasma membrane or escape of the EVs from the endosomal system.

EVs play various roles in the homeostasis of healthy organisms and diseases like cancer, neurodegenerative or infectious diseases. In healthy organisms, they regulate cell development [139] and immune responses [140] like antigen-presentation.[141] In cancer, for example, EVs exert various roles to promote tumor growth [142], metastasis [143], and immune evasion.[144]

1.2.2 Isolation methods

EVs can be isolated from various body fluids, as well as from cell culture medium.[145] The EV isolation from blood plasma is more challenging due to the high viscosity of plasma and potential contaminants like lipoproteins and protein aggregates.[146] When isolating EVs from cell culture medium, added fetal calve serum contains potential contaminants. Serum-derived EVs could be co-isolated with cell culture-derived EVs and

should be depleted before usage during EV harvesting. Another source of contamination is the high abundance of serum albumin.

Differential ultracentrifugation (UC) is the original and still predominant purification method for plasma and cell culture-derived EVs.[147] Differential UC was used by Raposo et al. to isolate exosomes secreted from B lymphocytes for the first time in 1996.[141] The protocol contains several low-speed centrifugation steps to remove cell debris, dead cells, and cells. Subsequently, exosomes are pelleted by a 100,000 x g centrifugation step. To reduce the viscosity of body fluids, the starting material can be mixed with phosphate buffered saline (PBS) previous to centrifugation.[145] A major downside of this isolation method is the potential damage of vesicle surface structures by centrifugation at 100,000 x g. Further, proteins aggregate and are pelleted at this centrifugation speed.[148-150]

An alternative to UC is size exclusion chromatography (SEC), which was used for EV isolation as well.[151-154] SEC is a size-based separation method that relies on a porous matrix. Larger particles can pass quickly as the pores in the Matrix do not capture them. Small particles pass slower due to the interaction with the porous matrix. When collecting fractions of the eluate, larger vesicles are eluted first. Subsequently, EVs are eluted, followed by lipoproteins and protein aggregates. Proteins are eluted last due to their small size.[151] Fractions containing small EVs with diameters between 30-80 nm can be contaminated with very low-density lipoproteins (VLDL) as they have a similar size range.[146] To process larger volumes of conditioned medium from cell culture, ultrafiltration can be used to pre-concentrate the sample before SEC.[155] The major advantage of SEC is that it preserves EV surface structures. This can result in a higher functionality of vesicles.[156] Both UC and SEC can be complemented by density gradient centrifugation. This technique separates particles according to buoyant density and can yield EV preparations with ultra-high purity when used in combination.[157]

Aside from SEC and UC, there are many other emerging technologies for EV isolation. Several isolation techniques rely on immunoprecipitation, where EVs are captured based on one or more surface markers.[158-161] Another set of techniques is based on flow fractionation such as asymmetric flow field-flow fractionation (AF4).[162-164]

1.2.3 Therapeutic and diagnostic application of EVs

Furthermore, EVs are getting recognized for their diagnostic and therapeutic potential. Glypican 1 (GPC1) was found to be enriched in tumor exosomes from various cancer types including pancreatic [165], breast [166], and colon cancer.[167] Therefore, the detection of GPC1-enriched EVs could be used for cancer diagnosis and monitoring of the tumor burden. The therapeutic potential of EVs was first discovered when using mesenchymal stem cells (MSCs) as regenerative cell therapy.[168,169] There, EVs were identified as the therapeutic agent.[170,171] MSC-derived EV treatment of patients with graft-versus-host disease showed remarkable results.[172] Therefore, the regenerative and immunomodulatory potential of MSC-derived EVs is explored further.[173]

1.2.4 EVs for drug delivery

EVs are natural NPs that play an important role in cell-to-cell communication as they transfer biologically active cargo between distant cells. The variety of properties necessary for this renders them to be ideal for use as drug delivery vehicles. EVs can carry different classes of cargo molecules. Lipophilic cargos can be integrated into the lipid bilayer, which increases their water solubility.[174] Hydrophilic cargo can be transported in the aqueous lumen of the vesicle, where they are protected from the surrounding environment.[175-177] Both are necessary for the transportation of the cargo through the bloodstream during systemic delivery. On a systemic level, EVs were reported to have an inherent targeting ability depending on the parent cell type. Tumor cell-derived EVs accumulated in tumors and metastatic nodes.[84,178,179] The effect is referred to as 'tumor-homing'. The molecular mechanisms for tumor-homing of EVs are largely unknown to date. A study by Hoshino et al. reported that the integrin expression profile on tumor-derived EVs determines their organ tropism. They further link the organ tropism of tumor-derived EVs to future sites of metastasis.[120] Another pharmacologically relevant and hardly accessible target is the brain, which is protected by the blood-brain barrier (BBB). This tight network of endothelial cells prevents the penetration of pathogens and many drugs into the brain.[180] EVs are currently under investigation as a possible shuttle to transport therapeutic cargo across the BBB. There is a variety of reports demonstrating the BBB crossing of EVs derived from different cell sources like mesenchymal stem cells [181], brain tumor cells [182], brain metastasis-promoting breast

cancer cells [183], and other cell types.[184] Banks et al. compared the brain-targeting capability of EVs from different cell culture cell types. Even though there are many studies on the BBB crossing of EVs from different cell sources, little is known about the prerequisites for BBB crossing. A better understanding of how EVs target specific organs or tumors would promote the usage of EVs as targeted drug delivery vehicles. Besides the potential for inherent targeting, EVs were able to penetrate spheroid tumor models deeper compared to liposomes.[185] Further, EVs were transported through extracellular matrix-simulating hydrogels quickly, which allowed them to reach their target cells more efficiently.[186] Both properties are beneficial for efficient drug delivery. Once the drug-loaded EVs reach their target cells, they must overcome multiple biological barriers including the plasma membrane and the intracellular endosomal system. Due to the equipment of EVs with surface proteins that interact with the cellular uptake machinery, they are superior in active cargo delivery compared to liposomes.[187,188] Studies on the delivery of RNA by EVs showed a remarkable efficiency to delivering active RNA to the cytosol, which requires cell uptake and endosomal escape.[128] A direct comparison of the RNA delivery efficiency of EVs to lipid NPs demonstrated that as little as 0.1-10 fM of total RNA packaged in EVs was sufficient for active delivery. For lipid NPs, the minimal dose was magnitudes higher.[138] In addition to this, EVs showed an excellent safety profile in numerous clinical trials.[189] However, the application of tumor cell-derived EVs must be inspected carefully because of their potential metastasis-promoting effect and the possibility of containing oncogenes.[190] Aside from this, there are technical challenges that impair the translation of EVs to clinical applications. EV preparations contain a heterogenic mixture of vesicles with presumably different biological activities. Furthermore, generating reproducibility between EV batches is challenging because small changes in critical parameters have a big impact on the resulting EV sample.[191,192] This makes it very difficult to generate a highly defined product.[193] Another practical consideration is that EV production upscaling is much more difficult than large-scale production of liposomes or other synthetic nanocarriers.[193]

1.2.5 Strategies for drug loading of EVs

When exploiting EVs for drug delivery one of the most important steps is to load the drug in EVs. Therefore, the loading strategy is crucial. In general, EV loading strategies can be divided into exogenous loading, where the cargo is loaded after the purification of the EVs, and endogenous loading, where the cargo is incorporated into the EVs

during their production by the producing cell. Exogenous loading is often based on the physical or mechanical disruption of the EV membrane, which likely compromises the surface properties and functionality of the EVs. For this purpose, techniques like sonication [194], electroporation [195,196], extrusion [197,198], and freeze-thaw cycles [197,199] are applied. The EV membrane can also be disrupted chemically for cargo loading. The mild surfactant saponin was used for the loading of hydrophilic small molecules [197,199] and the enzyme catalase.[200] Some studies compared the encapsulation efficiency of different loading methods with varying results. For some cargo molecule EV combinations, saponins resulted in the highest loading and/or highest therapeutic efficacy.[197,200] In another study, osmotic shock and freeze-thaw cycles yielded the highest encapsulation efficiency without reducing the EVs' cell uptake.[199] These findings suggest that the best loading strategy must be evaluated for each cargo EV combination. An exogenous, but not damaging, loading technique is the passive loading of cargo molecules, where the cargo is incubated with the purified EVs.[197] This approach is especially suitable for hydrophobic cargo like curcumin, which has poor water solubility and is preferentially associated with the EV membrane.[174] Furthermore, passive loading was also applied to gold NPs as cargo.[201] Another less invasive exogenous loading strategy is the usage of a glycosylphosphatidylinositol (GPI) anchor which inserts into the EV membrane due to its lipid nature.[202]

In contrast to exogenous loading, endogenous loading takes place during the biogenesis of the EVs and utilizes the producing cell's machinery. Therefore, it is mainly limited to molecule classes that can be produced by living cells, such as proteins and nucleic acid. For RNA loading, the producing cell can be genetically modified to simply over-express the RNA molecule of interest. There are also more advanced genetic-engineering approaches reported where the loading is actively enhanced by making the cargo artificially interact with EV components. Peptides or proteins can e.g. be fused to EV membrane proteins like CD63 or CD9.[203,204] However, there are also attempts to load small molecules by incubating the producing cell with cargo molecules.[205] This approach can be challenging because of the possible cytotoxic effects of the drug molecule on the producing cells or the limited stability of the cargo when exposed to cells. A possible solution for this problem is encapsulating the drug cargo into mesoporous silica NPs and then utilizing the producing cells' particle uptake and

EV loading machinery for packaging the drug-loaded NPs into EVs during EV biogenesis.[84]

1.2.6 Synthetic NP/EV hybrid particles for drug delivery

Synthetic NP/EV hybrids can open new possibilities for drug delivery as they are thought to combine the best features of synthetic NPs with those of EVs. Many studies on hybrid NPs exploited the ability of tumor-derived EVs to specifically accumulate in tumor tissue and metastasis.[84,112,178,179] Depending on the NP cargo NP/EV hybrids were developed for drug delivery and theranostic approaches. Due to their ability to encapsulate drug molecules in their porous structure, mesoporous silica NPs were loaded with the small chemotherapeutic molecule doxorubicin for cancer therapy.[84,112] Gold NPs were used as an imaging agent for biodistribution studies [178], for intracellular EV tracing in electron microscopy [206], and for photothermal therapy.[179] Metal-organic framework NPs combine both as they can capture therapeutic cargo such as small chemotherapeutic molecules [207] and even proteins [208] and additionally can be detected by magnetic resonance imaging. Generating these hybrid particles can be more challenging than loading other therapeutic cargo into EVs. There are various strategies reported for the generation of hybrid NPs that can also be distinguished into exogenous (after purification of EVs) and endogenous (during intracellular formation of EVs) loading strategies. Exogenous loading of NPs into EVs was achieved by passive incubation of NPs, which was reported for metal-organic framework particles, gold NPs, and mesoporous silica NPs.[112,206] In some reports, the exogenous loading process was promoted by physical intervention like ultrasonication, extrusion, or electroporation. The incorporation of metal-organic framework particles into EVs was for example facilitated by a combination of ultrasonication and extrusion.[208] Manganese carbonyl NPs were incorporated by electroporation [209] and gold NPs were incorporated by extrusion.[181] For platinum NPs, a different strategy was reported. Here, platinum NPs were assembled *in situ* directly inside of EVs from Pt^{2+} precursors to create a better tolerable alternative to the anticancer drug cisplatin.[179] Another class of hybrid NPs is the fusion of liposomes with pre-isolated EVs. This strategy aims to conserve the targeting properties of exosomes while increasing the packaging capacity to deliver e.g. larger nucleic acids like CRISPR/Cas9 expression vectors.[210] For silica [84] and gold NPs [83,178,179] there are reports where the cellular exosome biogenesis machinery was used to incorporate the NPs into EVs. The proposed packaging mechanism starts with the uptake of the

NPs by the producing cells through endocytosis (**Figure 1.2.2**). Subsequently, endosomal escape of the NPs is required to enter the cytosol. From the cytosol, NPs have access to packaging into exosomes by inward budding into multivesicular bodies. There is experimental evidence demonstrating the intracellular co-localization of NPs with CD63, which serves as a marker for multivesicular bodies.[84,178] Furthermore, transmission electron micrographs showed gold NP clusters inside intracellular vesicles.[83] After the maturation of the multivesicular body, NP-loaded exosomes are released by the fusion of the multivesicular body membrane with the plasma membrane. This step was demonstrated by the co-localization of NPs with CD81, which is another exosome marker, in the extracellular space.[83]

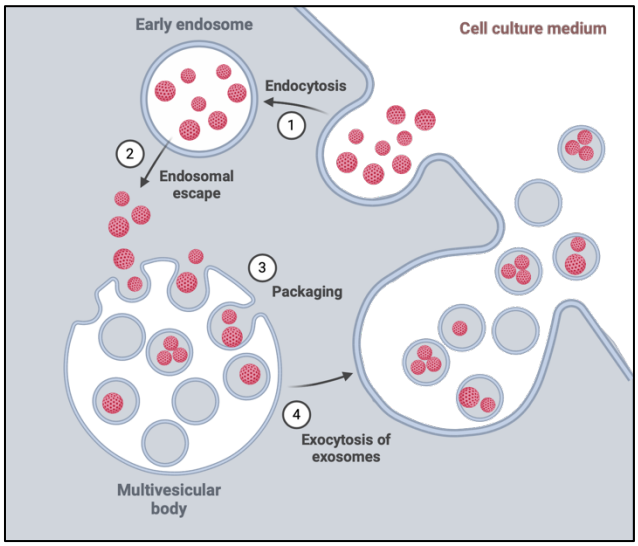

Figure 1.2.2: Schematic depiction of NP packaging via the cellular exosome biogenesis pathway. (1) Endocytosis of NPs by cell. (2) Endosomal escape. NPs enter the cytosol. (3) Packaging into exosomes by inward budding of the multivesicular body membrane. (4) Fusion of the multivesicular body membrane with the plasma membrane results in the release of NP-loaded exosomes. This graphic was created with BioRender.com.

There are reports of successful packaging of NPs into EVs using the cellular machinery. However, little is known about the actual packaging rates and how they differ depending on cell type, NP material, and incubation protocol. This is due to a lack of methodology to quantify encapsulation reliably and comparably. Yong et al. have proven packaging qualitatively by co-localization of NP and EV signals in confocal fluorescence imaging and transmission electron microscopy (TEM).[84] Sancho-Albero et al. performed a statistical analysis of TEM images to calculate packaging rates.[179] Lara et al. demonstrated packaging by cryo-TEM images and bulk detection of EV fluorescence and total gold mass.[178] While these techniques offer valuable hints towards NP packaging in EVs all of them exhibit limitations. The resolution of confocal microscopy

is too low to discriminate between packaged particles and aggregates formed by NPs and exosomes. TEM imaging of EVs results in capturing typical 'cup-shaped' objects due to the vacuum condition [141], which makes it very difficult to interpret TEM images of NP/EV hybrids. Cryo-TEM imaging can capture better depictions of EVs since their native bubble shape is preserved. This is especially important when analyzing more complex objects like NP/EV hybrids. However, statistical analysis to determine packaging rates based on cryo-TEM images would be extremely laborious considering the labor-intensive procedure and data acquisition of this technique.

1.2.7 Protein corona formation on EVs

The protein corona is a layer of proteins that adsorb to nano surfaces upon incubation in biological fluids like blood. The concept of protein corona formation originated from the synthetic biomedical NP field. The 'chemical identity' of the NP transforms into the 'biological identity' by adsorption of the protein corona. This ultimately determines the NP's fate in the human body and can impair its biomedical application.[36] In 2019, the protein corona concept was transferred to viruses as the first natural NP.[211] Ezzat et al. characterized the protein corona composition of the respiratory syncytial virus (RSV) and the herpes simplex virus type 1 (HSV-1).[211] Both human plasma-derived protein coronae contained complement proteins, but also proteins that were unique to each virus. Further, the presence of the protein corona around the virus particles was visualized by TEM imaging. Tóth et al. were the first to report the formation of a protein corona on THP-1 cell-derived EVs.[212] Apolipoproteins, complement proteins, fibrinogen, and immunoglobulins were the most abundant proteins found in the EV protein corona. All these proteins were often found in different combinations on various synthetic NPs as well.[38,46,213] Furthermore, the EV protein corona was visualized by confocal fluorescence microscopy and TEM. Functional studies revealed that the protein corona was integral to the biological activity of EVs. Tóth et al. showed that immune activation of dendritic cells upon EV treatment was increased in the presence of a protein corona.[212] A second study by Wolf et al. investigated the protein corona on placental-expanded stromal cells.[214] Here, angiogenesis and wound healing were increased in the presence of a protein corona. Taken together, these studies expand the view that the biologically active cargo is contained in the EV lumen. Also, the proteins interacting with the EV surface contribute to their functionality. This suggests reevalu-

ating former proteomic analysis of EVs isolated from blood plasma and serum-containing cell culture supernatants. These studies often found serum proteins which were assumed to be contaminants rather than components of the EV protein corona.[215,216]

The EV protein corona might not only contribute to their biological functionality but could also influence the blood clearance and biodistribution of intravenously injected nanocarrier EVs. There might even be a difference in the protein corona composition of native blood-derived EVs and that forming on transplanted EVs. These considerations are especially important for the use of EVs as drug nanocarriers. For many synthetic nanocarriers including liposomes, opsonizing proteins in the protein corona enhance their uptake by phagocytic immune cells of the MPS.[217,218] Due to the location of the MPS in the liver, spleen, lungs, and lymph nodes, this leads to a rapid accumulation in these organs. As a result, the therapeutic efficacy of the nanotherapeutics is drastically reduced.[218] To avoid this, stealth molecules, such as PEG, were grafted on the NP surface, which improved the therapeutic efficacy.[52,219-221] Wiklander et al. compared the biodistribution of transplanted EVs from different cell sources in mice and found accumulation in the liver and spleen.[222] Further, it was reported that the PEGylation of EVs increased their blood circulation time.[202] These results suggest that transplanted EVs encounter sequestration by the MPS similar to synthetic nanocarriers and that this poses an obstacle to further clinical translation. However, the role of the EV protein corona for the engagement with the MPS remained unclear and was addressed in the here presented PhD thesis.[223]

2 Materials and Methods

2.1 Establishing nanoparticle packaging and extracellular vesicle isolation protocol

2.1.1 Synthesis of polystyrene NPs

Polystyrene NPs were synthesized by [redacted]. As previously published, the polystyrene NPs were synthesized using miniemulsion polymerization [224,225]. For the continuous phase, 2.11 g Lutensol® AT50 (poly(ethylene glycol)-hexadecyl ether) (BASF SE, Ludwigshafen, Germany) were dissolved in 72 g Milli-Pore water. To prepare the amino-functionalized NPs 0.539 g 2-aminoethylmethacrylamide hydrochloride (AEMH) (Sigma-Adrich, St. Louis, USA) were added to the Lutensol solution. The dispersed phase for the preparation of plain and amino-functionalized NPs contained 18.02 g of distilled styrene (Thermo Fisher Scientific, Waltham, USA), 752.2 mg of hexadecane (TCI, Eschborn, Germany), 18.3 mg BODIPY (523/535 nm) and 300.76 mg V59 initiator (2,20-azobis(2-methylbutyronitrile)) (Wako Chemicals, Neuss-Uedesheim, Germany). The dispersed phase for the preparation of carboxy-functionalized NPs contained 17.1 g of distilled styrene (Thermo Fisher Scientific, Waltham, USA), 903.7 mg acrylic acid, 777 mg of hexadecane (TCI, Eschborn, Germany), 16.3 mg BODIPY (523/535 nm) and 300.76 mg V59 initiator (2,20-azobis(2-methylbutyronitrile)) (Wako Chemicals, Neuss-Uedesheim, Germany). For pre-emulsification, the continuous and dispersed phase solutions were mixed and stirred at room temperature for 1 h. The solution was homogenized using a Branson W 450 digital sonifier equipped with a ½" tip (Branson Ultrasonics, Brookfield, USA). Sonication was done for 120 s at an intensity of 90% while the samples were cooled in an ice water bath. The polymerization took place at 72°C for 16 h. To purify the NPs, the samples were centrifuged at 8,442 x g for 1 h and resuspended in water. The samples were washed three times.

2.1.2 HCT116 cell culture

Human colorectal tumor (HCT) 116 cells were cultured in Dulbecco's Modified Eagle Medium (DMEM) - high glucose supplemented with 10% fetal bovine serum (FBS), 100 U/mL penicillin, and 100 mg/mL streptomycin. Cells were grown in a humidified

incubator at 37°C and 5% CO_2. For passaging of HCT116 cells, 0.25% Trypsin-ethylenediaminetetraacetic acid (EDTA) was used at 37°C and 5% CO_2 for 5 min before centrifugation at 300 g for 5 min (all reagents from Thermo Fisher Scientific, Waltham, USA).

2.1.3 Packaging of PS-NPs

HCT116 cells were seeded in T175 cell culture flasks with a density of $3x10^6$ cells/flask and were grown to confluency. Subsequently, cells were incubated with 250 µg/mL polystyrene NPs in DMEM without FBS (both Thermo Fisher Scientific, Waltham, USA) for 18 h. Before the exocytosis phase, the medium was discarded, cells were washed three times with phosphate-buffered saline (PBS) and FBS-free DMEM was added. The cells were continued to incubate in the fresh medium for 24 h before harvesting the conditioned medium (CM). The CM was centrifuged at 3,000 g at 4°C for 20 min and the supernatant was concentrated 20-fold with an Amicon Ultra-15 30 kDa MWCO centrifugal filter (Merck Millipore, Darmstadt, Germany). Particles were isolated by size exclusion chromatography (SEC) according to Böing et al. [226] In brief, 10 mL syringes were packed with Sepharose CL-2B (Thermo Fisher Scientific, Waltham, USA). Columns were washed with one column volume PBS before applying 2 mL of concentrated and precleared CM. Fractions of 1 mL were collected and analyzed for particle count by differential light scattering (DLS) and fluorescence intensity. For DLS measurements, 200 µL of undiluted sample was used. Measurements were performed using a Zetasizer Nano S90 (Malvern Panalytical GmbH, Germany) at 25°C. For measuring the fluorescence intensity, 100 µL of the undiluted sample was measured with a Tecan Infinite M1000 plate reader (Tecan, Männedorf, Switzerland). Fractions 4-6 were collected as particle-rich fractions and concentrated 30-fold using Amicon Ultra-2 30 kDa MWCO centrifugal filters (Merck Millipore, Darmstadt, Germany). The resulting sample was used for further analysis.

2.1.4 Western blot

The protein content was measured using Pierce 660 nm Protein Assay Reagent (Thermo Fisher Scientific, Waltham, USA). Absorption was measured at 660 nm with a M1000 plate reader (Tecan, Männedorf, Switzerland). Subsequently, 5 µg of protein were separated on a NuPAGE™ 10% Bis-Tris Bolt™ polyacrylamide gel (Thermo Fisher Scientific, Waltham, USA). Therefore, the required volume of sample was mixed

with 4 µL NuPAGE™ Reducing Agent and 10 µL NuPAGE™ LDS Sample Buffer and was filled up to 26 µL with water. To denature the proteins, the samples were boiled at 95°C for 10 min. The samples and SeeBlue™ Plus2 Pre Stained Standard were applied to the SDS gel and run at 130 V for 1 h using 1X NuPAGE™ MES SDS buffer (both from Thermo Fisher Scientific, Waltham, USA). To transfer the proteins to the western blot membrane, an iBlot™ Dry Blotting System (Thermo Fisher Scientific, Waltham, USA) was used. Therefore, the bottom stack was put into the iBlot device, and the wetted gel was laid on top. A wetted filter paper was placed on top of the gel, followed by the top stack. The blot was run using P2 for 6 min. For protein detection, the WesternBreeze™ Chromogenic Kit (Thermo Fisher Scientific, Waltham, USA) was used according to the manufacturer's instructions. In brief, the membrane was blocked for 30 min on a rotary shaker using the kit's blocking solution. Subsequently, the membrane was washed twice for 5 min in water. To prepare the primary antibody solution, the αCD63 Recombinant Rabbit Monoclonal Antibody (SY21-02) (Thermo Fisher Scientific, Waltham, USA) was diluted 1:1000 in the antibody solution provided by the kit. The membrane was washed 4 times with 20 mL antibody wash provided by the kit for 5 min. Subsequently, the second antibody solution was applied for 30 min on a rotary shaker, and after thorough washing of the membrane, 5 mL of the chromogenic substrate solution was applied until purple bands appeared.

2.1.5 Flow cytometry

Cell uptake and exocytosis of PS-NH_2 NPs were quantified by flow cytometry. Therefore, 75,000 cells per well were seeded in a 24-well plate (Greiner Bio-One, Frickenhausen, Germany). The next day, cells were incubated with particles at 37°C and 5% CO_2 for 2 or 18 h at a concentration of 25 and 2.5 µg/mL in an FBS-free medium. Subsequently, the particle-containing medium was discarded, the cells were washed three times with PBS and fresh medium without FBS was added. After incubation for another 4 h (2 h uptake) or 24 h (18 h uptake), the cells were detached with Trypsin-EDTA (Thermo Fisher Scientific, Waltham, USA) for 2 min at 37°C and centrifuged at 500 x g for 5 min. The cells were resuspended in 1 mL PBS for flow cytometry measurement. 2 of 3 replicates per condition were stained with Zombie Aqua™ Fixable Viability Kit (BioLegend, San Diego, USA) diluted 1:500 in PBS. The NP uptake was measured with an Attune NxT Flow Cytometer (Thermo Fisher Scientific, Waltham, USA). Measurements were stopped, after reaching 10,000 events for the cells.

The BODIPY signal of the PS-NPs was detected in channel BL1 and the cell viability staining was detected in VL1. The Attune NxT Software was used for data analysis. FSC/SSC scatter plots were used for cell population selection and events were depicted as percentage of gated cells and median fluorescent intensities.

2.1.6 Confocal laser scanning microscopy (cLSM)

The intracellular localization of PS-NPs in HCT116 cells was verified by cLSM images taken with a Leica TCS SP5 (Leica, Wetzlar, Germany). The microscope was equipped with a multi-laser combination and five detectors (range of 400-800 nm). BODIPY-labelled PS-NPs were excited at 514 nm and a detector range of 530-600 nm. CellMask™ Deep Red plasma membrane stain (Thermo Fisher Scientific, Waltham, USA) was excited at 633 nm and a detector range of 646-799 nm. Images were taken in sequential mode using the LAS X software. For post-processing, brightness and contrast settings were adjusted using ImageJ. 12,500 HCT116 cells were seeded per well in µ-Slide 8 Well ibiTreat slide (IBIDI, Gräfelfing, Germany) the day before the uptake. The cells were incubated with 2.5 µg/mL PS-NPs in an FBS-free medium at 37°C and 5% CO_2 for 18 h. Subsequently, the NP-containing medium was removed, the cells were washed and fresh medium was added for 24 h before imaging. As controls, the cells were imaged untreated or after incubation with PS-NPs for 18 h. CellMask™ Deep Red was diluted 1:1000 in PBS and incubated with the cells for 2 min before washing and imaging.

To analyze the sample after the packaging procedure, 200 µL sample were incubated on a µ-Slide 8 Well ibiTreat slide (IBIDI, Gräfelfing, Germany) for 2 h at room temperature. After removing the sample, sedimented particles were fixed with 4% PFA (Carl Roth, Karlsruhe, Germany) for 15 min and incubated in 1% bovine serum albumin (BSA) (Merck, Darmstadt, Germany) for 15 min subsequently. The cells were washed three times and were incubated with the antibody solution in 1% BSA for 1 h at room temperature. For detection of the extracellular vesicle (EV) membrane a mixture of 0.5 µL CD9 Monoclonal Antibody (MEM-61), Alexa Fluor™ 647, and 0.5 µL CD63 Monoclonal Antibody (H5C6), eFluor™ 660, eBioscience™ (both Thermo Fisher Scientific, Waltham, USA) was used. Before image acquisition, the samples were washed three times with PBS. The PS-NPs were excited as described above and the antibody mixture was excited at 633 nm using a detector range of 646-799 nm.

2.2 Packaging of SiNC in EVs

2.2.1 Synthesis of silica nanocapsules

The silica nanocapsules (SiNCs) were synthesized by [redacted]. Ultrasmall SiNCs were synthesized with concurrent processes of Ostwald ripening and a sol-gel reaction of alkoxysilane following our previous report.[227] 5.21 mg of cyanine 5 N-hydroxysuccinimide ester (NHS) ester (Cy5-NHS ester) (Lumiprobe, Hannover, Germany) was mixed with 3.64 µL of (3-aminopropyl)triethoxysilane (TCI, Portland, Oregon) and 3 g of anhydrous chloroform (Carlo Erba, Emmendingen, Germany). The mixture was stirred overnight (mixture A). An oil phase was formed by mixing 0.5 mL of mixture A with 0.134 mL of cyclohexane and 2 mL of tetraethyl orthosilicate (TEOS) (Thermo Fisher Scientific, Waltham, USA). The oil phase was then added to an aqueous phase of 3.8 mg/mL dimethyloctadecyl[3-(trimethoxysilyl)propyl]ammonium chloride (TPOAC) (Thermo Fisher Scientific, Waltham, USA) in water under vigorous stirring. The emulsion was stirred for 30 min before being sonicated under ice-cooling in a pulse regime (3 s on, 3 s off, 50% amplitude) with a Branson SFX 550 Sonifier (Branson Ultrasonics, Brookfield, USA). The resulting miniemulsion was stirred at 25ºC for 20 h and then at 40ºC for 6 h. The dispersion volume was then adjusted to 30 mL by adding deionized water. To remove large SiNC (>10 nm in diameter), the synthesized dispersion was centrifuged at 10,397 x g at 4ºC for 45 min. The supernatant was collected after centrifugation and then the centrifugation process was repeated one more time.

Large SiNC were synthesized as follows. 0.5 mL of mixture A, 0.169 mL of hexadecane, and 2 mL of TEOS (Thermo Fisher Scientific, Waltham, USA) were mixed to form an oil phase. The oil phase was then added to an aqueous phase of 3.8 mg/mL TPOAC (Thermo Fisher Scientific, Waltham, USA) in water under vigorous stirring. The emulsion was stirred for 30 min and then was sonicated under ice-cooling in a pulse regime (3 s on, 3 s off, 50% amplitude) with a Branson SFX 550 Sonifier (Branson Ultrasonics, Brookfield, USA). Subsequently, the resulting miniemulsion was stirred at 25ºC for 20 h.

The functionalization of SiNC with polyethylene glycol (PEG) was prepared as follows. 60 mg of 5,000 Da PEG-methoxysilane (Rapp Polymer, Tübingen, Germany) was dissolved in 1 mL of water. The solution was added dropwise into a 2.5 mL dispersion of either ultrasmall SiNC or large SiNC under stirring. The mixture was then stirred at 25ºC for 24 h.

The PEG-functionalized SiNC were purified by dialysis using dialysis tubing with a MWCO of 12–14 kDa. The dispersion of SiNC was dialyzed against 600 mL of deionized water for 2 days; the water was changed 3 times per day.

2.2.2 HCT116 cell culture

HCT116 cells were cultured as described in **section 2.1.2**.

2.2.3 Flow cytometry

Cell uptake and exocytosis of SiNCs were quantified by flow cytometry. Therefore, 75,000 cells per well were seeded in a 24-well plate (Greiner Bio-One, Frickenhausen, Germany). The next day, cells were incubated with particles at 37°C and 5% CO_2 for 2, 6, or 24 h at a concentration of 200 µg/mL or for 2 h with concentrations ranging from 10 µg/mL to 200 µg/mL. After incubation, cells were detached with Trypsin-EDTA (Thermo Fisher Scientific, Waltham, USA) for 2 min at 37°C and centrifuged at 500 g for 5 min. Cells were resuspended in 1 mL PBS for flow cytometry measurement. The NP uptake was measured with an Attune NxT Flow Cytometer (Thermo Fisher Scientific, Waltham, USA). Measurements were stopped, after reaching 10,000 events for the cells. The Cy5 signal of the SiNC was detected in the RL1 channel with excitation at 638 nm and a 670/14 nm band pass filter. The Attune NxT Software was used for data analysis. FSC/SSC scatter plots were used for cell population selection and events were depicted as percentage of gated cells and median fluorescent intensities.

2.2.4 Confocal laser scanning microscopy (cLSM)

The intracellular localization of SiNC in HCT116 cells was verified by cLSM images taken with a Leica TCS SP5 (Leica, Wetzlar, Germany). The microscope was equipped with a multi-laser combination and five detectors (range of 400-800 nm). Cy5-labeled SiNCs were excited at 633 nm and a detector range of 646-799 nm. CellMask™

Plasma Membrane Stain Orange (Thermo Fisher Scientific, Waltham, USA) was excited at 561 nm and detected at 578-618 nm. Images were taken in sequential mode using the LAS X software. For post-processing, brightness and contrast settings were adjusted using ImageJ. 75,000 HCT116 cells were seeded per well in µ-Slide 8 Well ibiTreat slide (IBIDI, Gräfelfing, Germany) the day before the uptake. Cells were incubated with SiNCs (200 µg/mL, prepared in FBS-containing medium) at 37°C and 5% CO_2 for 2 h before imaging.

2.2.5 Packaging of SiNCs

SiNCs were packaged as described in **section 2.1.3**. The protocol was adapted according to SiNCs. Here, the cells were incubated with 100 µg/mL SiNCs in DMEM with FBS (both Thermo Fisher Scientific, Waltham, USA) for 2 h. Before the exocytosis phase, the medium was discarded, cells were washed three times with PBS and FBS-free DMEM was added. The cells were continued to incubate in the fresh medium for 4 h before harvesting the CM. The purification of particles from the CM was not changed compared to **section 2.1.3**.

2.2.6 Transmission electron microscopy (TEM)

The sample preparation and imaging were done by [redacted]. The samples were drop casted on grids (Plano, Wetzlar, Germany) with a 10 nm carbon film. Images were acquired with a JEOL JEM1400 transmission electron microscope (JEOL, Freising, Germany).

2.2.7 Cryo-TEM and electron energy loss spectroscopy (EELS)

The sample preparation was done by [redacted] and cryo-TEM imaging and EELS was done by [redacted]. CryoTEM samples were prepared on glow-discharged 300 mesh 2/1 Quantifoil grids (Quantifoil Micro Tools, Großlöbichau, Germany). 4 µL of sample was added to the grid and blotted using Vitrobot Mark (Thermo Fisher Scientific, Waltham, USA) for 1 sec using force 5 at 20ºC in 100% humidity. The grid was then plunge-frozen in liquid ethane and imaged with a K3 camera (Gatan, Pleasanton, USA) in the Titan Krios G4 cryo-TEM (Thermo Fisher Scientific, Waltham, USA). To analyze the spatial distribution of the element silica in the sample, EELS was applied. The sample was imaged under cryo conditions using a Gatan Continuum EELS spectrometer in combination with a Gatan K3 direct electron detection camera

(both Gatan, Pleasanton, USA). While recording the EEL spectrum for every pixel of the STEM image, the microscope was operated in scanning TEM (STEM) mode. The digital Micrograph GMS 3 software (Gatan, Pleasanton, USA) was used for data acquisition.

2.2.8 Fluorescence cross-correlation spectroscopy (FCCS)

The samples analyzed by FCCS were produced by myself (EVs and EV/SiNC hybrids) and [redacted] (SiNCs), whereas the FCCS measurements were performed by [redacted]. The FCCS experiments were performed on an LSM 880 commercial setup (Carl Zeiss, Jena, Germany). For excitation of the Alexa 488 and Cy5 labeled species, respectively an argon ion laser (488 nm) and a He/Ne-laser (633 nm) were used. The excitation lasers were focused on the studied solutions by a C-Apochromat 40x/1.2 W high numerical aperture water immersion objective (Carl Zeiss, Jena, Germany). An eight-well polystyrene, chambered cover glass (Laboratory-Tek, Nalge Nunc International) was used as a sample cell. The fluorescence was collected with the same objective and after passing through a confocal pinhole, directed to a Quasar spectral detection unit (Carl Zeiss, Jena, Germany). In this unit, emission was spectrally separated by a grating element on a 32-channel array of GaAsP detectors operating in a single photon counting mode. The emission of Alexa 488 was detected in the spectral range 500-550 nm and that of Cy5 in the range 640-700 nm. The temporal fluctuations δFg(t) and δFr(t) of the “green” (Alexa 488) and “red” (Cy5) fluorescence signals were recorded and used to calculate the auto- Ggg(τ), Grr(τ), and the cross-correlation Ggr(τ) functions:

$$G_{gg,rr}(\tau) = 1 + \frac{\langle \delta F_{g,r}(t) \delta F_{g,r}(t+\tau) \rangle}{\langle F_{g,r}(t) \rangle \langle F_{g,r}(t) \rangle} \quad (1)$$

$$G_{gr}(\tau) = 1 + \frac{\langle \delta F_{g}(t) \delta F_{r}(t+\tau) \rangle}{\langle F_{g}(t) \rangle \langle F_{r}(t) \rangle} \quad (2)$$

The experimental auto- and cross-correlation curves were fitted with the theoretical model function for freely diffusing fluorescence species.[228]

$$G(\tau) = 1 + \frac{1}{N} \frac{1}{\left[1+\frac{\tau}{\tau_D}\right]\sqrt{1+\frac{\tau}{S^2\tau_D}}} \quad (3)$$

Here, N is the average number of diffusing fluorescence species in the confocal observation volume, τD is the diffusion time of the species and S is the so-called structure parameter, S = z0/r0, where z0 and r0 represent the axial and radial dimensions of the confocal volume V, respectively. Furthermore, the diffusion time, τ_D, is related to the respective diffusion coefficient, D, through: $\tau_D = \frac{r_0^2}{4D}$. The fits yielded the corresponding diffusion times, and subsequently the diffusion coefficients and through the Stocks-Einstein relation the hydrodynamic radii of the fluorescent species.

Furthermore, the amplitude of the cross-correlation curve Ggr(0) is directly proportional to the concentration of dual-colored species Cgr in the studied solution through [228]:

$$C_{gr} = \frac{[G_{gr}(0)-1]V_{gr}}{[G_g(0)-1]V_g[G_r(0)-1]V_r} \quad (4)$$

The fractions of dual-colored species compared to all green or red species were calculated as:

$$\frac{C_{gr}}{C_g} = \frac{N_r V_{gr}}{N_{gr} V_r} \quad \text{and} \quad \frac{C_{gr}}{C_r} = \frac{N_g V_{gr}}{N_{gr} V_{gr}} \quad (5)$$

As the values of r0 and S and thus V depend on the specific characteristics of the optical setup and the respective wavelengths, calibration experiments were performed using fluorescent dyes with known diffusion coefficients, i.e., Alexa 488 and Atto 643 in water.

2.2.9 Multi-angled DLS

Multi-angled DLS measurements were performed by [redacted]. An ALV spectrometer equipped with a goniometer and an ALV-5004 multiple-tau full-digital correlator (320 channels) was used. The light source was a He-Ne laser at a wavelength of 632.8 nm. To control the temperature a thermostat (Julabo) was used. The water used for dilutions was filtered with a GS filter (0.2 µm) (Merck Millipore, Billerica, USA) and the 5-SiNC PEG particle stock solution was added unfiltered. The measurements were performed in quartz cuvettes with an inner radius of 9 mm (Hellma, Mühlheim, Germany) that were cleaned with acetone in a Thurmond apparatus.[229] The data was analyzed using a multicomponent fit method as previously reported.[230]

2.3 Exocytosis of NPs from cells

2.3.1 Silica NPs

Mesoporous silica NPs (SiNP) in the sizes 10 nm, 30 nm, 50 nm, and 100 nm from the sicastar®-redF series were purchased from micromod Partikeltechnologie GmbH (Rostock, Germany). According to the manufacturer, particles were produced via the Stöber process [231] and contain covalently bound rhodamine B as fluorescent labeling (excitation: 569 nm, emission: 585 nm).

2.3.2 HCT116 cell culture

Cell culture was done by [redacted] under my supervision. HCT116 human colorectal cancer cells were cultured as described in **section 2.1.2**.

2.3.3 Protein corona adsorption

Protein corona adsorption was done by [redacted] under my supervision. Human citrate blood plasma was taken from healthy donors at the Department of Transfusion Medicine in Mainz after physical examination and after obtaining written informed consent in accordance with the Declaration of Helsinki. The blood plasma of 10 healthy donors was pooled and stored at -20°C. The study was approved by the local ethics committee “Landesärztekammer Rheinland-Pfalz” (Bearbeitungsnummer: 837.439.12 (8540-F)). The protein corona was adsorbed as described previously by our group.[91,232,233] In brief, human citrate plasma (0.5 mL) and SiNP (1 mg/mL) were incubated for 1 h at 37°C and 300 rpm. Plasma was removed by centrifugation at 20,000 x g and 4°C for 1 h. Subsequently, the pellet was resuspended PBS and centrifuged again. For cell uptake experiments, the pellet was washed twice and resuspended in DMEM without FBS after the last run. For fluorescence calibration, both particles with and without protein corona were measured with an M1000 plate reader (Tecan, Männedorf, Switzerland). For liquid chromatography-mass spectrometry (LC-MS) measurement, the pellet was washed three times with PBS. The final pellet was resuspended in desorption buffer (SDS (2% (w/v)) + Tris*HCL (62.5 mM) in H_2O (3 mL)). Subsequently, it was incubated at 95°C for 5 min and subjected to digestion.

2.3.4 In-solution digestion and LC-MS measurement

The in-solution digestion and LC-MS measurements were performed by [redacted]. The data was reviewed by me and [redacted]. The in-solution digestion and LC-MS measurements were performed as previously described by our group.[91,232,234] In short, SDS was removed by using Pierce Detergent Removal Spin Columns (Thermo Fisher Scientific, Waltham, USA) followed by protein precipitation using ProteoExtract protein precipitation kit (Merck Millipore, Darmstadt, Germany). After isolation, proteins were resuspended in RapiGest SF (Waters, Milford, USA), reduced with dithiothreitol (Sigma-Aldrich, St. Louis, USA), and alkylated with iodoacetamide (Sigma-Aldrich, St. Louis, USA). Tryptic digestion of the protein was performed at a protein:trypsin ratio of 50:1 for 18 h at 37°C. After stopping the digestion by adding HCl (2 µL) (Sigma-Aldrich, St. Louis, USA) and removing the degradation products of RapiGest by centrifugation, the peptides were proceeded to LC-MS measurements. Therefore, the samples were diluted with formic acid (0.1%) and spiked with Hi3 E. coli (50 fmol/µL) (Waters, Milford, USA). Measurements were performed at a nanoACQUITY UPLC system coupled to a Synapt G2-SI mass spectrometer (Waters, Milford, USA). Electrospray ionization was performed in positive mode with a NanoLockSpray source. As a reference, Glu-Fibrinopeptide (150 fmol/µL) at a flow rate of 0.5 µL/min was injected and a sample flow rate of 0.3 µL/min was set. The mass spectrometer was operated in a resolution mode performing data-independent acquisition (MSE). Data was processed using MassLynx 4.1 and proteins were identified using Progenesis QI 2.0. A reviewed human database downloaded from UniProt was used for protein identification. Noise reduction thresholds were set for low energy, high energy, and peptide intensity at 120, 25, and 750 counts, respectively. A maximum protein mass of 600 kDa, one missed cleavage, fixed carbamidomethyl modification for cysteine, variable oxidation for methionine, and a false discovery rate of 4% for proteins was set for protein and peptide identification. For peptide identification at least three assigned fragments and for protein identification at least two assigned peptides and five assigned fragments are required. The TOP3/HI3 approach was used for the quantification of each protein in fmol.[235]

2.3.5 Flow Cytometry

Flow cytometry experiments were done by [redacted] under my supervision. The data was reviewed by me. HCT116 cells were seeded into 24-well plates (Greiner Bio-one,

Frickenhausen, Germany). Cells (150,000) were seeded per well. The next day, the cells were incubated with SiNPs in the presence or absence of a pre-formed protein corona (5 µg/mL) in serum-free DMEM for 2 h, 4 h, or 24 h. For measuring exocytosis of SiNPs, the cell culture medium was exchanged after 2 h, and the cells were incubated for another 2 h or 22 h. As a control for dead cells, cells were incubated either for 2 h, 4 h, or 24 h with dimethyl sulfoxide (DMSO; 20%; Sigma-Aldrich, St. Louis, USA). The cells were detached with Trypsin-EDTA (Thermo Fisher Scientific, Waltham, USA) and subsequently centrifuged at 300 x g, 22°C for 5 min. Two of three pellets of one condition were stained with LIVE/DEAD™ Fixable Green (Thermo Fisher Scientific, Waltham, USA) according to the manufacturer´s instructions. The pellets were resuspended in 1 mL PBS and measured with the Attune NxT Flow Cytometer (Thermo Fisher Scientific, Waltham, USA). For the excitation of the particles, the yellow laser (561 nm) and an emission filter in the range of 530/30 nm were used. For the detection of LVE/DEAD™ Fixable Green, the blue laser (488 nm) and an emission filter in the range of 585/16 nm were used. For data analysis, the Attune NxT software was used. Forward scatter/side scatter (FSC/SSC) scatter plots were used to discriminate the cell population and events were depicted as percentages of gated cells and MFI. Subsequently, the fluorescence intensity of the SiNP dispersion was used to adjust the difference in fluorescence for particles with and without protein corona. Results were depicted using GraphPad Prism 9 (Dotmatics, Boston, USA).

2.3.6 Confocal Laser Scanning Microscopy (cLSM)

cLSM images were acquired by [redacted] and me. HCT116 cells were seeded into a µ-Slide 8 Well chamber (ibidi, Gräfelfing, Germany). Cells (100,000) were seeded per well. The next day, cells were incubated with SiNPs in the presence or absence of a pre-formed protein corona (10 µg/mL) in serum-free DMEM for 2 h. The plasma membrane was stained with CellMask™ Deep Red Plasma Membrane Stain (Thermo Fisher Scientific, Waltham, USA) and lysosomes were stained with Invitrogen™ LysoTracker™ Green DND-26 (Thermo Fisher Scientific, Waltham, USA) according to manufacturer's instructions. The cells were measured live. The images were acquired with an LSM SP5 STED Leica Laser Scanning Confocal Microscope (Leica, Wetzlar, Germany) and a Leica TCS SP8 (Leica, Wetzlar, Germany), equipped with a multi-laser combination and five detectors (range of 400-800 nm). SiNPs were excited at 561 nm and detected at 575-640 nm. CellMask™ Deep Red Plasma Membrane

Stain was excited at 633 nm and detected at 644-800 nm. LysoTracker™ Green DND-26 was excited at 469 nm and detected at 503-541 nm. Images were taken by sequential scanning using the LAS X software. For processing and analysis, Fiji was used. Brightness and contrast were adjusted to reflect differences in fluorescence intensity of the different-sized SiNPs.

2.3.7 ζ-potential measurement

The measurements were done by [redacted] and me. A Zetasizer Nano Z (Malvern Panalytical GmbH, Germany) was used for the zeta potential determination of SiNPs. For the measurement, the SiNP stock solution (5 µL) was diluted in potassium chloride solution (KCl) (1 mL, 1 mM). The measurement was performed at 20°C after an equilibration time of 2 min. Each measurement was performed in triplicates and mean values as well as standard deviations were calculated.

2.3.8 Multi-angled DLS

The multi-angled DLS measurements were performed by [redacted]. An ALV spectrometer equipped with a goniometer and an ALV-5004 multiple-tau full-digital correlator (320 channels) was used. The light source was a He-Ne laser at a wavelength of 632.8 nm. To control the temperature a thermostat (Julabo) was used. The water used for dilutions was filtered with a GS filter (0.2 µm) (Merck Millipore, Billerica, USA) and the particle stock solution was added unfiltered. The stock solution of the 10 nm SiNPs was filtered with an LCR filter (0.45 µm) (Merck Millipore, Billerica, USA) before dilution. The measurements were performed in quartz cuvettes with an inner radius of 9 mm (Hellma, Mühlheim, Germany) that were cleaned with acetone in a Thurmond apparatus.[229] The data was analyzed using a multicomponent fit method as previously reported.[230]

2.3.9 Transmission electron microscopy

The sample preparation and imaging was done by [redacted]. The samples were drop casted on grids (Plano, Wetzlar, Germany) with a 10 nm carbon film. Images were acquired with a JEOL JEM1400 transmission electron microscope (JEOL, Freising, Germany).

2.4 Protein corona on EVs and liposomes

2.4.1 Cell culture

THP-1 cells were cultured in RPMI 1640 medium supplemented with 10% FBS, 100 U/mL penicillin, 100 mg/mL streptomycin, and 2 mM Glutamax. HCT116 cells were cultured as described in **section 2.1.2**. Cells were grown in a humidified incubator at 37°C and 5% CO_2. For passaging of THP-1 cells, cells were centrifuged at 300 x g for 5 min. For passaging of HCT116 cells, 0.25% Trypsin-EDTA was used at 37 °C and 5% CO_2 for 5 min before centrifugation at 300 x g for 5 min (all reagents from Thermo Fisher Scientific, Waltham, USA).

2.4.2 Generation of monocyte-derived dendritic cells

Monocyte-derived dendritic cells were isolated and cell uptake was performed by [redacted]. Buffy coats, received from healthy donors upon informed consent (blood bank of the University Medical Center Mainz) were used to isolate peripheral blood mononuclear cells (PBMCs).[236] PBMCs were isolated from other blood cells by centrifugation for 20 min at 900 x g at room temperature through a Histopaque-1077 density gradient media (Sigma-Aldrich, USA). Subsequently, PBMCs were collected from the interphase and washed with PBS. $CD14^+$ monocytes were enriched using magnetic cell separation via CD14 MicroBeads (MACS) (Miltenyi Biotec., Bergisch Gladbach, Germany). The cells were subsequently cultured at a concentration of 10^6/mL in 3 mL in 6-well plates (Greiner, Kremsmünster, Austria) using IMDM medium supplemented with 10% FBS, 1% GlutaMAX, 1 β-mercaptoethanol, 1% non-essential amino acids, 1 mM sodium pyruvate, 100 U/mL penicillin and 100 g/mL streptomycin. Further, 200 U/mL granulocyte-macrophage colony-stimulating factor (GM-CSF) and 200 U/mL interleukin-4 (IL-4) were added to each well. Before cell uptake, cells were cultured for 6 days at 37°C and 5% CO_2. 1 mL of culture medium was carefully removed from the wells and replenished with 1 mL fresh medium supplemented with 600 U/mL GM-CSF and 600 U/mL on day 2 and day 4.

2.4.3 EV isolation from the cell culture medium

30 mL of CM was collected from approximately $2x10^7$ sub-confluent HCT116 cells cultured in serum-free medium for 24 h. CM was centrifuged at 3,000 x g at 4°C for 20 min. Supernatants were collected and concentrated 20-fold using Amicon Ultra-15

30 kDa MWCO centrifugal filters (Merck Millipore, Darmstadt, Germany). EVs were isolated by SEC according to Brahmer et al.[226] 10 mL syringes were packed with Sepharose CL-2B (Thermo Fisher Scientific, Waltham, USA). Columns were washed with one column volume PBS before applying 2 mL of concentrated and pre-cleared CM. Fractions of 1 mL were collected and analyzed for particle count by NP tracking analysis. Fractions 4-6 were collected as particle-rich fractions and concentrated 30-fold using Amicon Ultra-2 30 kDa MWCO centrifugal filters (Merck Millipore, Darmstadt, Germany). Protein content was measured using Pierce 660 nm Protein Assay Reagent (Thermo Fisher Scientific, Waltham, USA). Absorption was measured at 660 nm with a M1000 plate reader (Tecan, Männedorf, Switzerland).

2.4.4 Liposome preparation

Liposomes were prepared by [redacted]. Liposomes were prepared from mixtures of cholesterol (Chol), 1,2-Dioleoyl-*sn*-glycero-3-phosphoethanolamine (DOPE), and L-*α*-phosphatidylcholine (egg PC) with different molar compositions to reach two different liposome formulations, DOPE 5% and DOPE 33%. The three liposome components were prepared at a concentration of 10 mg/mL in chloroform and stored at -20°C. Then, the different liposome membrane compositions were obtained by mixing 1.44 mL eggPC, 120 µL DOPE, and 440 µL Chol, to achieve eggPC:DOPE:Chol = 55:5:40 molar ratio; and 835 µL eggPC, 767 µL DOPE, and 398 µL Chol, to get eggPC:DOPE:Chol = 1:1:1 molar ratio. All chemicals were purchased from Merck, Darmstadt, Germany. The lipid mixtures together with 2 mL of chloroform (Merck, Darmstadt, Germany) with 1 vol% EtOH (Carl Roth, Karlsruhe, Germany) were added in a 50 mL round-bottomed flask. To obtain the dried lipid films the solvent was evaporated with a rotary evaporator (450 mbar and 3 mbar each for 30 min at 42°C).

The lipid films were hydrated by the addition of 4 mL of PBS buffer (0.1 M, pH = 7.4) (Merck, Darmstadt, Germany). Then the mixtures were stirred overnight at 500 rpm and subsequently sonicated in a water bath for 20 min. Finally, the liposomes were extruded 11 times per pore size through polycarbonate membranes with pore sizes of 800 nm, 400 nm, and 200 nm using a 1 mL syringe (Avanti Polar Lipids, Alabaster, USA). Liposomes were stored at 4°C until further use.

2.4.5 Labeling HCT116 EVs and liposomes with Cyanine 5 (Cy5)

100 µg of freshly isolated HCT116 EVs or liposomes were incubated with 4 µL 1 mM Cy5 NHS-Ester (Lumiprobe, Hunt Valley, USA) at room temperature for 1 h. Unreacted dye molecules were removed by washing the samples with PBS using Amicon Ultra-2 30 kDa MWCO centrifugal filters (Merck Millipore, Darmstadt, Germany). For the labeling of EVs, an excess of fluorophores was used.

The labeling reaction was done in 100 µL at a working concentration of 40 µM Cy5-NHS. That corresponds to $2.4x10^{15}$ available fluorophore molecules. 100 µL of isolated EVs contained approximately $5x10^{9}$ particles. Therefore, the labeling reactions were performed at a fluorophore excess of $4.8x10^{5}$. Considering that there are multiple available NH_2 groups per EV particle, it is likely that at this ratio there was an excess of fluorophores over NH_2 groups. To verify that all unbound fluorophores have been washed out to the extent that they do not affect cell uptake studies, a control containing only fluorophores but not particles was prepared. Therefore, the same amount of fluorophore was incubated with PBS and washed according to the staining protocol. Incubation of this sample with HCT116 cells did not result in an intracellular uptake signal above the cell background in flow cytometry measurements.

2.4.6 Dynamic light scattering (DLS)

For DLS measurements, 10 µL of liposome sample were diluted in 200 µL PBS buffer. For EV measurements, 200 µL of the undiluted sample was used. Measurements were performed using a Zetasizer Nano S90 (Malvern Panalytical GmbH, Germany) at 25°C. The size distribution was obtained by cumulants fitting.

2.4.7 Nanoparticle tracking analysis (NTA)

We thank [redacted] for the opportunity to use their NTA device. The measurement was performed by me under the supervision of [redacted]. For NTA measurements, ZetaView (Particle Metrix GmbH, Germany) and the corresponding software ZetaView version 8.05.16 SP3 (Particle Metrix GmbH, Germany) were used. The following instrument parameters were used: Scatter mode with a sensitivity of 80 and a shutter of 100. For analysis, a max area of 1000, a min area of 10, and a min brightness of 30 were chosen. The binning was set to 5 nm. Samples were diluted with PBS and measurements were done at 25°C. The particles of 11 long videos and a total

of 959 objects were analyzed and mean and standard deviation were calculated from number-weighted mean values.

2.4.8 Zeta potential

A Zetasizer Nano Z (Malvern Panalytical GmbH, Germany) with disposable folded capillary cells was used to determine the zeta potential of the EV and liposome samples. For the measurements, 10 µL of each liposome dispersion or 100 µL of EV solution were diluted with 1 mL of a 1 mM potassium chloride (KCl) solution. The measurement was performed at 25°C after 2 min of equilibration. Each measurement was performed in triplicates and mean values as well as standard deviations were calculated.

2.4.9 Protein corona adsorption

Human citrate blood plasma was taken from healthy donors at the Department of Transfusion Medicine at the University Medical Center Mainz after physical examination and after obtaining written informed consent in accordance with the Declaration of Helsinki. The blood plasma of 10 healthy donors was pooled and stored at -20°C. The study was approved by the local ethics committee “Landesärztekammer Rheinland-Pfalz” (Bearbeitungsnummer: 837.439.12 (8540-F)). Protein corona was adsorbed as previously described by our group.[91,232,233] The protocol was adapted to EV properties. 100 µg of Cy5-labeled or unlabeled EVs or liposomes were incubated with 1 mL of human citrate plasma at 37°C under constant agitation (300 rpm) for 1 h. For EV proteome analysis 100 µg EVs were incubated with 1 mL PBS. Subsequently, EVs and liposomes were pelleted at 100,000 x g at 4°C for 1 h with an Avanti J-26S XP ultracentrifuge (Beckman Coulter, Pasadena, USA). For mass-spectrometry analysis of the protein corona, pellets were washed 3x with PBS and subjected to digestion for liquid chromatography-mass spectrometry (LC-MS). For cell uptake experiments pellets were washed 1x in PBS and the final pellets were resuspended in 1 mL cell culture medium.

2.4.10 Flow cytometry and cytotoxicity

Cell uptake of EVs and liposomes with and without protein corona into THP-1 cells, HCT116 cells, and monocyte-derived dendritic cells (moDCs) was measured by flow cytometry. Therefore, 150,000 cells per well were seeded in 24-well plates (Greiner Bio-One, Frickenhausen, Germany) and directly incubated with EVs or liposomes

(10 µg/mL) at 37°C and 5% CO_2 for 16 h. Subsequently, cells were centrifuged at 300 x g for 5 min and resuspended in 1 mL PBS for flow cytometry measurement. For binding assays in the absence and presence of Fc receptor block, 100,000 cells were pre-treated with 0.5 µL Human TruStain FcX (Biolegend, San Diego, USA) for 10 min at room temperature. Subsequently, cells were centrifuged at 300 x g for 5 min and resuspended in 10 µL cell culture medium without serum. Diluted EV or liposome solution (20 µg/mL) was added and incubated with cells at 4°C for 40 min. Subsequently, cells were centrifuged at 300 x g for 5 min and resuspended in 1 mL PBS for flow cytometry measurement. NP uptake was measured with an Attune NxT Flow Cytometer (Thermo Fisher Scientific, Waltham, USA). Measurements were stopped, after reaching 10,000 events for the cells. Cy5 signal of EVs or liposomes was detected in the RL1 channel with excitation at 638 nm and a 670/14 nm band pass filter. The Attune NxT Software was used for data analysis. FSC/SSC scatter plots were used for cell population selection and events were depicted as percentage of gated cells and median fluorescent intensities. For cell viability measurement, 5,000 cells per well were seeded in 96-well plates (Greiner Bio-One, Frickenhausen, Germany) and were directly incubated with EVs or liposomes (10 µg/mL) at 37°C and 5% CO_2 for 16 h. As dead cell control, cells were incubated with a medium containing 20% dimethyl sulfoxide (Sigma-Aldrich, St. Louis, USA) for 16 h. CellTiter-Glo Luminescent Cell Viability Assay (Promega, Madison, USA) reagent was prepared according to the manufacturer's protocol and then 100 µL reagent was added per well. Luminescence was measured with an M1000 plate reader (Tecan, Männedorf, Switzerland).

2.4.11 Confocal laser scanning microscopy (cLSM)

The intracellular localization of liposomes and EVs in THP-1 cells was verified by cLSM images taken with a Leica TCS SP8 (Leica, Wetzlar, Germany). The microscope was equipped with a multi-laser combination and five detectors (range of 400-800 nm). Cy5-labeled liposomes and EVs were excited at 633 nm and a detector range of 646-799 nm. CellMask™ Plasma Membrane Stain Orange (Thermo Fisher Scientific, Waltham, USA) was excited at 561 nm and detected at 578-618 nm. LysoTracker™ Green DND-26 (Thermo Fisher Scientific, Waltham, USA) was excited at 488 nm and detected at 504-541 nm. Images were taken in sequential mode using the LAS X software. For post-processing, Image J was used, and brightness and contrast settings were adjusted to account for differences in liposome and EV fluorescent labeling. For

+ and -PC images of the same particle, identical brightness, and contrast settings were used.

150,000 THP-1 cells were seeded per well in 48-well plates (Greiner Bio-One, Frickenhausen, Germany) and directly incubated with EVs or liposomes (120 µg/mL) at 37°C and 5% CO_2 for 16 h. Cells were centrifuged at 300 x g for 5 min and stained with CellMask and LysoTracker shortly before imaging. For imaging, 10 µL cell suspension was applied to a High Precision Microscope Cover Glass 24 x 60 mm 170±5 µm in thickness (Carl Roth, Karlsruhe, Germany) and covered with a second cover glass 170±5 µm in thickness and 24 mm in diameter (Carl Roth, Karlsruhe, Germany).

2.4.12 Cryo-TEM

Sample preparation and cryo-TEM imaging were performed by [redacted]. The statistical analysis was done by me. Cryo-TEM was done as described in **section 2.2.7**. For statistical analysis of the vesicle diameter distribution, 5 images and a total of 34 objects were taken into account. Vesicle diameters were measured by hand using Image J.

2.4.13 In-solution digestion and LC-MS measurement

The in-solution digestion and LC-MS measurements were done by [redacted]. The in-solution digestion and LC-MS measurements were performed as previously described by our group.[91,232,233] In short, SDS was removed by using Pierce Detergent Removal Spin Columns (Thermo Fisher Scientific, Waltham, USA) followed by protein precipitation using ProteoExtract protein precipitation kit (Merck Millipore, Darmstadt, Germany). After isolation, proteins were resuspended in RapiGest SF (Waters, Milford, USA), reduced with dithiothreitol (Sigma-Aldrich, St. Louis, USA), and alkylated with iodoacetamide (Sigma-Aldrich, St. Louis, USA). Tryptic digestion of the protein was performed at a protein:trypsin ratio of 50:1 for 18 h at 37°C. After stopping the digestion by adding 2 µL HCl (Sigma-Aldrich, St. Louis, USA) and removing the degradation products of RapiGest by centrifugation, the peptides were proceeded to LC-MS measurements. Therefore, the samples were diluted with 0.1% formic acid and spiked with 50 fmol/µL Hi3 E. coli (Waters, Milford, USA). Measurements were performed at a nanoACQUITY UPLC system coupled to a Synapt G2-SI mass spectrometer (Waters, Milford, USA). Electrospray ionization was performed in positive mode

with a NanoLockSpray source. As a reference, Glu-Fibrinopeptide (150 fmol/µL) at a flow rate of 0.5 µL/min was injected and a sample flow rate of 0.3 µL/min was set. The mass spectrometer was operated in a resolution mode performing data-independent acquisition (MSE). Data was processed using MassLynx 4.1 and proteins were identified using Progenesis QI 2.0. A reviewed human database downloaded from UniProt was used for protein identification. Noise reduction thresholds were set for low energy, high energy, and peptide intensity at 120, 25, and 750 counts, respectively. A maximum protein mass of 600 kDa, one missed cleavage, fixed carbamidomethyl modification for cysteine, variable oxidation for methionine, and a false discovery rate of 4% for proteins was set for protein and peptide identification. For peptide identification at least three assigned fragments and for protein identification at least two assigned peptides and five assigned fragments are required. The TOP3/HI3 approach was used for the quantification of each protein in fmol.[237]

3 Results and Discussion

3.1 Establishing nanoparticle packaging and extracellular vesicle isolation protocol

Copyright: Unpublished data

Motivation:

NPs have been widely employed as drug nanocarriers to protect and deliver therapeutic cargo *in vivo*. To improve blood circulation time and enhance the specific targeting of nanocarriers, a wide range of surface functionalizations including PEGylation and antibody attachments were developed. However, the mono-functionalization of nanocarriers was shown to be insufficient to meet the complexity and dynamics of the physiological environment in the human body. Organisms like the human body produce specialized nanovesicles, named extracellular vesicles, to transfer a mixture of biomolecules between distant sites. Hereby, the vesicle membrane executes a variety of functions necessary for the successful shuttling of the cargo. Before aiming to package ultra-small and weakly fluorescent silica nanocapsules, we wanted to establish all relevant protocols by utilizing highly fluorescent polystyrene nanoparticles as model nanoparticle. As a basis for the development of a packaging protocol, we first established a protocol to isolate empty EVs from cell culture supernatants of HCT116 cells. This protocol was also used to produce EVs to study their human plasma protein corona as described in **section 3.4**. Building on the isolation protocol for empty extracellular vesicles, we further developed a protocol for packaging of synthetic NPs using PS-NPs as model NP.

Contribution:

I established and performed the cell culture for the packaging of PS-NPs, as well as for the production of empty EVs. I also established and performed the SEC-based EV and NP-loaded EV isolation from cell culture supernatants. I analyzed the resulting SEC fractions with DLS, Pierce assay, and Western blot and measured the fluorescence intensity. [redacted] synthesized the three differently functionalized PS-NPs and measured DLS. I measured the fluorescence intensity of the PS-NPs. I established and performed the single-particle cLSM of the bare and packaged PS-NH_2. I also

measured the cell uptake and exocytosis of PS-NPs with flow cytometry and imaged the cell uptake and exocytosis with cLSM. I prepared and edited the figures. [redacted] advised on the purification of EVs from cell culture supernatants and the confirmation of EV isolation. [redacted] and [redacted] supervised the project.

3.1.1 Abstract

Here, we aimed to establish a model workflow for packaging of synthetic nanoparticles into extracellular vesicles by engaging the cellular EV biogenesis machinery. As model nanoparticles, we used polystyrene nanoparticles as they have a bright fluorescence and a suitable diameter. Later, this workflow can serve as a blueprint for the packaging of other therapeutically relevant nanocarriers. We designed a cell culture protocol that involves nanoparticle uptake and exocytosis for intracellular packaging of synthetic nanocarriers into extracellular vesicles. Further, we developed a size-exclusion chromatography-based protocol for the isolation and concentration of extracellular vesicles from cell culture supernatants. We developed a fluorescence microscopy method for the detection of hybrid particles. This workflow can be transferred to other therapeutically relevant nanocarriers.

3.1.2 Introduction

The application of NPs for drug delivery has been translated to clinical practice for many years. While the first nanocarriers served as physical protection of the therapeutic cargo against degradation in physiological environments [4], later formulations were functionalized with ligands like polyethylene glycol (PEG) to further prolong the blood circulation time.[238] To avoid side effects and increase the delivery efficiency, a variety of targeting ligands such as antibodies [239-241], proteins[183,242], and sugars [243,244] were explored. Despite the effort to modify and functionalize the NP surface, precise *in vivo* targeting is still a major challenge to the clinical translation of drug nanocarriers.

A major challenge for the development of effective targeting strategies is the lack of knowledge of the molecular mechanisms underlying the *in vivo* behavior of NPs. Additionally, the physiological environment is highly complex and changes multiple times on the delivery route.[57] This requires a dynamic adaptation of the nanocarrier functionalization. An approach to transfer these properties to the NP surface without detailed molecular knowledge of the processes is to utilize biomaterials for the surface coating of NPs.[245] Here, cell membranes of different cellular sources like red blood cells (RBCs) [107,108], cancer cells [111], or leucocytes [110] have been used for NP coating and could improve drug delivery. Recently, nano-sized extracellular vesicles (EVs) secreted by cells for information transfer to distant target cells have drawn attention as natural drug delivery vehicles.[131] However, the loading of therapeutic molecules into

EVs is currently a major obstacle to their application for drug delivery. Therapeutic molecules are either incubated with the producing cell for random incorporation in EVs [205], or pre-isolated EVs are mechanically disrupted for the loading of therapeutic molecules.[195,197] In the case of cytotoxic molecules, the incubation of the therapeutic molecules with the producing cell can harm the cells. The mechanical disruption of the EV membrane can harm the bioactivity of the EVs as it can damage the membrane and protein integrity. To use the full potential of the EV membrane as a biomaterial for the surface coating of synthetic nanocarriers novel drug-loading strategies are required.

To establish a general workflow and gain first insights into the packaging of nanocarriers by human colorectal tumor (HCT) 116 cells, we used PS-NPs with a diameter between 135 nm and 145 nm as model NP. PS-NPs are an ideal model particle as their bulk material is non-toxic and particles are not biodegradable.[246] This ensures that the particles remain intact during intracellular trafficking and that the fluorescent molecules cannot leak out. Hence, its fluorescence can be detected intracellularly, as well as after secretion. EVs are a heterogeneous mixture of vesicle populations with different diameters. Depending on the cell source and purification method, the isolated vesicles can range between 30 nm and 1000 nm in diameter.[117] Therefore, the PS-NPs would not fit into small EVs but can fit into medium to large-size EVs.

Here, we aimed to develop a workflow for the packaging of PS-NPs into EVs by engaging the cellular EV biogenesis machinery using HCT116 cells. PS-NPs were used as model NPs that can be detected easily by their fluorescence signal. The workflow established here is supposed to serve as a blueprint strategy to develop packaging protocols for other, therapeutically more relevant nanocarriers in the future. The insights generated in this section were directly applied to the development of a packaging protocol for the therapeutically relevant SiNCs described in **section 3.2**.

3.1.3 Results and Discussion

As a first step, before attempting to package NPs in EVs, we established the isolation of EVs from cell culture supernatant by size exclusion chromatography (SEC). This cell culture and SEC isolation protocol was supposed to serve as a basis for the development of a protocol including the packaging of NPs. The protocol depicted in **Figure 3.1.1 A** was adapted from Brahmer et al. and Böing et al., who isolated EVs from blood plasma.[152,247] Therefore, we needed to adapt it for the EV isolation from the cell culture

medium. To ensure a high EV particle yield, we used a 40 mL conditioned medium (CM) derived from $2x10^7$ HCT116 cells. To use a 10 mL Sepharose CL-2B column, we had to concentrate the starting material to 2 mL by ultrafiltration. As ultrafiltration in the presence of fetal bovine serum (FBS) can result in massive particle aggregation, we collected the EVs in an FBS-free cell culture medium. This also avoids contamination of the EV sample with FBS-derived EVs. To identify the EV-containing SEC fractions, we analyzed the fractions for their particle count rate and protein concentration (**Figure 3.1.1 B**). The highest particle count rate was detected for fractions 5-7 and the protein concentration increased rapidly in fractions 8-10. This is in good accordance with the results of Brahmer et al., who report the highest particle count in fractions 4-6 and showed a rapid protein increase starting from fraction 8.[152] According to the elution mechanism of SEC, the particle size decreases with increasing fraction number. Therefore, the protein concentration increases at later fractions which results from the elution of protein aggregates and free proteins whereas the protein contamination in fractions 5-7 is low. Based on this, we pooled fractions 5-7 and analyzed the particle size distribution with differential light scattering (DLS) (**Figure 3.1.1 C**). The mean diameter was 241.7 nm with an experimental error of 10%. Given that DLS is a bulk analysis method that neglects smaller particles and overweighs larger particles, this diameter fits well with the typical diameter of a mixture of exosomes and larger microvesicles.[117] The resulting sample was further characterized to confirm the isolation of EVs with this protocol which is depicted in **Figure 3.4.3**. In brief, cryo-TEM images revealed the presence of vesicles with a mean diameter of 91±109 nm (**Figure 3.4.3 B** and **Table 3.4.1**). The NTA measurement confirmed the smaller diameter given by cryo-TEM (**Figure 3.4.2** and **Table 3.4.1**). Further, the main EV markers including CD9, CD64, and CD81 were identified by mass spectrometry as depicted in **Figure 3.4.3 C**. Taken together, these results demonstrate that the adapted protocol was capable of isolating EVs and can be used as a basis for developing a packaging protocol.

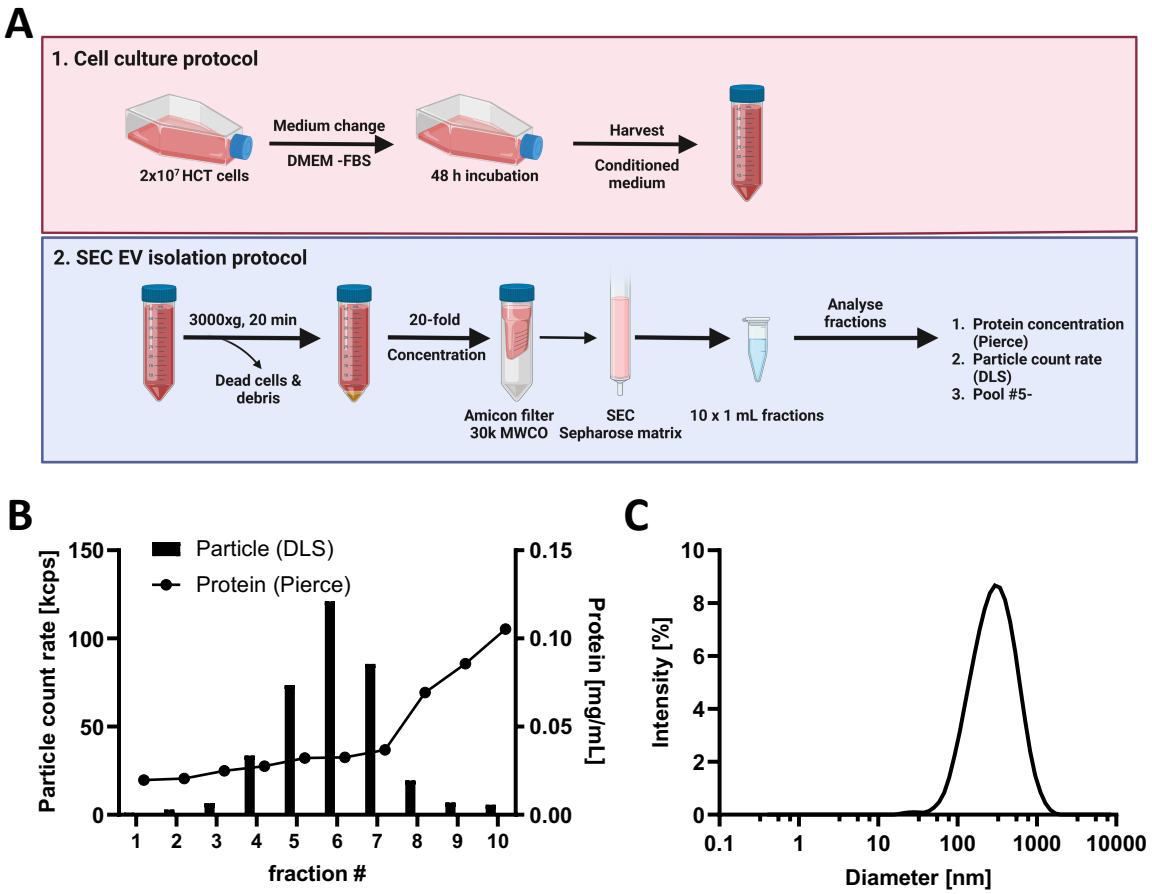

Figure 3.1.1: EV isolation from HCT116 cell culture supernatant with SEC. A. Schematic depiction of cell culture and SEC isolation protocol. HCT116 cells were cultured in FBS-free Dulbecco's Modified Eagle's Medium (DMEM) for 48 h before harvesting the conditioned medium. The conditioned medium was pre-cleared and concentrated before SEC. This graphic was created with BioRender.com. B. 10 SEC fractions were collected and analyzed for their protein concentration with Pierce assay and particle count rate with DLS to determine EV-containing fractions. C. Fractions 5, 6, and 7 were pooled, concentrated, and subjected to DLS to obtain the particle diameter distribution of the sample. The DLS measurements were done at 20°C in PBS. The EV production protocol was performed by me, as well as the DLS and Pierce Assay measurement.

For developing an NP packaging protocol utilizing the cellular EV biogenesis machinery, we used fluorescent polystyrene NPs (PS-NP) as a model particle. PS-NPs are used as model NPs because they are biocompatible, stable in biological media, and can be functionalized easily.[232,246] For the establishment of a packaging protocol, we used three differently functionalized PS-NPs. We synthesized plain PS-NPs (PS-plain), carboxy-functionalized PS-NP (PS-COOH) and amino-functionalized PS-NPs (PS-NH_2). To be able to detect the PS-NP during the packaging process and after secretion, high fluorescence intensity was crucial. The three PS-NPs had similar fluorescence intensities between 600 and 850 AU at a concentration of 10 µg/mL in DMEM (**Figure 3.1.2**). The NPs' diameters ranged from ~135-140 nm (**Table 3.1.1**), which would allow fitting into slightly larger EV particles.

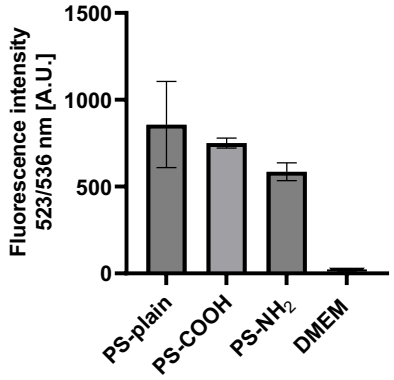

Figure 3.1.2: Comparison of PS-NP fluorescence. The NPs were measured at a concentration of 10 µg/mL in DMEM without FBS. As a negative control, DMEM without FBS was measured. The fluorescence intensity of PS-NPs was measured at 523/526 nm. The mean and standard deviation of n = 3 are shown. The measurement was performed by me.

Table 3.1.1: Diameter and fluorescence of PS-NPs. The hydrodynamic diameter of the PS-NPs was measured by DLS at 90°C. The experimental error (10%) is given. The fluorescence intensity of the NP dispersions was measured at a concentration of 10 µg/mL in DMEM without FBS. As a negative control, DMEM without FBS was measured. The Fluorescence intensity of PS-NPs was measured at 523/526 nm. The mean and standard deviation of n = 3 are shown. DLS and fluorescence measurements were done by me.

PS-NP	D_h **[nm] DLS**	**Fluorescence [AU]**
PS-plain	135±13.5	857.33±202.53
PS-COOH	143±14.3	750.33±23.49
PS-NH2	139±13.9	585.67±41.52
DMEM	-	12.00±0.0

As a first naïve approach to include packaging of PS-NPs into the cell culture protocol developed beforehand, we decided to incubate HCT116 cells with a high dose (250 µg/mL) of PS-NPs for 18 h to ensure a high NP loading of the cells. After removal of the NP-containing medium and thorough washing of the cells, we continued the incubation in an NP-free medium for another 24 h to collect secreted EVs. The NP incubation, as well as the EV collection, was performed in an FBS-free medium, to increase particle loading and to avoid aggregation during ultracentrifugation, respectively. After collection of the CM, ultrafiltration and SEC isolation were performed as described for the EV isolation protocol. The adapted protocol is depicted in **Figure**

3.1.3 A. The collected fractions were analyzed for PS-NP fluorescence to identify NP-containing fractions (**Figure 3.1.3 B**). The highest fluorescence intensity for all PS-NPs was found in fractions 4, 5, and 6. However, considering the similar diameter of the PS-NPs compared to EVs they would be eluted in the same fraction. Therefore, further investigation of the sample was necessary. As all PS-NPs irrespective of the surface functionalization were present in the relevant SEC fractions to a similar extent, we decided to focus on PS-NH_2 for further investigation. To confirm the presence of EVs in the NP-containing fractions, we performed a chromogenic western blot for the detection of the EV marker CD63 (**Figure 3.1.3 C**). At fractions 4, 5, and 6 we detected a band corresponding to CD63 at ~49 kDa. As CD63 can have different glycosylation states its band ranges from 40-60 kDa.[248] As the fractions 4, 5, and 6 exhibited the highest PS-NP fluorescence intensity and contained CD63, we decided to pool these fractions to generate the final sample.

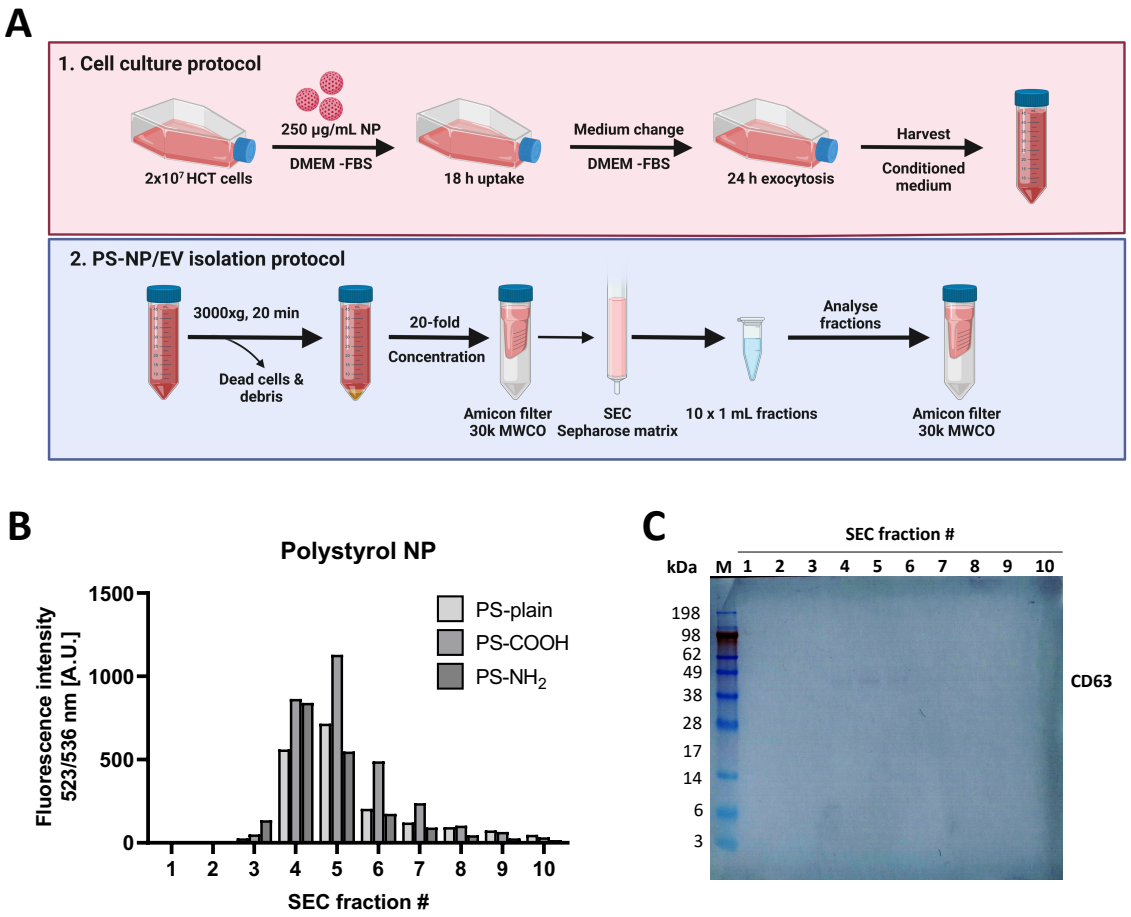

Figure 3.1.3: EV isolation from HCT116 cell culture supernatant with SEC. A. Schematic depiction of PS-NP packaging protocol. This graphic was created with BioRender.com. B. 10 SEC fractions from PS-NP packaging were collected and analyzed for their fluorescence intensity at 523/536 nm. C. Western blot of SEC fractions resulting from the CM of HCT116 cells incubated with PS-NH_2. The western blot was treated with a αCD63 antibody and developed with a chromogenic substrate. The packaging protocol, the fluorescence measurement, and the Western blot were performed by me.

To confirm the packaging of PS-NH_2 into HCT116-derived EVs by the established packaging protocol, we wanted to investigate the pooled and concentrated SEC fractions on a single-particle level. Therefore, we immobilized either bare PS-NH_2 or packaged PS-NH_2 on a microscopy slide by PFA fixation. Like conventional immunocytochemistry staining of cell organelles in PFA-fixed cell samples, we aimed to stain the EV membrane with fluorescent antibodies against the common EV markers CD9 and CD63. The NPs were fluorescently labeled and could also be detected by cLSM. Both EV marker antibodies were labeled with a red fluorophore and were excited at 633 nm. To ensure minimal spectral overlap, the PS-NPs were labeled with a green fluorophore, which can be excited at 514 nm. In the micrographs, particles were represented as puncta, and double-positive puncta represent NPs closely associated with an EV membrane. As can be seen in **Figure 3.1.4**, bare immobilized PS-NH_2 did not show any co-

localization with the EV marker antibodies. Further, in this sample, there was no antibody signal at all, which indicates there is no unspecific binding of the antibodies. In contrast, the packaged PS-NH_2 sample exhibited some double-positive puncta, which were highlighted by the squares. Furthermore, this sample had puncta only positive for the PS-NH_2 signal or the antibody signal. This indicated the presence of bare PS-NH_2 and empty EVs which were expected to be present in the sample as a size-based isolation method was used.

The investigation of the sample by cLSM on a single-particle level gives a qualitative impression of the sample and can be used to confirm the presence of hybrid particles. A similar approach to proving the presence of EV-packaged NPs was reported by Yong et al.[84] However, the resolution of cLSM is not high enough to discriminate larger aggregates from single EVs filled with one or more NPs. Furthermore, this method crucially depends on the fluorescence intensity of the NP to allow detection. Another downside is, that the events cannot be easily quantified in a statistically significant manner as usually only some hundred events are imaged. With colocalization rates in the single-digit realm, cLSM does not give a reliable statistic. This makes it difficult to compare packaging rates between different particles, cell types, and incubation times. For the analysis of NPs that are not as bright as PS-NH_2 and to quantify packaging rates more reliably, eventually, a different method needs to be found. A possibility would be fluorescence cross-correlative spectroscopy, which is highly sensitive in terms of detection of fluorescence and can be used to analyze the binding of binding partners in the nanometer range. Furthermore, packaging rates can be calculated from this analysis.

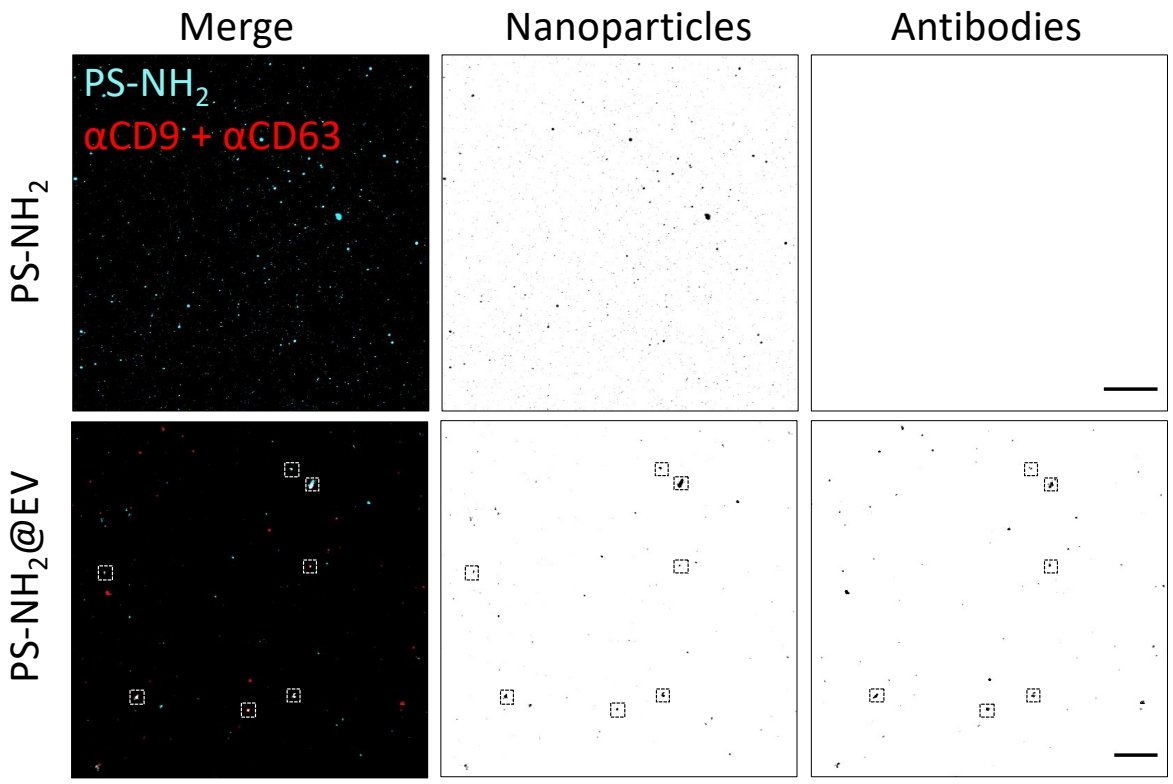

Figure 3.1.4: Single-particle cLSM of PS-NH_2 and PS-NH_2/EV hybrids. The NPs were immobilized on microscopy slides before double-labeling with αCD63 and αCD9 antibodies. PS-NH_2 contained BODIPY (523 nm/536 nm) and the antibodies were labeled with a red fluorescent dye excitable at 633 nm. Double-positive puncta were highlighted with a square. The scale bars represent 15 µm. The production of the PS-NH_2/EV hybrid particles, as well as the cLSM imaging, was done by me.

Nevertheless, this experiment confirms the packaging of PS-NH_2 into EVs by the developed cell culture and SEC isolation protocol in a qualitative manner. To exclude bare PS-NH_2 and empty EVs or increase the yield of packaged NPs, the protocol could be further optimized. Unwanted species could for example be depleted by using an additional purification method such as density gradient or immunoprecipitation. The yield of packaged NPs could eventually be increased by optimizing the cell culture protocol.

By optimizing the cell culture protocol we wanted to improve the uptake and exocytosis of PS-NH_2 in HCT116 cells. Therefore, we incubated HCT116 cells with 25 µg/mL or 2.5 µg/mL PS-NH_2 for either 2 h or 18 h before changing the medium and allowing exocytosis for another 4 h or 24 h. Having a short and a long uptake and a short and long exocytosis phase, we wanted to investigate, if this influences the exocytosis fraction and could be used to optimize the packaging protocol. However, analyzing the intracellular PS-NH_2 signal after uptake and exocytosis with flow cytometry did not reveal exocytosis irrespective of short or long incubation times (**Figure 3.1.5**). Instead,

the intracellular PS-NH_2 signal increased further after removing the particles from the cell culture medium. It is possible that PS-NH_2 remains in the cell culture well despite thorough washing by adhering to the walls or the cell surface and can later be taken up, which results in a further increase of the intracellular signal. Hence, the flow cytometry experiment did not give further insights into the optimization of the incubation scheme to enhance NP exocytosis.

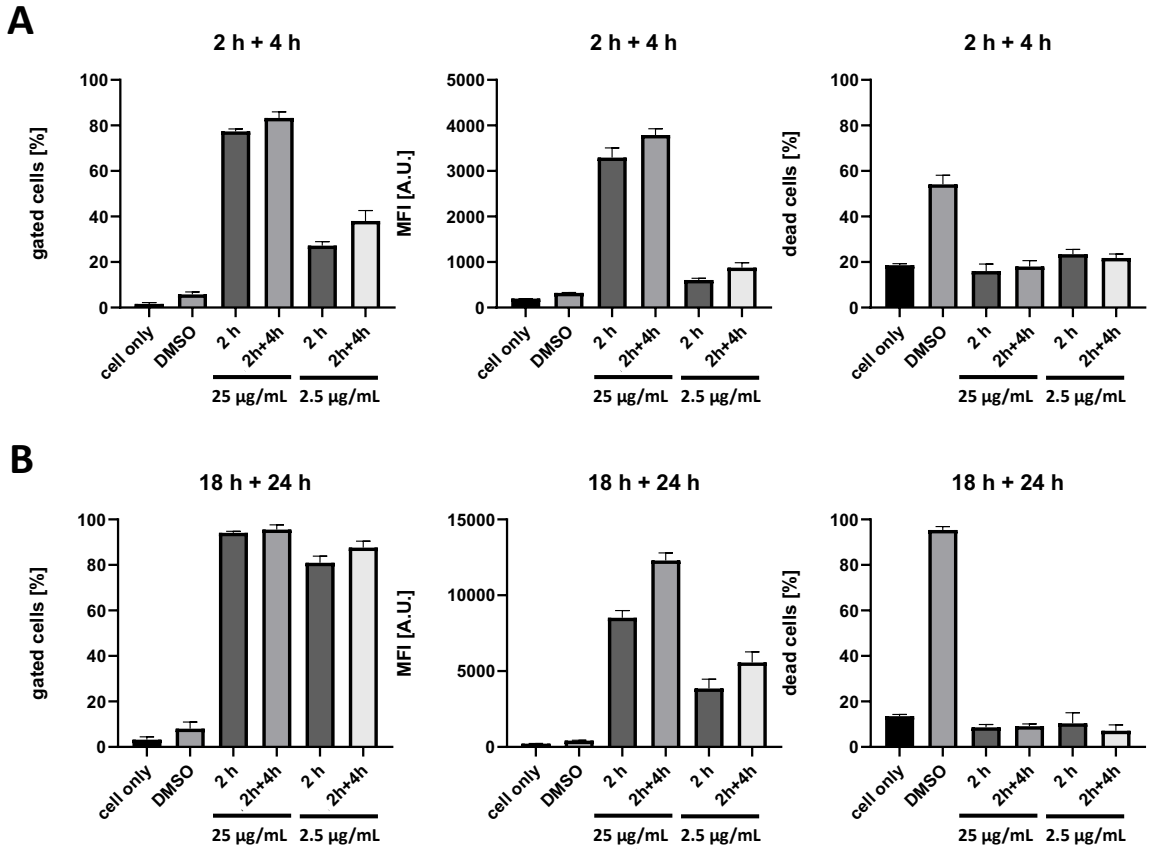

Figure 3.1.5: Flow cytometry analysis of PS-NH_2 exocytosis from HCT116 cells after an uptake period of 18 h. The cells were incubated with 2.5-250 µg/mL PS-NP-NH_2 in DMEM –FBS. Subsequently, the cells were washed and further incubated in a particle-free medium for 24 h. A. and B. depict the percentage of gated cells and the median fluorescence intensity. C. depicts the ATP content of untreated cells, cells incubated with PS-NH_2, and cells incubated with 20% DMSO (positive control). Means and standard deviations are shown (n = 3). The flow cytometry experiments were done by me.

In addition, we used cLSM to qualitatively assess PS-NH_2 endocytosis and exocytosis in HCT116 cells. In this experiment, we focused on the incubation scheme as applied in the packaging experiment. After incubation with PS-NH_2 for 18 h, the NP signal was detected intracellularly. 24 h after removing the NPs from the cell culture medium, there were no NPs found inside the cells anymore. Given that PS-NPs are not biodegradable [246], this can most likely be explained by the exocytosis of the PS-NH_2. Interestingly, we

could capture exocytosis by the cLSM experiment but not by flow cytometry. As stated above, it is possible that PS-NH_2 adheres to the cells or the walls of the cell culture well and can later be taken up despite thorough washing between medium changes. Eventually, this effect is less pronounced in the cell culture wells used for cLSM due to their different ratio between volume and surface area resulting in the visibility of the exocytosis after incubating without additional NPs in the supernatant.

Summing up, we observed exocytosis of PS-NH_2 after 24 h of incubation in particle-free medium. This supports the cell culture scheme that we applied in the packaging protocol. However, the incubation scheme can be optimized further.

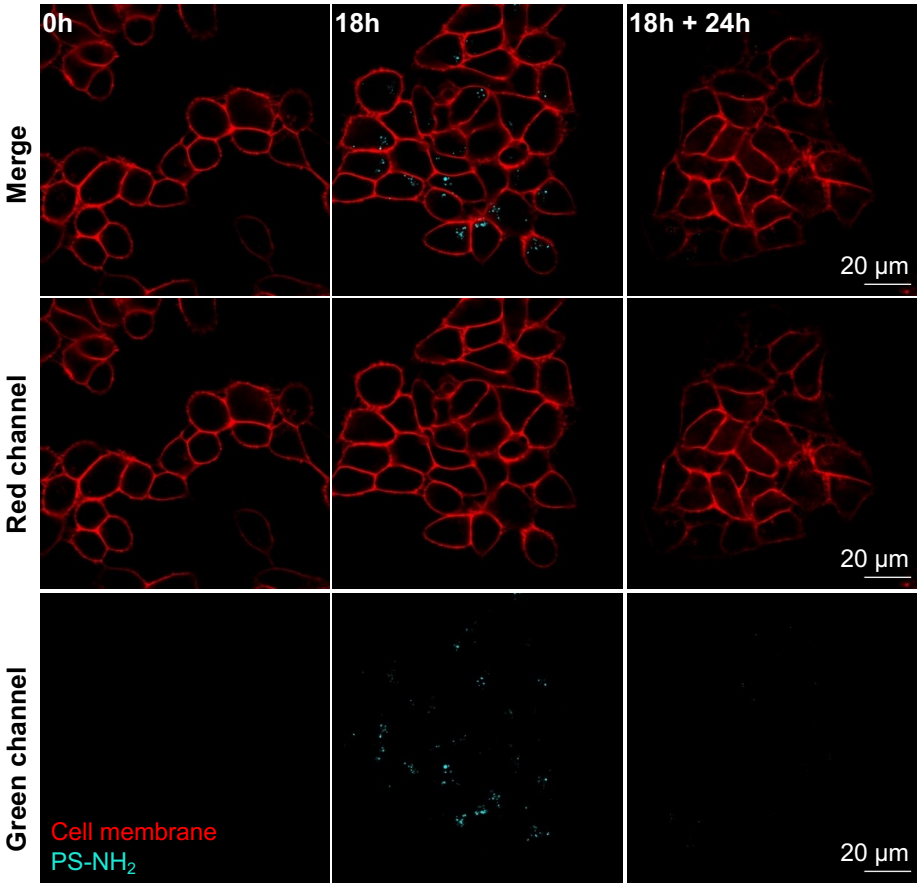

Figure 3.1.6: Imaging of PS-NH_2 exocytosis from HCT116 cells after an uptake period of 18 h. The cells were incubated with 2.5 µg/mL PS-NP-amino in DMEM –FBS. Subsequently, the cells were washed and further incubated in a particle-free medium for 24 h. The cell membrane was stained with a cell mask red and is depicted in red. PS-NH_2 are depicted in cyan. The cLSM images were acquired by me.

3.1.4 Conclusion

Here, we presented the successful establishment of a protocol for isolating EVs from the HCT116 cell culture supernatant. The isolation was based on SEC, which is a common method for the isolation of EVs from different sources. SEC isolation causes less damage to the EV membrane compared to other common methods like ultracentrifugation.[152,247] It is important to preserve the membrane integrity and functionality for using it as a functional surface coating for NPs. The EV purification protocol developed here was also used for EV production to investigate the EV protein corona as described in **section 3.4**.

Next, we adapted the EV isolation protocol to incorporate NPs into EVs during their biogenesis. Therefore, we used PS-NPs as model NPs to establish the protocol. As a starting point, we decided to use a long NP incubation time to ensure high loading of the cells. After removing the particles, we collected the EVs for 24 h to ensure the accumulation of a high number of EVs. Yong et al. reported the packaging of silica NPs by a similar cell culture procedure but used shorter incubation and exocytosis times.[84] Here, fine-tuning the incubation and exocytosis times are parameters that can be further optimized to increase the yield of NP-loaded EVs. After detecting the fluorescence signal of the PS-NPs in some of the fractions resulting from SEC separation, we confirmed the packaging of PS-NPs with cLSM on a single-particle level. However, this method requires the NPs to be highly fluorescent and we might need to find more sensitive methods with a higher resolution.

The insights that we gathered while establishing a packaging protocol for PS-NPs directly inform the development of a protocol for other more relevant nanocarrier types, such as SiNC, as described in **section 3.2**.

3.2 Packaging of SiNC in EVs

Copyright: We plan to submit this in a revised version.

Motivation:

Extracellular vesicles have been envisioned as drug delivery vehicles. However, the loading of extracellular vesicles with therapeutic molecules beyond their natural constituents is still a major challenge. Instead of directly loading the extracellular vesicles with therapeutic molecules outside of cells, we aimed to load them with synthetic nanoparticles intracellularly that bear the potential to carry therapeutic molecules as cargo. To load the synthetic nanoparticles, we wanted to pursue a novel approach that involves the cellular biogenesis machinery of extracellular vesicles. **Section 3.1** describes the development of cell culture and size exclusion chromatography-based extracellular vesicle isolation protocol as a basis for the detection of the packaging of nanoparticles. In the second step, polystyrene nanoparticles were used as highly fluorescent model nanoparticles to develop a packaging protocol. In this section, the developed protocol was adapted for ultra-small silica nanocapsules, which are capable of encapsulating therapeutic molecules and are therefore, relevant for drug delivery.

Contribution:

SiNCs were produced by [redacted]. I performed the flow cytometry and cLSM cell uptake experiments, as well as the flow cytometry exocytosis kinetic. I developed the packaging protocol including the cell culture scheme and isolation protocol. Based on that, I prepared the SiNC/EV hybrids that were analyzed with FCCS by [redacted], who also calculated hydrodynamic diameters and packaging rates from this. I prepared the cell uptake of SiNC for cryo-TEM studies. [redacted] prepared the sample for cryo-TEM and [redacted] and [redacted] obtained EELS cryo-TEM images of the species. Further, [redacted] obtained TEM images of bare SiNC and [redacted] measured multi-angle DLS of the particles.

3.2.1 Abstract

In vivo, targeting of synthetic drug nanocarriers is highly relevant for successful drug delivery and is often addressed by biochemical functionalization of the nanocarrier surface. However, the *in vivo* environment is highly complex, dynamic, and not yet fully understood. To circumvent the necessity to understand the molecular details of all processes involved, natural membranes, such as cell membranes, are explored as multifunctional surface coating material. Recently, extracellular vesicles have attracted a lot of interest as natural drug delivery platform as these vesicles serve as a systemic transport system for biomolecules under physiological conditions. Furthermore, it was demonstrated that EVs transferred RNA several orders of magnitude more efficiently compared to liposomes in cell culture which highlights their advanced cell penetrating ability. In this study, we aimed to transfer these key delivery functions, integrated into the membrane of extracellular vesicles, to synthetic nanocarriers. Therefore, we loaded fluorescently labeled silica nanocapsules as model drug carriers into HCT116 cell-derived extracellular vesicles by exploiting the cellular vesicle biogenesis pathway. Here, we demonstrated the development of a protocol for packaging two differently sized silica nanoparticles with a diameter of 5 nm and 25 nm into extracellular vesicles by hijacking the cellular extracellular vesicle machinery. After the uptake and exocytosis of silica nanocapsules in cell culture, we isolated and concentrated the secreted extracellular vesicles by a combination of size exclusion chromatography and ultrafiltration. To confirm the generation of silica nanocapsules/extracellular vesicle hybrids we used fluorescence cross-correlation spectroscopy. This particle diffusion-based method confirmed the presence of hybrids and allowed for the quantification of packaging rates. This was supported by the observation of silica nanocapsules inside multivesicular bodies in HCT116 cells using electron energy loss spectroscopy and electron microscopy. The association of silica nanocapsules with multivesicular bodies indicated exocytosis via the cellular exosome pathway.

3.2.2 Introduction

Precise *in vivo* targeting is a major challenge to the clinical translation of drug nanocarriers. This is due to the high level of complexity of the *in vivo* environment and its dynamic change as the nanocarrier is transported through different tissues and organs.[57]

Additionally, the molecular details of the underlying mechanisms are still not fully understood, which impedes the development of *in vivo* targeting strategies further. Using naturally derived membranes as a multi-functional surface coating for nanocarriers [107,110,111] is an alternative strategy to modifying the physicochemical properties [249] of the nanocarrier or biochemical attachment of targeting ligands.[93,95,96]

Recently, the membrane of nano-sized biologically derived vesicles came into focus as a biomaterial for the coating of nanocarriers.[84,112] These vesicles, termed extracellular vesicles (EVs), are secreted by cells for information transfer to distant target cells.[117] Hence, we speculated that the EV membrane is equipped with a variety of functionalities to navigate the complex and dynamic *in vivo* environment.

However, the transfer of the EV membrane to the nanocarrier surface is delicate as the EV membrane integrity can be disrupted easily. Harsh chemical or physical methods to disrupt the EV membrane for loading after their isolation are likely to damage the membrane itself or embedded EV proteins. Therefore, loading of nanocarriers during the biogenesis process of EVs inside the producing cell would be a gentle alternative. Uptake of the NPs by the cell most likely results in entering the endosomal system.[80] This is a dynamic network of intracellular vesicles constantly fusing and separating while shuttling the extracellular cargo to its intended destination.[78,79] After escaping the endosomal system, the particles are localized in the cytosol. From here, the particles can associate with the plasma membrane and are eventually exocytosed in plasma membrane-derived vesicles, termed microvesicles. Alternatively, the particles can associate with large intracellular vesicles that form exosomes by inward budding of their membrane and subsequent fusion with the plasma membrane. This would facilitate the packaging of the NPs in exosomes.[117] Due to a lack of experimental separation methods, samples usually contain a mixture of microvesicles and exosomes, which are commonly referred to as EVs.

In this study, we wanted to utilize the human colorectal cancer cell line HCT116 for the packaging of fluorescent silica nanocapsules (SiNCs) by hijacking the cellular uptake and EV biogenesis machinery. SiNCs are biocompatible and suitable for encapsulation of hydrophobic therapeutic cargos. To allow packaging even in small EV populations with diameters between 30 nm and 100 nm, we created ultra-small SiNC with a diam-

eter of 5 nm and 25 nm by controlled Ostwald ripening and PEGylated them subsequently (termed 5-SiNC PEG and 25-SiNC PEG). To confirm the generation of EV/SiNC hybrid particles, we employed dual-fluorescence FCCS to detect correlations between EV and SiNC fluorescent signals with a nanometer resolution. This even allowed for the quantification of packaging rates. Finally, we could also localize 25-SiNC PEG inside multivesicular bodies in HCT116 cells by electron energy loss spectroscopy and electron microscopy, which indicates exocytosis via the cellular exosome machinery.

3.2.3 Results and Discussion

Fluorescent silica nanocapsules (SiNC) with two different sizes were prepared by a sol-gel reaction at the oil-water interface of a miniemulsion. To further decrease the capsule size for the preparation of ultrasmall SiNC, controlled Oswald ripening was performed simultaneously. For stable fluorescent labeling of the SiNC, Cy5-ester was polymerized into the silica matrix during the sol-gel process. As evident from the statistical analysis of the transmission electron microscopy (TEM) images of the SiNC, this resulted in particles with shell diameters of 5 nm and 25 nm (**Figure 3.2.1**). Additionally, the hydrodynamic radii of the SiNCs were determined by multi-angle differential light scattering (DLS) and fluorescence cross-correlation spectroscopy (FCCS) (**Table 3.2.1**). As there is a hydration shell forming around the PEG layer of the SiNC, the measurements resulted in larger diameters. For the 5-SiNC PEG, 32±3.2 nm and 41±4.1 nm for DLS and FCCS were measured, respectively. Taking the experimental error into account, these measurements were in good accordance. For the 25-SiNC PEG, 41±4.1 nm and 62±6.2 nm for DLS and FCCS were measured, respectively. These measurements were also in good accordance considering the very small size of the particles.

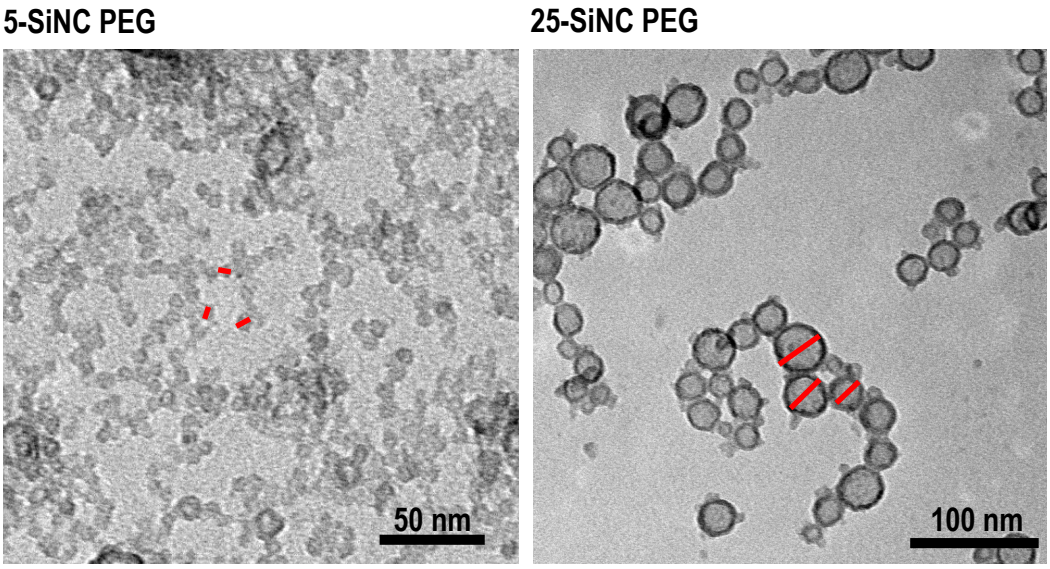

Figure 3.2.1: TEM images of SiNCs. The red lines showcase the measured diameter. The images were acquired by [redacted] and the statistical analysis was performed by me.

Table 3.2.1: Physical characterization of SiNCs. The hydrodynamic diameter was determined by multi-angle DLS (25°C) and FCCS. 5-SiNC PEG was measured with multi-angle DLS. 25-SiNC PEG was measured at an angle of 90°C. The experimental error (10%) is given for DLS and FCCS values. The diameter of the silica shell was determined by analyzing TEM images. Means and standard deviations are shown. DLS was measured by [redacted], FCCS was measured by [redacted], and the TEM images were analyzed by me.

SiNC	D_h [nm] DLS	D_h [nm] FCCS	D [nm] TEM
5-SiNC PEG	32±3.2	41±4.1	5.95±1.00
25-SiNC PEG	84±8.4	62±6.2	25.53±7.05

Next, we assessed the cell uptake behavior of SiNCs in HCT116 cells to identify ideal parameters for establishing the packaging protocol. First, we measured SiNC uptake at different concentrations and time points by flow cytometry (**Figure 3.2.2**). While the uptake of 5-SiNC PEG and 25-SiNC PEG was similar after 2 h, the 5-SiNC PEG uptake was higher after 6 h and 24 h. The uptake of both nanocarriers was concentration dependent (**Figure 3.2.2 A**). The uptake increase was linear at lower concentrations and stagnated towards a concentration of 200 µg/mL. However, nearly 100% of cells were NP-positive even at the lowest concentration of 10 µg/mL (**Figure 3.2.3 A**). The median fluorescence intensity (MFI) increased linearly with increasing uptake time (**Figure 3.2.2 A**). After 2 h of uptake, nearly 100% of cells had taken up NPs (**Figure 3.2.3 B**). Taken together, the SiNC were taken up fast and with a high loading per cell. As

nearly 100% of cells were positive for NPs after an incubation time of 2 h, this incubation time seems to be sufficient for the loading of the majority of cells with SiNC. To ensure a high loading with NPs per cell, we decided to use the highest concentration (200 µg/mL) of SiNC for incubation in subsequent experiments.

For the detection of NP exocytosis, the particles must be fully internalized before starting the exocytosis phase. As NPs that are not fully internalized but only attach to the cell surface contribute to the detection of NP-positive cells by flow cytometry, we aimed to proof the internalization of SiNC into HCT116 cells. Therefore, HCT116 cells were incubated with 200 µg/mL SiNC for 2 h before obtaining cLSM images to detect the localization of the particles (**Figure 3.2.2 B**). The cLSM images of both SiNCs demonstrate full internalization of nanocapsules into the cells after uptake for 2 h. The SiNC signal was found in the cytosol close to the nuclear border.

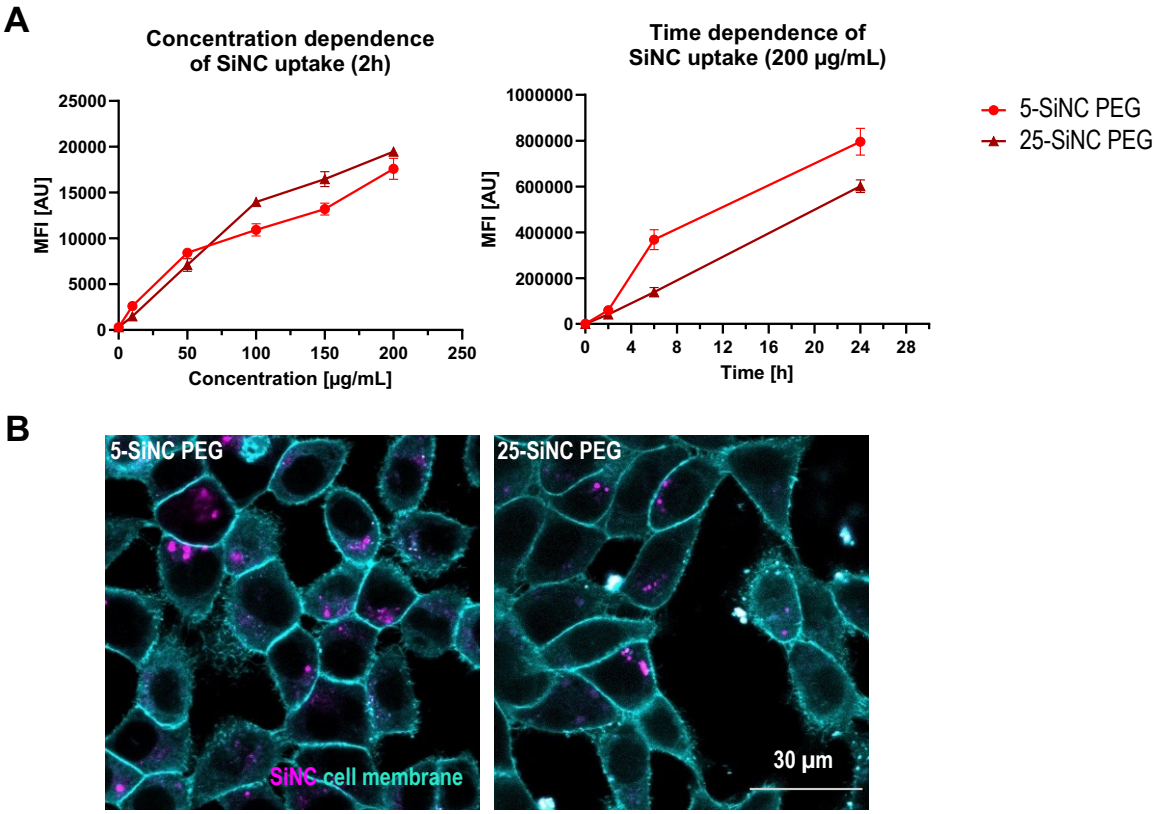

Figure 3.2.2: Uptake of SiNC into HCT116 cells. A. Flow cytometry analysis of particle uptake into HCT116 cells at different concentrations and time points. The 0 µg/mL and 0 h points depict untreated cells. Means and standard deviations of median fluorescence intensities are shown (n = 3). B. Confocal laser scanning microscopy images of HCT116 cells treated SiNC for 2 h at a concentration of 200 µg/mL. The cell membrane is pseudo-colored in cyan blue and the SiNCs are pseudo-colored in magenta. Scale bar 30 µm. The flow cytometry experiment, as well as the cLSM imaging, was done by me.

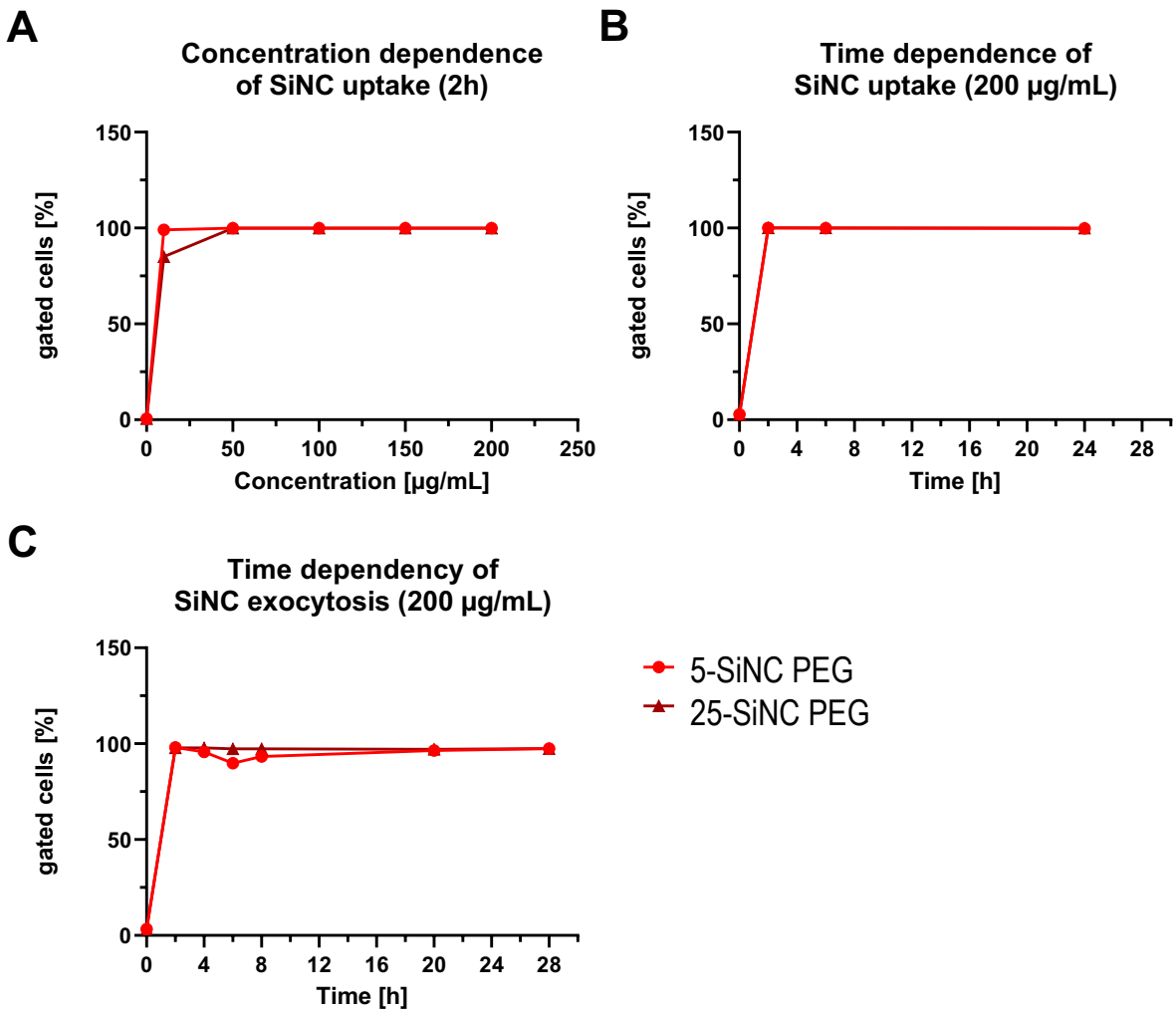

Figure 3.2.3: Flow cytometry analysis of uptake and exocytosis of SiNC in HCT. A. and B. Particle uptake into HCT116 cells at different concentrations and time points. The 0 µg/mL and 0 h points depict untreated cells. Means and standard deviations of gated cells are shown (n = 3). C. Exocytosis of SiNCs from HCT116 cells after an uptake period of 2 h. The means and standard deviation of the percentage of gated cells (n = 3) are shown. The flow cytometry experiment was done by me.

Assessing the cell uptake behavior of SiNCs demonstrated that the HCT116 cells were highly loaded with particles after incubation with 200 µg/mL SiNC for 2 h and that the particles were located in the cytosol. As a next step, we aimed to assess the exocytosis kinetic of SiNCs to identify an ideal time point for the harvesting of exocytosed NPs. We used a particle incubation time of 2 h. This short incubation time has the advantage of not monitoring an overlap of multiple processes, for example, simultaneous exocytosis of particles and re-uptake of exocytosed particles. Further, the intracellular degradation of SiNCs during such a short period is unlikely. To measure the exocytosis of SiNC from HCT116 cells, we incubated the cells with 200 µg/mL of SiNC for 2 h. Subsequently, the particle-containing medium was discarded and the cells were washed three times before replacing it with fresh SiNC-free medium. The intracellular SiNC

content at different time points after medium replacement was measured by flow cytometry (**Figure 3.2.4 A**). The MFI values were normalized to the MFI value obtained after incubation for 2 h. The exocytosis kinetics of both SiNC were similar. 2 h after the medium change, the intracellular SiNC signal was reduced to approximately 50% of the initial value. 4 h and 6 h after the uptake, the intracellular SiNC signal was at a similar low level, before the signal increased again 18 h after the medium change. 26 h post medium change, the intracellular SiNC signal increased to nearly 100% of the starting MFI directly after the uptake. This can be attributed to a re-uptake of exocytosed SiNCs. The exocytosis kinetic observed here is in good accordance with other studies. Slowing et al. demonstrated a rapid uptake of mesoporous silica NPs (MSNs) into the cells within 3 h and the exocytosis as soon as 40 min later.[250]

Yanes et al. reported the uptake of MSNs within 2 h and the almost complete exocytosis of MSNs 6 h after the uptake. This result was even confirmed by direct measurement of the element silicon with inductively coupled plasma atomic emission spectroscopy (ICP-OES).[86] This cross-validates that the observed decrease in intracellular SiNC signal is due to exocytosis and not related to quenching of the fluorescent signal during trafficking of the SiNC through different intracellular compartments. Focusing on a short time frame of 4 h also decreases the contribution of cell division to the decrease of intracellular SiNC signal.

Based on the exocytosis kinetics measured for SiNCs in HCT116 cells, we developed a cell culture protocol for the isolation of the exocytosed SiNC from cell culture supernatants (**Figure 3.2.4**). $2x10^7$ HCT116 cells were incubated with 200 µg/mL SiNCs for 2 h. Subsequently, the NP-containing cell culture medium was removed. The cells were washed three times, before adding fresh NP-free cell culture medium to remove adhering SiNCs. After incubation for 4 h, the conditioned medium was collected and subjected to a size exclusion chromatography (SEC) protocol typically used for EV isolation from cell culture medium.[247] To remove cell debris and dead cells, the conditioned medium was centrifuged at 3,000 x g. Before SEC, the medium was concentrated 20-fold by 30 kDa MWCO ultrafiltration. The EV-containing fractions collected from SEC were further concentrated by ultrafiltration. By using the fractions that typically contain EVs, free 5-SiNC PEG should be separated from EV-associated 5-SiNC PEG. However, the separation of free and packaged 25-SiNC PEG is more inaccurate due to the overlap in diameter. Empty and SiNC-filled EVs cannot be separated by this

isolation method as the size range is identical. However, this protocol isolates and concentrates particles in the size range of EVs including the complete population of hybrid EV/SiNCs that are of main interest to this project.

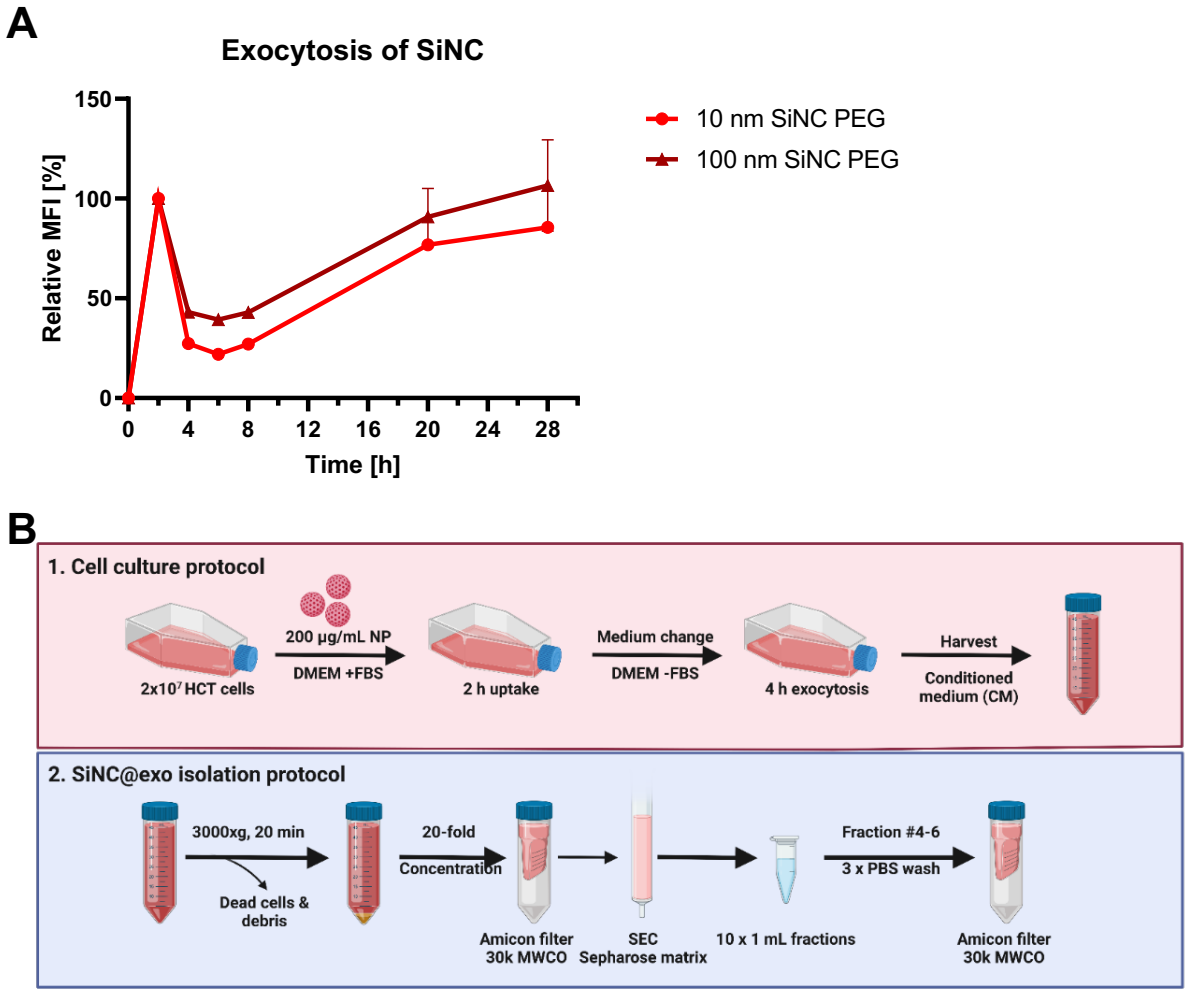

Figure 3.2.4: Packaging of SiNCs into HCT116 EVs. A. Flow cytometric analysis of SiNC exocytosis from HCT116 cells after an uptake period of 2 h. The MFI relative to the MFI after 2 h of uptake is shown. Means and standard deviation of n = 3 are shown. B. Packaging protocol. The cell culture protocol was adapted from the exocytosis kinetic depicted in A. After a 2 h uptake and a 4 h exocytosis period, the conditioned medium was collected and EVs were isolated by size exclusion chromatography. This graphic was created with BioRender.com. Flow cytometry was done by me. The packaging protocol was developed and performed by me.

Before further analyzing the resulting sample, we aimed to capture the intracellular localization of the SiNCs during the packaging process. Therefore, we obtained cryo-TEM images of HCT116 cells incubated with 25-SiNCs for 2 h (**Figure 3.2.5**). As depicted in **Figure 3.2.5 A** and **B**, the SiNCs could not be identified unambiguously based on contrast images. Therefore, we used electron energy loss spectroscopy (EELS) to detect silicon. The silicon signal revealed intact, round particles with diameters be-

tween 20 nm and 30 nm inside a multilammelar intracellular vesicle that likely represents a multivesicular body (MVB). Some of the silicon signals appeared to be surrounded by a membrane as visible in the contrast mode. This suggests that the SiNCs were captured in intraluminal vesicles. Once released into the extracellular space by the fusion of the MVB membrane with the plasma membrane these intraluminal vesicles are termed exosomes. Another possible scenario is that the observed SiNCs were contained in an autophagosome or in amphisomes which results from the fusion of an autophagosome with endosomal compartments.[251] Aside from releasing its content to the extracellular space, fusion of the compartment with a lysosome and subsequent degradation of the content would be possible alternative.[252] As we found multiple similar-looking structures inside cells, we concluded that these images capture the presence of SiNCs inside MVBs after packaging into exosomes. The MVB captured here was almost filled with intraluminal vesicles and some of them contained SiNCs. Considering its ripeness, this MVB was likely to fuse with the plasma membrane next to release its luminal content into the extracellular space. Given that this image was captured after incubation with SiNC for 2 h, it is likely that this MVB would release its content soon enough to harvest its content within the next 4 h as scheduled. This suggests that the incubation and exocytosis time scheme applied in the packaging protocol is in realistic alignment with the time frame of the intracellular packaging and release process. Hence, this observation supports that the SiNCs can be released inside exosomes and that the applied time scheduled is in good alignment with the intracellular events.

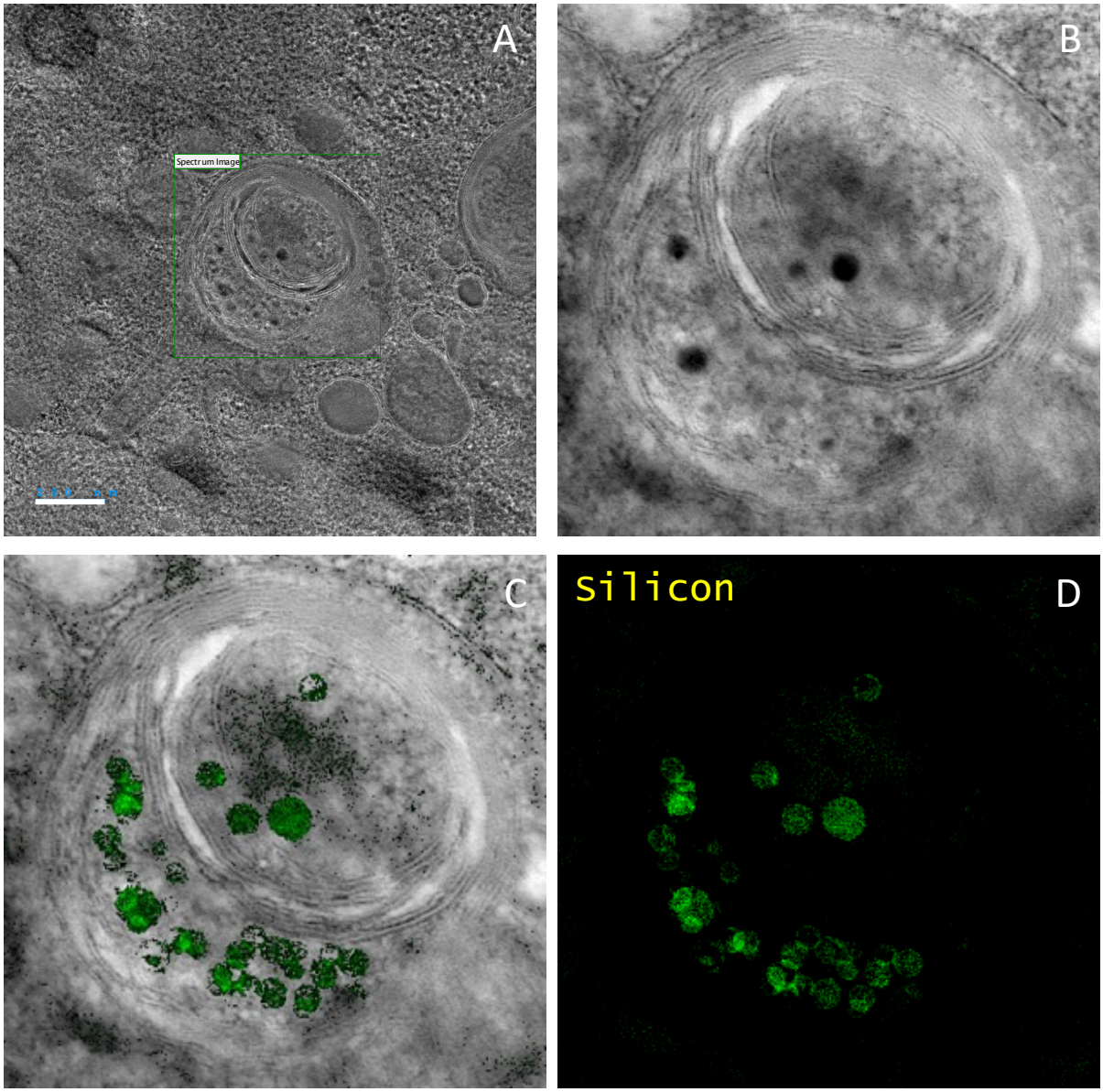

Figure 3.2.5: Cryo-TEM micrographs of 25-SiNC PEG uptake into HCT116 cells after 2 h. The cells were incubated with 200 µg/mL SiNCs. A. Overview of the intracellular region further analyzed with EELS. The scale bar represents 200 nm. B. Close-up of the rectangular selection analyzed with EELS. C. Overlay of contrast image and silicon spectrum. The silicon signal was depicted in green D. Silicon spectrum of the selected area. The silicon signal is depicted in green. The cell uptake of NPs was done by me, the sample preparation for TEM was done by [redacted], and the imaging and EELS were performed by [redacted].

As a first characterization of the samples resulting from the packaging protocol depicted in **Figure 3.2.4**, DLS spectra of naked and packaged SiNC were obtained (**Figure 3.2.6**). For the 5-SiNC PEG, there is a shift in the volume spectrum noticeable. The peak of naked 5-SiNC PEG centered around 10 nm, whereas the peak of the packaged 5-SiNC PEG centered around 50 nm and had a long shoulder towards larger particle diameters. The particle size change gives a first hint about the packaging of SiNC but from this, it is not evident that the 5-SiNC PEG were indeed inside the EV

lumen. The spectrum could also be explained by empty EVs and eventually naked 5-SiNC PEG. The spectra of naked and packaged 25-SiNC PEG were similar, except for the shoulder towards larger particle sizes that was only visible for packaged 25-SiNC PEG. The shoulder represents most likely larger EV particles, but it is not evident if they are filled with 25-SiNC PEG.

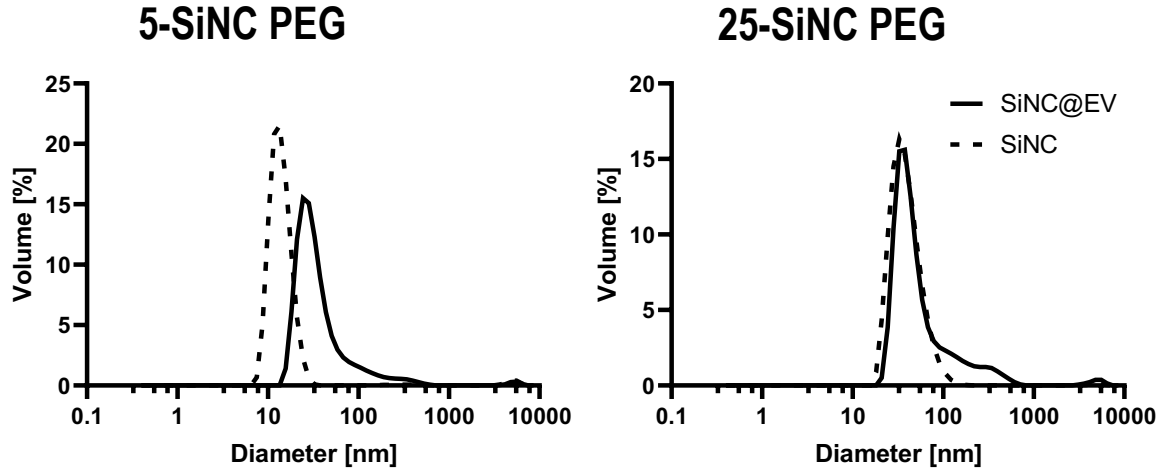

Figure 3.2.6: Volume distribution of hydrodynamic diameter of bare and packaged SiNC measured by DLS in PBS at 20°C. The SiNC/EV hybrids were generated by me, the SiNCs were produced by [redacted]. The DLS spectrum was obtained by me.

As the DLS spectra of naked and packaged SiNC opened the possibility that the SiNC were packaged in EVs, the association of single SiNC and EVs needed to be demonstrated by additional methods. Therefore, we wanted to analyze the co-localization of SiNC and EVs on an nm-length scale by dual-color fluorescence cross-correlation spectroscopy (DC FCCS). DC FCCS is a powerful method to investigate the nanoscale interactions between two fluorescent species in solution and has found numerous applications in studying processes ranging from DNA renaturation [253] and drug loading of nanocarriers [254] to NP formation.[255] The method relies on the dual-color labeling of the binding partners with spectrally well-distinguishable fluorophores, e.g. “green” and “red”. Next, two collinear laser beams with wavelengths that can excite the “blue” and “red” fluorophores respectively, are coupled to a confocal microscope to create two overlapping confocal observation volumes into the studied solutions. The temporal fluctuations of the “green” and “red” fluorescence signals caused by the diffusion of the respective species through the confocal observation volume are independently monitored and recorded. Auto-correlation analysis of the “green” and the “red” signals is used to determine the size of the studied species, while cross-correlation analysis of

these signals yields information on the co-localization of the species [256] (see SI for further details). Therefore, the SiNCs were fluorescently labeled with the red-emitting dye Cy5, and the EV membrane was stained with αCD63-antibodies labeled with the green-emitting dye Alexa Fluor 488 (AF488) (**Figure 3.2.7 A**). This fluorophore selection ensures a minimal spectral overlap. Typical experimental auto- and cross-correlation curves are depicted in **Figure 3.2.7 B** and **Figure 3.2.8 A**. By fitting of the autocorrelation curves, the diffusion time and average hydrodynamic diameter of the fluorescent species can be calculated (**Table 3.2.2**). Comparing the hydrodynamic diameter of the αCD63-antibodies mixed with either bare or EV-packaged SiNCs shows an increase from 10 nm to 88 nm. This indicates that binding of the αCD63-antibodies to a larger species only occurred in samples with packaged SiNCs. Further, this demonstrates that the antibody binds specifically to EVs and has no affinity for naked SiNCs. It is important to note that EVs are biologically derived NPs and therefore have a much higher polydispersity compared to the average synthetic NP. This was also demonstrated by analyzing the diameter of vesicles in cryo-TEM images in **section 3.4.3**. Here vesicles between 30 nm and above 200 nm were found and resulted in a large standard deviation (**Table 3.4.1**). The diameter of EVs can range between 30 nm and 1000 nm but usually centers around 100 nm.[117] This fits well with the average diameter obtained for the αCD63-antibodies when mixed with EVs. The hydrodynamic diameter of both SiNCs also increased upon packaging. The diameter of 5-SiNC PEG increased from 41 nm to 57 nm upon packaging, whereas the diameter of the 25-SiNC PEG increased from 62 nm to 68 nm. The increase in the diameters suggests the packaging of the SiNCs. The hydrodynamic diameters calculated here represent an average of a bulk-analysis and therefore, do not account for different populations like a mixture of bare and packaged SiNCs. This most likely explains the difference between the hydrodynamic diameter of the antibody upon mixing with packaged SiNCs and the hydrodynamic diameter of the packaged SiNC. The antibody diameter reflects an average of the EV population, whereas the SiNC diameter is smaller as it reflects an average of naked SiNCs and filled EV populations.

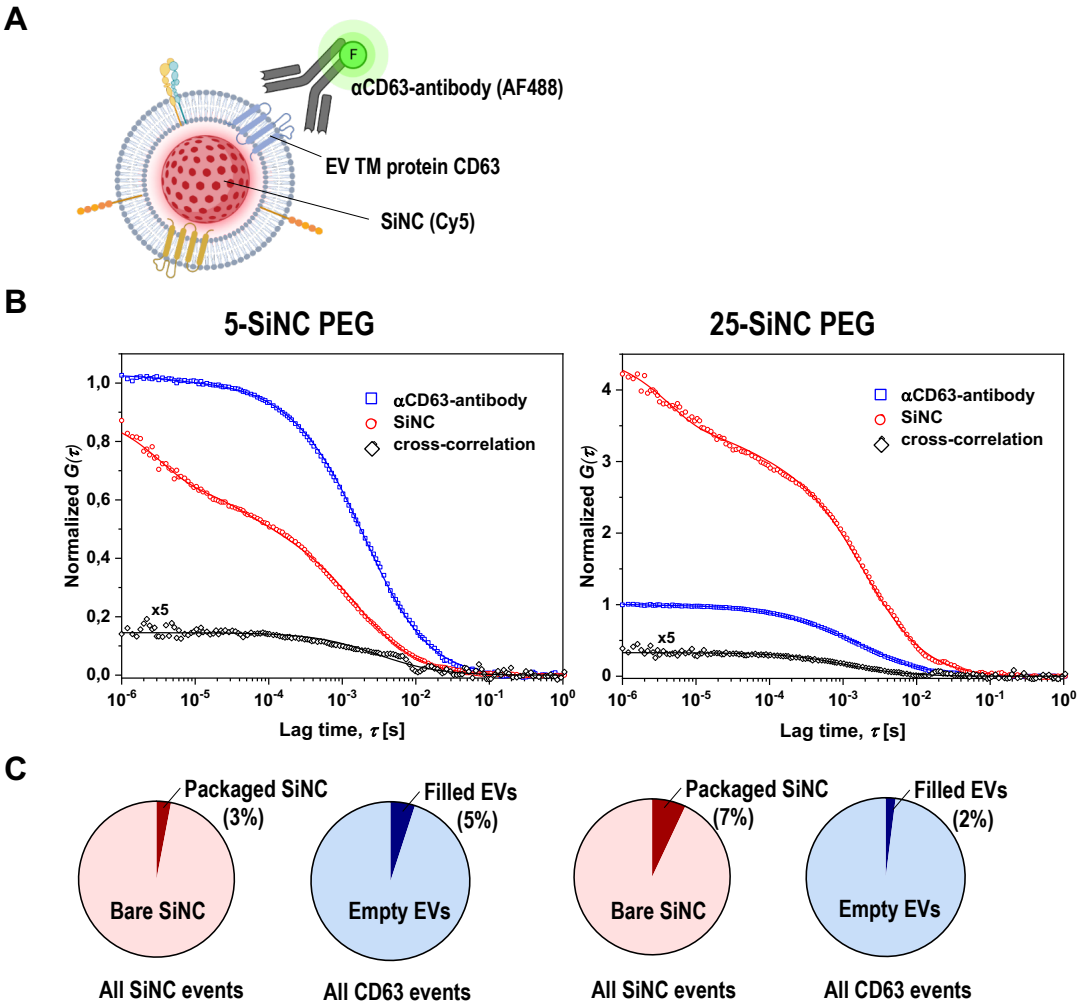

Figure 3.2.7: Characterization of SiNC-EV hybrid particles. A. Schematic depiction of hybrid particle detection by FCCS. The SiNCs are fluorescently labeled with Cy5. The EV membrane is detected with an Alexa Fluor 488-labeled antibody directed against the EV marker protein CD63. This graphic was created with BioRender.com. B. FCCS analysis of particles retrieved from the cell culture supernatant after exocytosis. The cross-correlation curve was magnified 5 times to enhance the visibility. C. Percentage of packaged SiNC and filled EVs calculated from the FCCS measurement. The SiNC/EV hybrids were generated by me, the SiNCs were produced by [redacted]. FCCS was measured and analyzed by [redacted].

Table 3.2.2: Hydrodynamic diameter of SiNC and αCD63-antibody by FCCS. The SiNCs were measured before and after packaging in EVs. The αCD63-antibody was measured after incubation with bare or packaged SiNCs. The experimental error (10%) is given. The SiNC/EV hybrids were generated by me, the SiNCs were produced by [redacted]. FCCS was measured and hydrodynamic diameter was calculated by [redacted].

	D_h [nm] FCCS	
	Bare particles	**Packaged particles**
5-SiNC PEG	41±4.1	57±5.7
25-SiNC PEG	62±6.2	68±6.8
αCD63-antibody	10±8.8	88±8.8

However, to unambiguously demonstrate the packaging of SiNC into EVs, the cross-correlation between the SiNC and EV signal must be demonstrated. Comparing the cross-correlation curve of antibodies and bare SiNCs (**Figure 3.2.8 C**) to the cross-correlation curve of antibodies and packaged SiNCs (**Figure 3.2.7 B**), demonstrates an increase in cross-correlation amplitude after packaging of SiNCs in EVs. This confirms that the packaging protocol described in **Figure 3.2.4** yields EV-packaged SiNCs. Ultimately, we aimed to quantify the packaging rate, which is the fraction of EV-coated SiNCs from all SiNCs events (**Figure 3.2.7 C**). Using equation (5) (see **section 2.2.8**) we estimated that for 5-SiNCs PEG, 3% of all SiNC events were double-positive for SiNC and EV fluorescence signal. For 25-SiNCs PEG, 7% of all SiNC events were double-positive for SiNC and EV fluorescence signals. We also calculated the EV filling rate based on all EV events detected. That is the fraction of EVs co-localizing with SiNCs (**Figure 3.2.7 C**). Here, 5% of EVs were filled upon packaging of 5-SiNCs PEG and 2% of EVs were filled upon packaging of 25-SiNCs PEG.

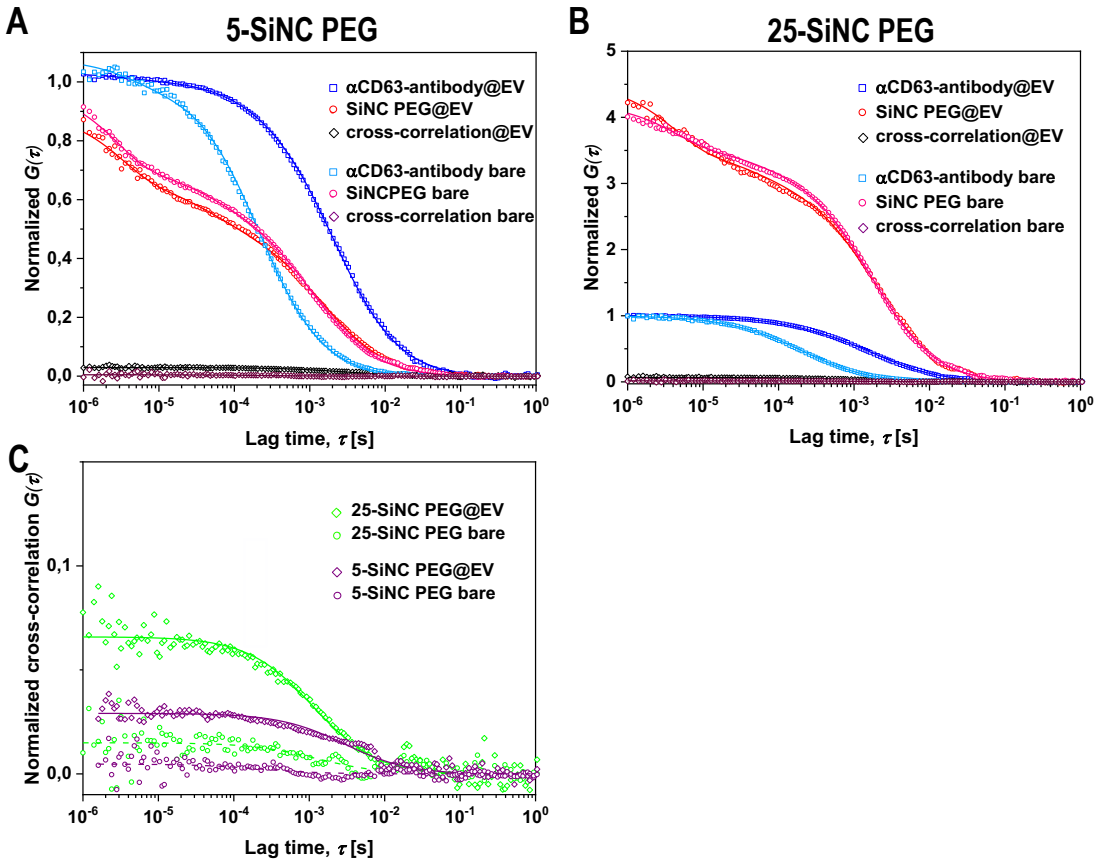

Figure 3.2.8: Characterization of SiNC-EV hybrid particles by FCCS. SiNCs were detected by Cy5 fluorescence. The EV membrane was marked with an Alexa Fluor 488-labeled αCD63-antibody. A. and B. FCCS analysis of bare SiNC or particles retrieved from the cell culture supernatant of cells treated with SiNC. Additionally, the antibody was measured alone or mixed with bare or packaged particles. C. Cross-correlation curves of the antibody SiNC mixture before (circle) and after (diamond) packaging. The SiNC/EV hybrids were generated by me, the SiNCs were produced by [redacted]. FCCS was measured and analyzed by [redacted].

Summing up, FCCS demonstrated the increase of the αCD63-antibodies' hydrodynamic diameter upon mixing with EV-containing samples, as well as the increase of 5-SiNCs PEG and 25-SiNCs diameters after packaging. This indicated packaging. Furthermore, we could confirm the loading of EVs with SiNCs by detecting co-localization events and even calculating loading rates. To our knowledge, our study is the first report that quantified the packaging of NPs in EVs. Others confirmed packaging qualitatively by analyzing hybrid particles with cLSM or TEM images.[84,178,179] While cLSM lacks the resolution for precise analysis at the nanoscale and the statistical significance for quantification, TEM possesses the resolution but is also challenging to quantify. FCCS instead, combines the nanoscale resolution, as well as the ability to quantify results in a statistically significant manner due to the high number of detected events. Furthermore, while FCCS was previously applied to determine drug loading of fully

synthetic carrier systems [257], here we successfully expanded this methodology for the characterization and quantification of a semi-synthetic SiNC/EV hybrid system.

In our study, the packaging rates were below 10% for both SiNCs. The loading rates determined by FCCS for osmotically-loaded EVs by Sanaee et al. ranged between 10 to 20%.[258] However, this group used a membrane intercalating dye for EV staining, while we used an antibody against the EV-specific surface marker protein CD63. This could partly explain the lower packaging rate in our study. EV markers are heterogeneously expressed in different EV populations. Wolf et al. demonstrated that only 8.9% of all PLX-EVs were $CD63^+$. In conclusion, only a subpopulation of EVs in the analyzed sample in our study may have been $CD63^+$. Therefore, only a subpopulation of EVs was presumably considered for the packaging rate calculation. In this respect, it would also be of interest to investigate, if the packaging is specific to one of the marker populations ($CD9^+$, $CD63^+$, and $CD81^+$).

It also needs to be considered that EVs are highly efficient in cargo delivery. This is evidenced by a study that investigated the functional delivery of RNA by EVs. Murphy et al. demonstrated that as little as 1 sgRNA per $3.6x10^5$ EV particles was sufficient to trigger a measurable signal in the recipient cell. In comparison, when using lipid NPs as RNA delivery vehicles, the lowest response triggering concentration was at least 100-fold higher compared to EVs.[138] That raises the question, of whether an NP loading rate of roughly 5-10% is sufficient to achieve a therapeutic response. As a next step, functional *in vitro* and *in vivo* studies are needed to assess the drug delivery performance of such SiNC/EV hybrid NPs.

3.2.4 Conclusion

In this study, we present the successful development of a protocol for packaging SiNC in EVs by hijacking the cellular EV pathways. The cell culture scheme developed in **section 3.1.3** was adapted based on the endocytosis and exocytosis kinetics of SiNC in HCT116 cells. The subsequent EV isolation protocol was developed in **section 3.1.3** and is based on ultrafiltration and SEC, which are techniques widely employed for EV isolation.[152,247] We observed the 25-SiNC inside of intraluminal vesicles of MVBs in HCT116 cells after 2 h of incubation with the particles. This was the first strong hint that the SiNCs were packaged into exosomes, which is a subpopulation of EVs generated in MVBs.[117]

To confirm SiNC packaging, we used dual-fluorophore FCCS. This approach was used for the quantification of drug loading into nanocarriers [254] and is capable of quantifying the packaging of SiNCs in EVs. To our knowledge, this is the first attempt to truly quantify the NP loading of biological vesicles, while other studies confirmed the packaging of synthetic NPs in EVs by image-based approaches.[84,178,179] We determined a loading rate of 3% for 5-SiNCs PEG and 7% for 25-SiNCs PEG. These loading rates were based only on $CD63^+$ vesicles. However, it was demonstrated before, that only a subpopulation of EVs isolated with particle size-based methods was positive for this EV marker.[214] Therefore, we estimate the real loading rate to be higher. However, due to the high delivery efficiency of EVs even lower loading rates could be sufficient for a therapeutic effect as shown for the delivery of RNA by EVs.[214] Optimizing the cell culture protocol by adjusting the length of the endocytosis and exocytosis periods could increase the packaging rates, if necessary. Furthermore, if a higher packaging rate is required, additional purification methods like density gradient centrifugation or immunoprecipitation of EVs can be used. Further purification of the sample would also reduce the overall yield of therapeutic EVs.

Here, we present a proof-of-principle study that demonstrates the packaging of hollow SiNCs into EVs by utilizing the cell's own EV machinery. For the first time, we could determine the packaging rates of the resulting sample. Quantitative characterization of the SiNC/EV hybrid NPs is a prerequisite to generating a well-defined therapeutic as needed for clinical translation. Next, a thorough *in vitro* and *in vivo* investigation of the drug delivery ability of SiNC/EV hybrids is necessary to assess the potential as a drug delivery vehicle.

3.3 Exocytosis of NPs from cells

Copyright: Manuscript has been submitted to Small.

Motivation:

The influence of the protein corona on the uptake of nanoparticles into cells is well understood. For drug delivery, nanoparticle exocytosis equally contributes to the overall delivery efficiency. While nanoparticle exocytosis was reported for various nanoparticles, the influence of the protein corona on this remains unknown. However, in an *in vivo* drug delivery scenario, the formation of a protein corona is inevitable. Thus, investigating the influence of a protein corona on nanoparticle exocytosis would give valuable insides into the overall drug delivery efficiency of nanocarriers. As a starting point, we wanted to investigate, if human plasma protein corona formation influences particle uptake at all. Hypothesizing that this might be influenced by the size of the nanocarrier, we used a variety of different-sized silica nanoparticles. In addition to the interest of this question for drug delivery applications, it is also interesting for the development of protocols for packaging of nanoparticles in extracellular vesicles using the cellular machinery. A pre-requisite for harvesting membrane-engulfed nanoparticles from cell supernatants is the exocytosis of nanoparticles. Finding parameters such as protein corona formation that enhance or impair nanoparticle exocytosis would be of interest for the optimization of a packaging protocol as described in **sections 3.2** and **3.3**.

Contribution:

[redacted] and I performed cell uptake and exocytosis of SiNPs (flow cytometry and cLSM. [redacted] and I prepared the protein corona on SiNPs. [redacted] performed the LC-MS sample preparation, measurement, and analysis. Julia Simon measured the zeta potential of the SiNPs. [redacted] prepared the TEM images of the SiNPs. [redacted] measured the multi-angled DLS of the SiNPs. [redacted] prepared the Figures. The LC-MS data of **Figure 3.3.8** was plotted by [redacted]. I edited all the figures and prepared the manuscript. [redacted] and [redacted] supervised the project.

3.3.1 Abstract

While the influence of the protein corona on nanoparticle uptake in mammalian cells is well understood, little is known about the influence of the protein corona on nanoparticle exocytosis. However, the exocytosis of nanoparticles also contributes to the therapeutic efficacy as it influences the net delivery of nanoparticles to a cell. Here, we report for the first time that the exocytosis of silica nanoparticles from HCT116 cells is increased by the pre-adsorption of a human plasma protein corona. This effect is also depending on the diameter of the nanoparticles. Small silica nanoparticles (10 nm) are exocytosed less, whereas larger silica nanoparticles (100 nm) are exocytosed extensively in the presence of a protein corona. Proteomic analysis of the plasma protein corona of the different-sized silica nanoparticles (10 nm, 30 nm, 50 nm, 100 nm) reveals different protein compositions. Apolipoproteins and coagulation proteins are enriched in a size-dependent manner with high amounts of apolipoproteins adsorbed to small silica nanoparticles. Our results demonstrate the importance of the nanoparticle protein corona for exocytosis and raise the need to design nanocarriers that are not exocytosed rapidly to enhance drug delivery.

3.3.2 Introduction

Nanoparticles are promising for the targeted delivery of a variety of therapeutically relevant cargo molecules such as nucleic acids, proteins, and small molecules for different treatment possibilities.[10] Especially the usage of lipid nanoparticles for vaccination against COVID-19 demonstrated the clinical importance of this technology.[259] To achieve that, a lot of research was conducted to understand the uptake of nanoparticles by target cells.[260] However, the possibility that nanoparticles can be exocytosed by cells and the consequences thereof were rarely addressed. Nevertheless, the exocytosis of nanoparticles also contributes significantly to the overall efficacy of a drug-loaded nanoparticle as it determines the net delivery to a cell.[261] A secondary problem is that exocytosed nanoparticles have adsorbed intracellular proteins or are covered with other biological components such as biomembranes.[84,250] This crucially alters their reuptake behavior and can lead to side effects and toxicity.[262] A factor that crucially influences the nanoparticles' uptake and eventually also their exocytosis is the formation of a protein corona. Therefore, we aim to investigate the influence of the nanoparticle plasma protein corona on exocytosis.

Nanometer objects in the size range between 10 nm and 100 nm show distinct interactions with biological cells. Particles with a diameter of 10 nm or smaller can sometimes even enter cells by passively penetrating the cell membrane, whereas particles with a diameter of 100 nm are likely taken up by clathrin-mediated endocytosis. However, nanoparticles in this size range can also be taken up by pinocytosis, caveolae-dependent endocytosis, and clathrin/caveolae-independent endocytosis.[260] Depending on the uptake mechanism, nanoparticles can enter different intracellular trafficking routes which determines their intracellular fate. After endocytosis, the nanoparticles are directed to their intracellular fate by the endosomal system which ultimately results in cargo release, nanoparticle degradation, storage, or exocytosis.[78,263] Nanoparticle exocytosis can occur via multiple pathways and often multiple pathways are involved simultaneously. The main routes of nanoparticle exocytosis are via the recycling endosome, lysosomal secretion, or associated with exosomes.[83,86,261] Exocytosis of nanoparticles was reported for many nanoparticle types. Mesoporous silica nanoparticles were endocytosed quickly and exocytosis was reported as early as 40 min to a few hours after removing excess mesoporous silica nanoparticles.[86,250] Furthermore, the exocytosis of gold nanoparticles with diameters between 2 nm and 100 nm was also reported.[83,264-266] These studies demonstrated that nanoparticle size and surface modifications are decisive factors for exocytosis.

The interaction of nanocarriers with cells is not only determined by the diameter or surface chemistry of the nanocarrier but crucially depends on the protein corona that forms on the nanoparticle surface. The protein corona is a layer of proteins that adsorbs to the nanocarrier upon contact with biological fluids like blood or blood plasma.[30,31] The process of protein corona formation is inevitable when administering a nanocarrier intravenously and is therefore highly important for drug delivery. The protein corona influences the biodistribution, cell uptake, and intracellular trafficking of nanoparticles.[267] This suggests that it could influence exocytosis as well, but this was rarely investigated so far. Another layer of complexity is added as the protein corona composition is dependent on the nanoparticle size and hence nanoparticle uptake.[268,269] The contribution of the individual factors particle size and protein composition for cell uptake and exocytosis are difficult to separate as they are intertwined.

Herein, we investigate the influence of a pre-formed human plasma protein corona on the exocytosis of SiNPs with different sizes. Therefore, we used flow cytometry analysis to determine the uptake and exocytosis of SiNPs with diameters of 10 nm, 30 nm, 50 nm, and 100 nm in the presence and absence of a pre-formed protein corona. In the presence of a protein corona, exocytosis was increased in a size-dependent manner. SiNPs with a diameter of 100 nm were exocytosed more compared to SiNPs with a diameter of 10 nm. We analyzed the composition of the protein corona and found a decrease in the lipoprotein amount with increasing particle size.

3.3.3 Results and Discussion

In this study, we used fluorescent SiNPs to investigate how a pre-adsorbed protein corona affects the exocytosis of nanoparticles with different biologically relevant sizes from cells. First, we characterized the physicochemical properties of the four different SiNPs. TEM micrographs of the SiNPs showed intact particles with diameters of approximately 10 nm, 30 nm, 50 nm, and 100 nm diameters (**Figure 3.3.1**). We further analyzed the nanoparticles´ hydrodynamic diameter (D_h) with multi-angle DLS and calculated the polydispersity index (PDI) from measurements at 90°C (**Table 3.3.1** and **Figure 3.3.2**). The D_h was in good accordance with the expected particle diameters. The PDI of the smaller SiNPs was higher, which indicates a broader size distribution, whereas the size distribution of larger SiNPs was narrower. To assess the influence of nanoparticle diameter on exocytosis, other surface properties of the SiNPs must be similar despite the difference in size. Therefore, we analyzed the ζ-potential of the SiNPs. The 10 nm and 30 nm SiNPs had a ζ-potential of approximately -25 mV and the 50 nm and 100 nm SiNPs had a ζ-potential of approximately -40 mV. The negative ζ-potential is caused by the free hydroxyl groups of the silica surface indicating that the surface chemistry of all SiNPs is similar and no additional surfactant is used for stabilization.

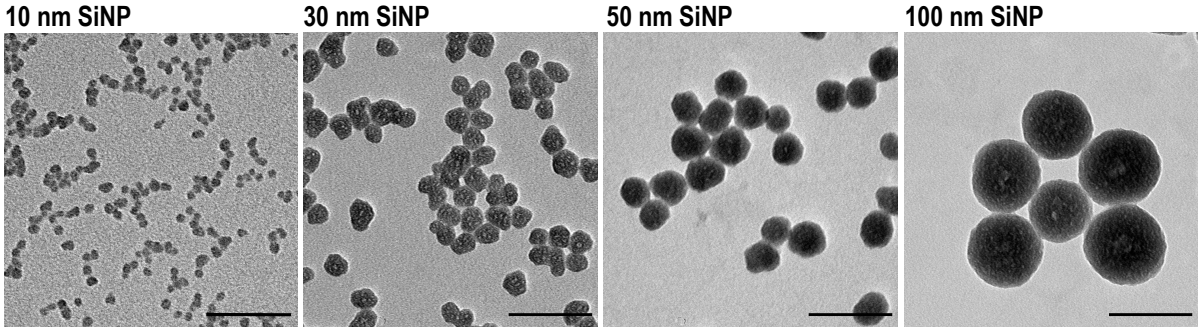

Figure 3.3.1: TEM images of 10 nm, 30 nm, 50 nm, and 100 nm SiNP. Scale bar: 100 nm. TEM images were obtained by [redacted].

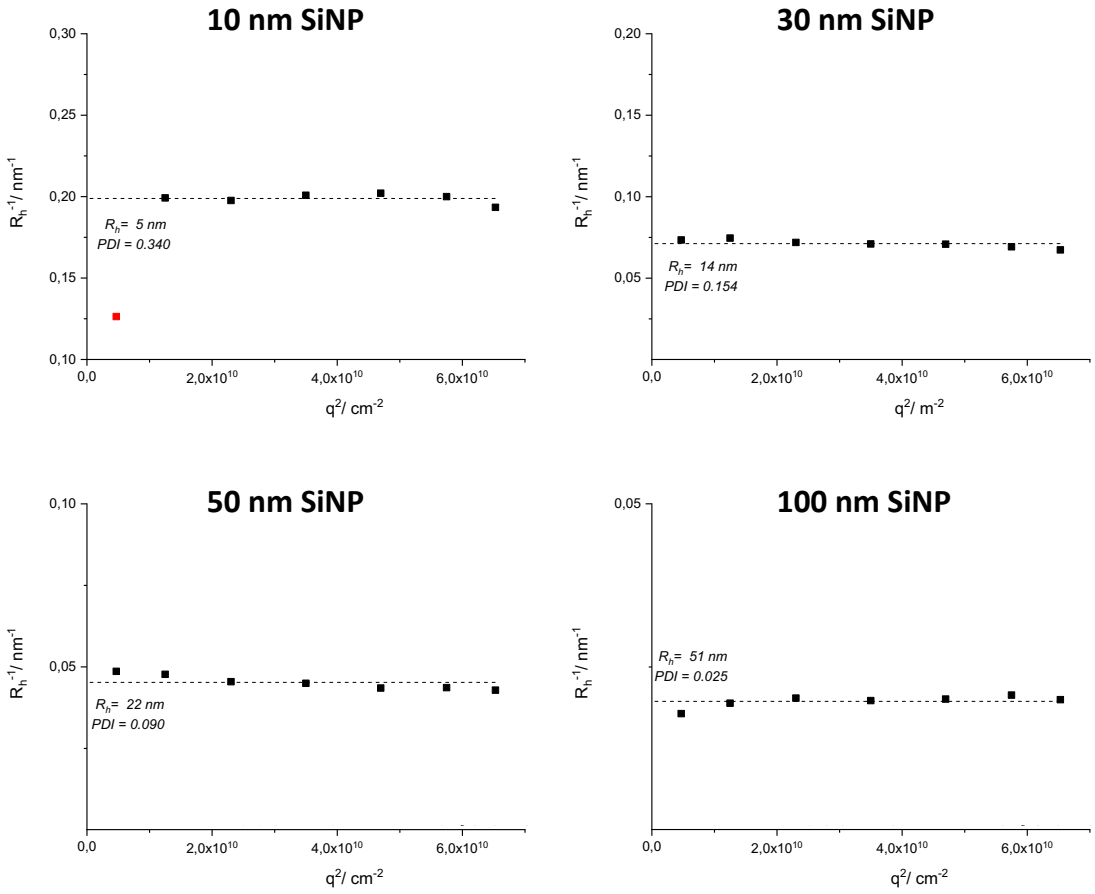

Figure 3.3.2: Hydrodynamic radii of SiNPs determined by multi-angle DLS in water at 20°C. The PDI was derived from 90°C measurements. The red data point was not taken into account for analysis. The measurements were done by [redacted].

Table 3.3.1: Physicochemical characterization of SiNPs. The *D*h of different-sized SiNPs was measured by multi-angle DLS in water at 20°C. The corresponding PDI was derived from 90°C measurements. ζ-potential was measured at 20°C in KCl. The fluorescence intensity of SiNP dispersion (1 mg/mL in water) was measured with excitation at 569 nm and emission at 585 nm. All measurements were done by [redacted].

	D_h [nm]	PDI	ζ-potential [mV]	Fluorescence [AU]
10 nm	10	0.340	-23±3.7	11150
30 nm	28	0.154	-24±2.9	9075
50 nm	44	0.090	-38±0.3	8996
100 nm	102	0.025	-42±3.2	10784

Before investigating the influence of a pre-adsorbed protein corona on SiNP exocytosis, we tested the influence on the uptake of SiNPs. **Figure 3.3.3 A** shows the uptake of SiNPs in the presence and absence of a pre-adsorbed human plasma protein corona in HCT116 cells after 2 h of incubation. In the absence of a protein corona, the cells took up the different-sized SiNPs to a similar extent. 50-70% of cells were positive for SiNPs and the uptake was not influenced by particle size. In contrast, the adsorption of a protein corona influenced the uptake of the different SiNPs differently. The uptake of 100 nm SiNPs was reduced to nearly 0% positive cells upon the adsorption of a protein corona. The uptake of 50 nm SiNPs was also reduced to approximately 10%. The uptake of 30 nm SiNPs was reduced from 60% positive cells to around 45% positive cells. Interestingly, the uptake of the 10 nm SiNPs was not reduced by the adsorption of a protein corona. This trend was also reflected by the median fluorescence intensity (MFI) of the cells. Here, the MFI in the presence of a protein corona decreased with increasing size. The MFI of cells incubated with SiNPs without protein corona was similar between different SiNPs (**Figure 3.3.4 A**). The cell viability was not affected by incubation with SiNPs (**Figure 3.3.4 B**).

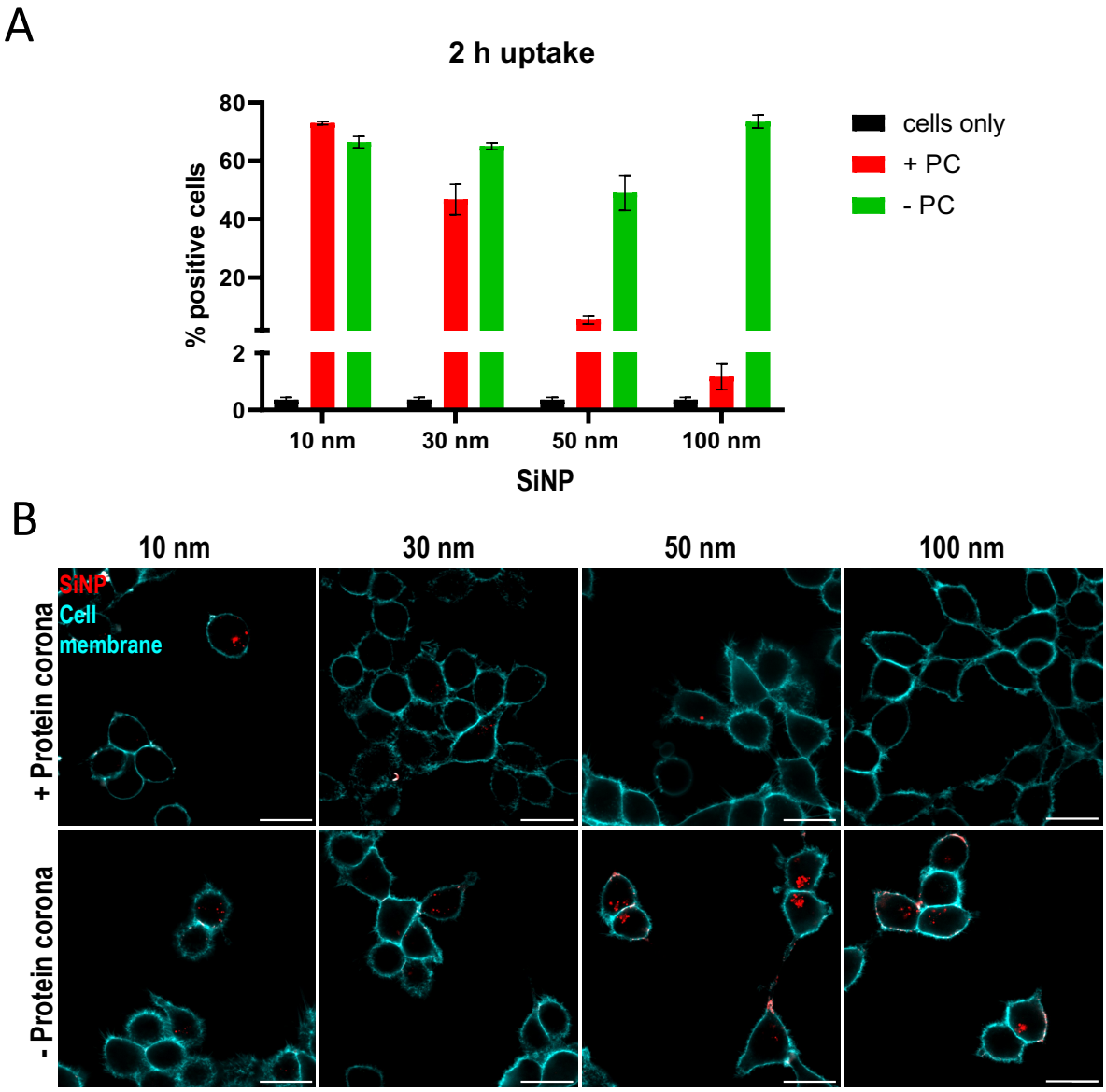

Figure 3.3.3: Uptake of different-sized SiNPs in the presence and absence of a protein corona. A. Flow cytometry measurement of 10 nm, 30 nm, 50 nm, and 100 nm SiNPs uptake in HCT116 cells after 2 h of incubation. Shown are the means and standard deviations of the percentage of positive cells (n = 3). B. cLSM image of HCT116 cells incubated with SiNPs in the presence and absence of a protein corona. Cell membrane is pseudocolored in cyan, SiNPs are pseudocolored in red. Scale bar: 20 µm. The protein corona preparation, cell uptake, and cLSM imaging were done by [redacted] under my supervision. I analyzed and interpreted the data.

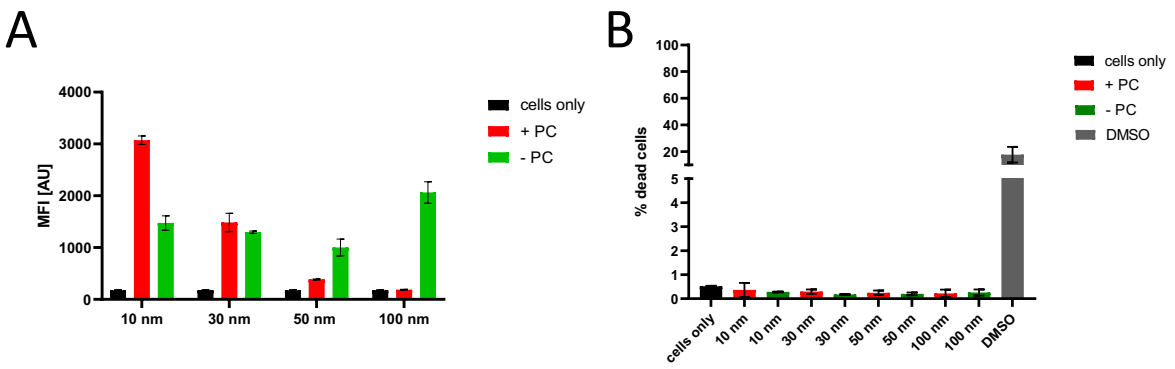

Figure 3.3.4: Uptake of different-sized SiNPs in the presence and absence of a protein corona. A Flow cytometry measurement of 10 nm, 30 nm, 50 nm, and 100 nm SiNPs uptake in HCT116 cells after 2 h of incubation. Shown are the means and standard deviations of the MFI of all cells (n = 3). B Cell viability after 2 h of incubation with SiNPs in the absence and presence of a protein corona as a percentage of dead cells. Mean and standard deviation of n = 3. The protein corona preparation, cell uptake, and viability assay were done by [redacted] under my supervision.

This experiment demonstrated that the influence of a protein corona on nanoparticle uptake is size-dependent. The uptake of small SiNPs was not impaired by the adsorption of a protein corona, whereas the uptake of bigger SiNPs was increasingly impaired in the presence of a protein corona. The reduction of nanoparticle uptake in the presence of a protein corona that we observed here was often observed in previous studies and is generally known as the stealth effect.[270] In the absence of a protein corona, the nanoparticle surface interacts with the cell membrane directly. This can lead to the passive penetration of the cell membrane and therefore a closer contact between the nanoparticle and the cell surface. For very small nanoparticles direct entry into the cytosol has been observed.[271]

In addition to flow cytometry, fluorescent micrographs of SiNP uptake in the presence and absence of a protein corona after 2 h confirmed the dependency of the protein corona influence on particle size (**Figure 3.3.3 B**). Further, the fluorescent micrographs confirmed that the SiNPs were located intracellularly after 2 h of uptake.

To investigate, if a pre-adsorbed protein corona has an impact on SiNP exocytosis, we incubated HCT116 cells with the different SiNPs for 2 h. Subsequently, the cell culture supernatant was discarded, and the cells were washed to remove any SiNPs attaching to the cell surface. Particle-free medium was added to the cells and the intracellular particle content was assessed 2 h and 22 h later (**Figure 3.3.5**).

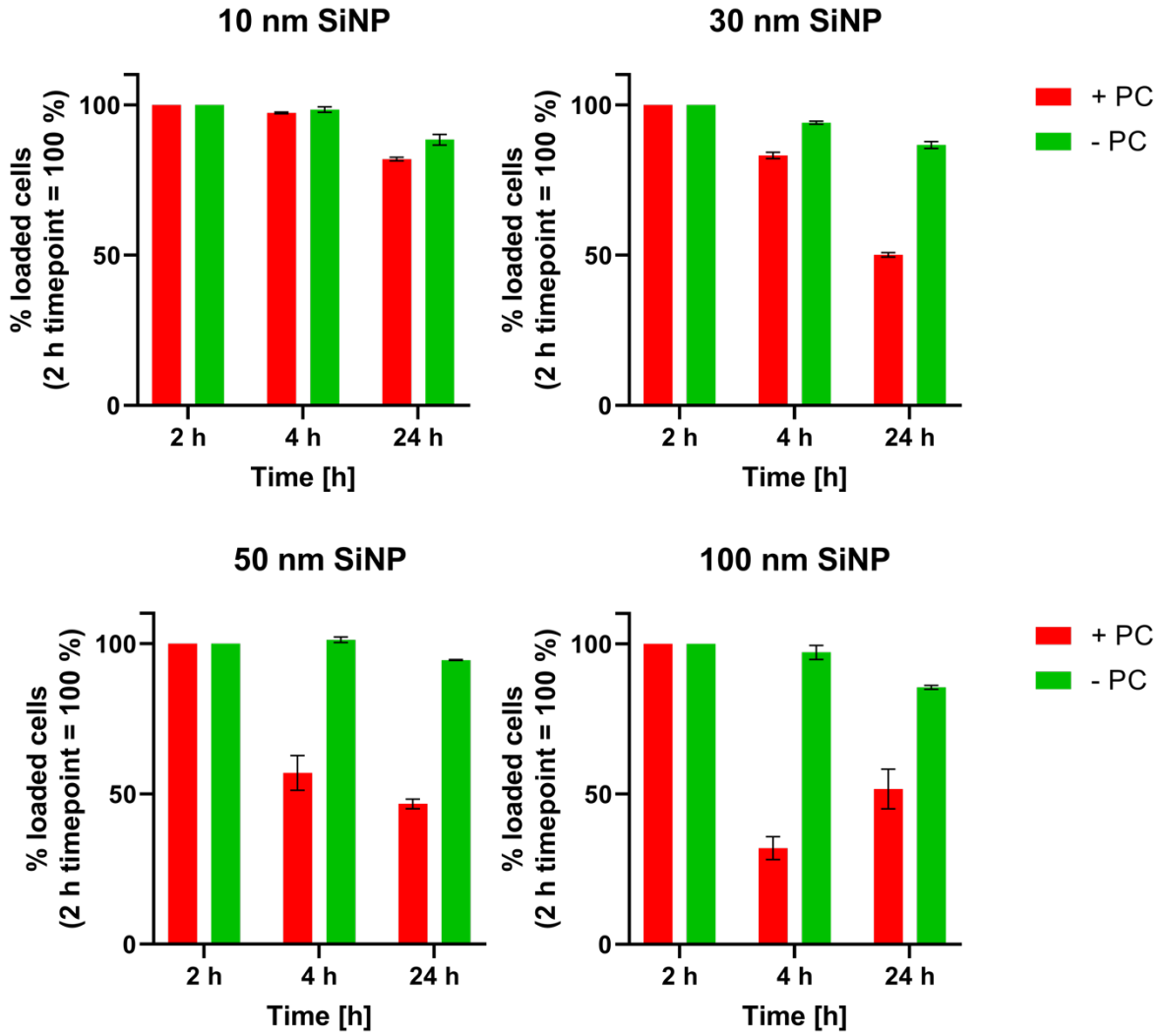

Figure 3.3.5: Exocytosis of different-sized SiNPs in the presence and absence of a protein corona. HCT116 cells were incubated with SiNP with or without pre-adsorbed protein corona for 2 h. Subsequently, the SiNPs were removed and the intracellular particle amount after 4 h and 24 h was measured by flow cytometry. The percentage of loaded cells relative to the loading after 2 h of particle uptake is shown. The means and standard deviation of n = 3 is depicted. The protein corona preparation and cell uptake were done by [redacted] under my supervision. I analyzed and interpreted the data.

The particles added without pre-adsorption of a protein corona were not strongly exocytosed. Around 90% of the cells that were positive directly after the uptake period remained particle-positive 22 h after removing the SiNPs. The MFI of the cells incubated with the 10 nm and 30 nm SiNPs decreased during the exocytosis period as the cells were oversaturated with nanoparticles due to the high uptake in the absence of a protein corona (**Figure 3.3.6**). However, the percentage of positive cells is a more robust measure for particle uptake and exocytosis. In contrast, for particles with a pre-adsorbed protein corona a time- and size-dependent decrease of the intracellular particle signal compared to the signal directly after the uptake period was observed. The exocytosis of SiNPs occurred rapidly as we could observe a decrease of intracellular

signal 2 h after the initial uptake period. In our study, we observed the strongest exocytosis for 100 nm SiNPs which showed a decrease of particle-positive cells to around 30% of the initial positive cells 2 h after the medium change. The percentage of cells positive for 50 nm SiNPs was reduced to around 50% after an exocytosis period of 2 h and the 30 nm SiNPs had a signal reduced only to around 80%. The 10 nm SiNPs did not show a reduced intracellular signal after 2 h of exocytosis. The MFI values of the cells incubated with 10 nm and 30 nm SiNPs decreased after removing the excess SiNPs as the cells were oversaturated with nanoparticles due to the high uptake in the absence of a protein corona (**Figure 3.3.6**). However, the percentage of positive cells is a more robust measure for particle uptake and exocytosis. Interestingly, the intracellular signals of 10 nm, 30 nm, and 50 nm SiNPs decreased even more after 22 h of exocytosis. For the 100 nm SiNPs, the intracellular signal increased again after 22 h of exocytosis which suggests a re-uptake of exocytosed particles.

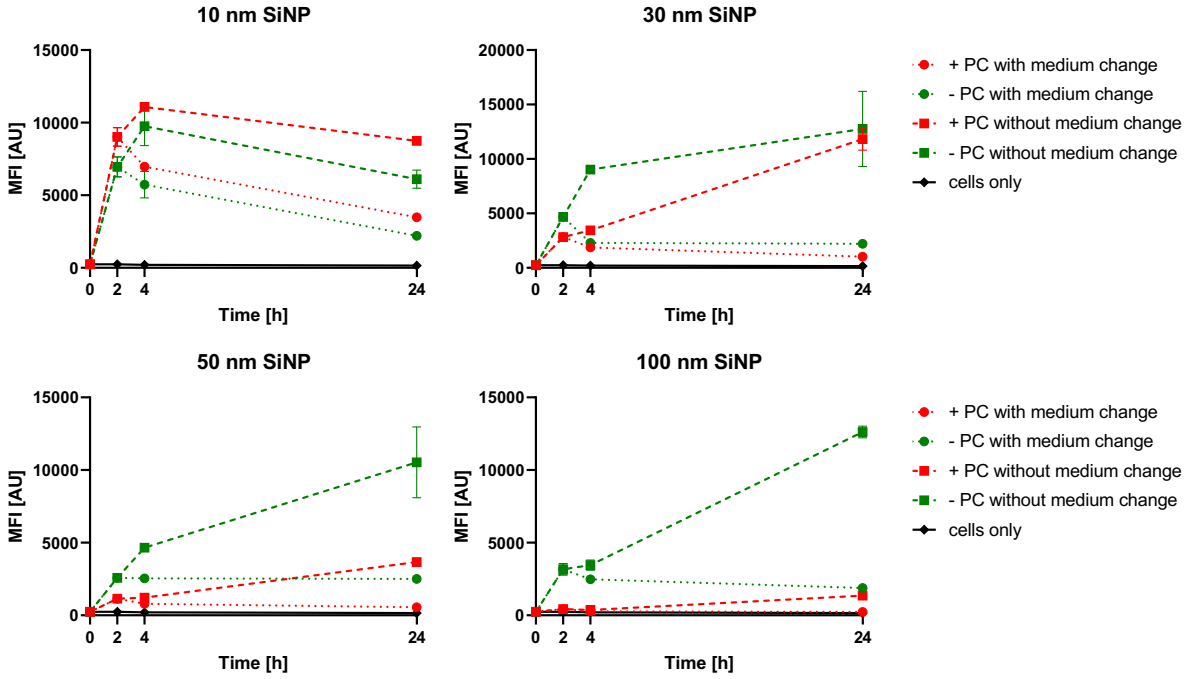

Figure 3.3.6: Exocytosis of different-sized SiNPs in the presence and absence of a protein corona. HCT116 cells were incubated with SiNPs with or without pre-adsorbed protein corona for 2 h. Subsequently, the SiNPs were removed and the intracellular particle amount after 4 h and 24 h was measured by flow cytometry. Additionally, cells were incubated with SiNPs for 2 h, 4 h, and 24 h without medium change. Shown are the means and standard deviations of the MFI of all cells (n = 3). Lines are guide to the eye only. The protein corona preparation and cell uptake were done by [redacted] under my supervision. I analyzed and interpreted the data.

We also measured the viability of the cells treated with the different conditions (**Figure 3.3.7**). Here, no severe toxicity was observed compared to untreated cells. Also, the

SiNPs without protein corona did not have a cytotoxic effect at the concentration and incubation time used here. Summing up, the exocytosis of SiNPs was strongly enhanced in the presence of a plasma-adsorbed protein corona, and smaller SiNPs were exocytosed less compared to bigger SiNPs. A rapid exocytosis of silica nanoparticles with a diameter of 100 nm 6 h after uptake was also observed by Yanes et al.[86] Furthermore, another study showed that exocytosis only happened in the presence of serum, which could be explained by the involvement of a protein corona in the exocytosis of nanoparticles.[272] In the absence of a protein corona, the nanoparticle surface interacts with the cell membrane directly and no active, receptor-mediated uptake process can take place. This can lead to the passive penetration of the cell membrane and direct entry into the cytosol, especially for very small nanoparticles.[271] This uptake mechanism would not result in a high degree of penetration of the nanoparticles into the endosomal system. As the endosomal system is the starting point for most exocytosis pathways this might suppress nanoparticle exocytosis.[78,263] This mechanism is a possible explanation for the very low exocytosis of nanoparticles in the absence of a protein corona and a protein corona might be a prerequisite for exocytosis.

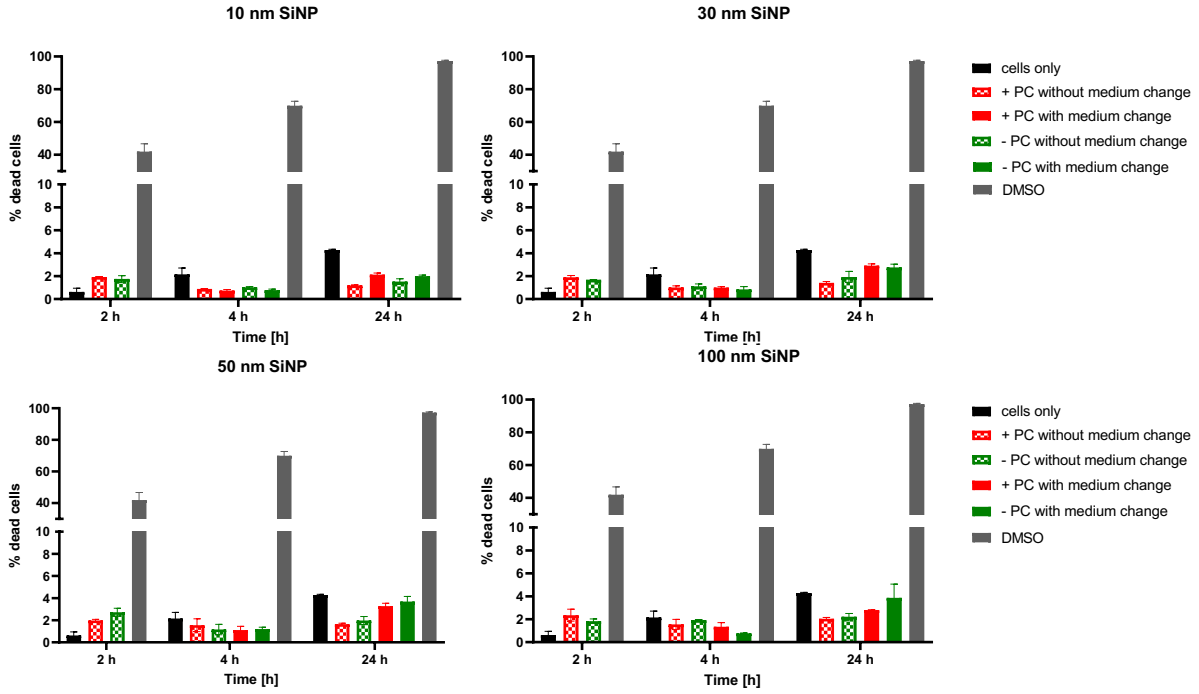

Figure 3.3.7: Cell viability after incubation of HCT116 cells with SiNPs in the absence and presence of a protein corona as a percentage of dead cells. Mean and standard deviation of n = 3. The protein corona preparation, cell uptake, and viability assay were done by [redacted] under my supervision.

As the protein corona had a big impact on the uptake and exocytosis of SiNPs in a nanoparticle size-dependent manner, we wanted to investigate the composition of the protein corona adsorbed to the different-sized particles further. It is known that small particles have a high surface curvature and therefore, less protein adsorb to their surface.[48,273,274] We also observed this effect on 10 nm, 30 nm, and 50 nm SiNPs which adsorbed increasing amounts of protein per surface area (**Figure 3.3.8 A**). For the 100 nm SiNPs, the adsorbed protein amount per surface area decreased slightly compared to the 50 nm SiNPs. The increasing amount of protein per surface area might explain the increasing influence that the protein corona had on cell uptake and exocytosis. Interestingly, the protein corona composition was highly dependent on the particle size as well. Especially, the amount of lipoproteins and coagulation proteins crucially depended on particle size. The protein corona of 10 nm SiNPs contained high amounts of lipoproteins but comparably small amounts of coagulation proteins (**Figure 3.3.8 B**). This ratio was increasingly inverted with increasing particle size. The protein corona of 100 nm SiNPs contained high amounts of coagulation proteins but comparably small amounts of lipoproteins. In contrast, the abundance of other protein classes like acute phase proteins, immunoglobulins, and complement system proteins was unaffected by particle size. We also observed a high dependency on particle size for individual proteins. The amount of apolipoprotein A-1, B-100, and E decreased with increasing particle size. In contrast, the abundance of coagulation factor XI, histidine-rich glycoprotein as well as plasminogen and α-2-macroglobulin (see SI_LC MS_protein list.xlsx) which belong to or are associated with coagulation proteins, showed to a tendency to increase with increasing particle size. Interestingly, the apolipoprotein C-III was adsorbed more to 100 nm SiNPs, although the total amount was lower than other apolipoproteins (see SI_LC MS_protein list.xlsx; can be requested from author of thesis).

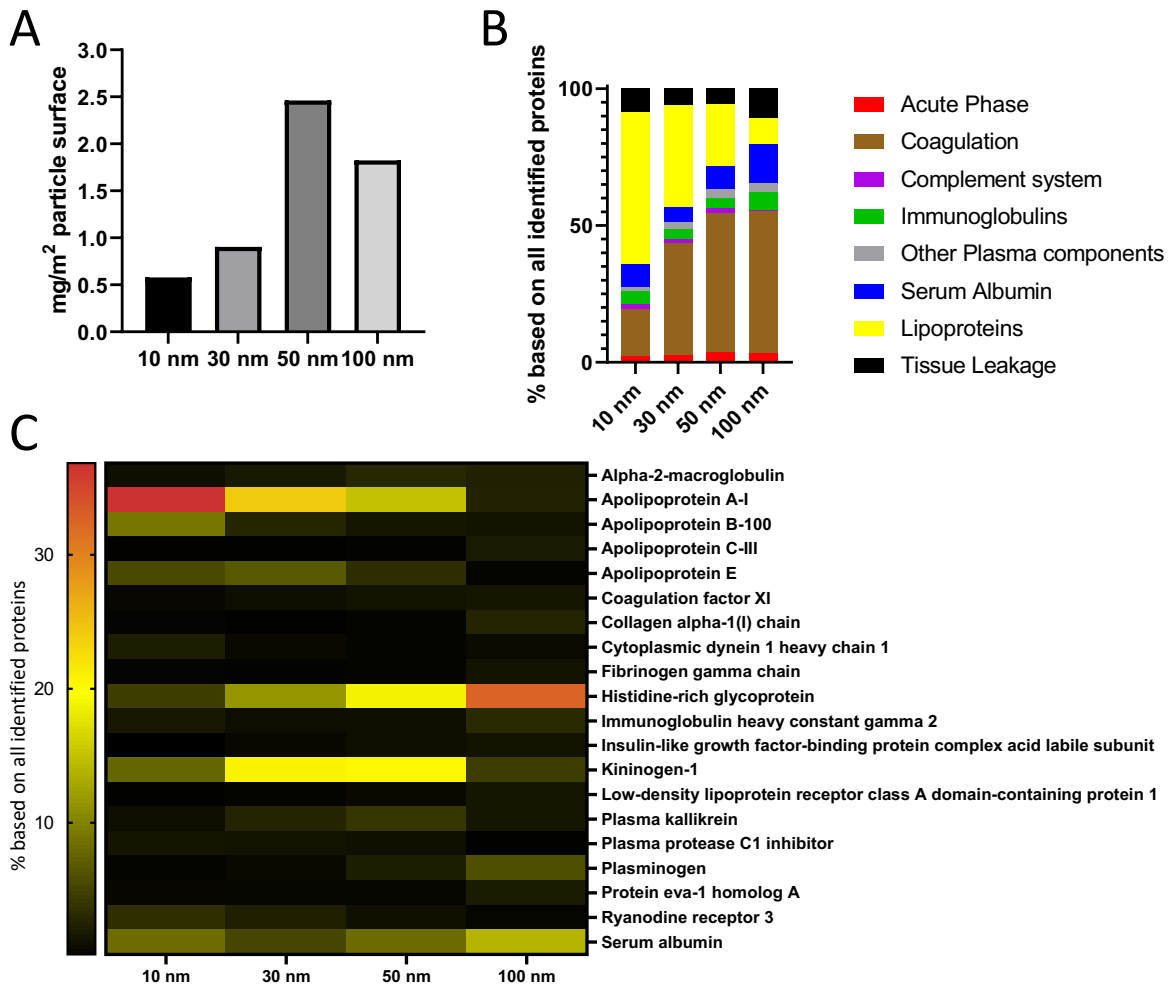

Figure 3.3.8: Proteomic characterization of the protein corona adsorbed on different-sized SiNP. A. Amount of protein adsorbed to SiNPs per surface area. B. Classification of corona proteins regarding their biofunctionality. C. Top 20 proteins found in LC-MS analysis of the protein coronas on different-sized SiNP. The protein corona preparation was done by [redacted] under my supervision. LC-MS analysis was done by [redacted]. I analyzed and interpreted the data.

Very small SiNPs seemed to attract more apolipoproteins, which are proteins known to naturally decorate lipoprotein complexes. This differential adsorption of apolipoproteins to SiNPs with a diameter of around 10 nm could be caused by their similarity in size to high density lipoproteins (HDL). HDLs also exhibit diameters of around 9 to 15 nm.[275] The 10 nm SiNPs were taken up equally well in the presence and absence of a protein corona. These particles, when carrying a protein corona, resembled HDLs in terms of size and apolipoprotein composition and thus might be able to use similar active uptake routes. Mimicking of HDL by nanoparticles was also proposed by Barrán-Berdón et al., who observed apolipoprotein-dependent uptake of nanoparticles by scavenger receptor class B type1(SR-B1).[276] This receptor is present on many tissues

including endothelium and facilitates receptor-mediated endocytosis of lipoprotein particles in cells.[277,278] However, in other experimental setups apolipoproteins were found to mediate stealth properties.[274] There, mainly apolipoprotein J (clusterin) was found to be responsible for the stealth effect.[56,274] Here, we also observed that the protein corona on 30 nm, 50 nm, and 100 nm SiNPs exhibited a stealth effect. However, apolipoprotein J was not found in the protein corona of any of the SiNPs used here with high abundance. Instead, the decrease in the amount of apolipoproteins present in the SiNP protein corona with increasing particle size might reduce the interaction with specific lipoprotein receptors. In addition, apolipoproteins adsorbed to larger particles might exhibit a different confirmation than on 10 nm SiNPs which can influence the recognition by lipoprotein receptors.[279] Therefore, the protein corona of larger SiNPs exhibited stealth properties rather than mediating the active uptake of SiNPs.

In addition to insights into the relation between the protein corona and SiNPs' uptake, we observed an exocytosis increase for all SiNPs. Similar to us Panyam et al. observed a nearly complete abolishment of exocytosis in the absence of serum.[280] They suggested that this was due to a lack of energy available in the cell culture medium and that exocytosis would be an energy-dependent process. Another possibility is that the presence of the protein corona changes the uptake route of the SiNPs and hence their intracellular trafficking route. This was demonstrated by da Costa Marques et al. before.[267] Therefore, it is possible that the protein corona can also influence the exocytosis of SiNPs. Here, it could be that the specific protein corona leads the SiNPs toward an intracellular trafficking route that is more likely to lead to exocytosis. The exocytosis of SiNPs was increased with increasing particle size. This is in line with the size-dependency of the protein corona composition observed here. Smaller SiNPs (10 nm) adsorbed high amounts of apolipoproteins and low amounts of coagulation proteins. This composition led to very low exocytosis. In contrast, large SiNPs (100 nm) adsorbed low amounts of apolipoproteins and high amounts of coagulation proteins.

3.3.4 Conclusion

Herein, we demonstrated that not only the endocytosis but also the exocytosis of SiNPs was strongly influenced by the presence of a protein corona. The SiNPs acquire a protein corona that enhances exocytosis in a nanoparticle size-dependent manner. Further, the depletion of apolipoproteins E, A1, and B-100 was associated with enhanced exocytosis. Small SiNPs were less prone to exocytosis even in the presence of a protein corona. In contrast, the formation of a protein corona enhanced the exocytosis of larger SiNPs. In the context of nanoparticle drug delivery, these findings have important consequences. To achieve a high intracellular drug delivery, it is important to prolong the residency of the nanoparticles inside the cell. Therefore, a rapid exocytosis of nanoparticles would be unfavorable and could decrease the efficacy of drug-loaded nanoparticles. In our study, we demonstrate that the presence of a human serum protein corona increases nanoparticle exocytosis *in vitro*. However, the formation of a protein corona upon injection of nanoparticles into the bloodstream is inevitable and likely also enhances the exocytosis of nanoparticles in an *in vivo* setup. This raises the question, of whether the development of nanocarriers with a reduced exocytosis ability is needed to enhance the net delivery of nanocarriers. Our study showed that it would be beneficial to use smaller SiNPs that acquire a protein corona that prevents exocytosis. On the other hand, there are attempts to use nanoparticle exocytosis as a mechanism for deeper tumor penetration or further systemic spreading of nanoparticles in cellular vesicles.[281] For this approach it would be interesting to employ larger SiNPs. Summing up, the protein corona is an important factor in nanoparticle drug delivery that is not only able to drastically reduce the uptake of nanoparticles into cells but can also enhance their exocytosis. Therefore, the protein corona influences the net delivery of nanoparticles which ultimately determines the efficacy of a drug delivery system.

3.4 Protein corona on EVs and liposomes

1 **Dietz, L.**, [redacted], [redacted], [redacted], [redacted], [redacted], [redacted], and [redacted]. (2023). Uptake of extracellular vesicles into immune cells is enhanced by the protein corona. J Extracell Vesicles *12*, e12399. 10.1002/jev2.12399.

Motivation:

Extracellular vesicles are becoming increasingly interesting as drug delivery vehicles. This is due to their advantageous features such as biocompatibility, the ability to cross biological barriers, and the potential for inherent organ targeting. Currently, different strategies are explored to load extracellular vesicles with therapeutically active cargo molecules. Such an attempt is presented in **sections 3.1** and **3.2**, where I report the loading of extracellular vesicles with synthetic nanocapsules. For many synthetic drug delivery systems, including liposomes, it is known that the formation of an opsonizing protein corona on the nanoparticle surface leads to rapid blood clearance by the mononuclear phagocytic system. This results in less delivery to the target site and decreases the drug efficiency. The formation of an opsonizing protein corona on drug nanocarriers has posed a major obstacle to their clinical application from early on and is an ongoing topic in drug delivery research. Furthermore, the first reports on the formation of a protein corona on extracellular vesicles revealed its contribution to the biological function of extracellular vesicles. However, the impact of the extracellular vesicle protein corona on the extracellular vesicle drug delivery ability remains unaddressed. Thus, I hypothesized that an opsonizing protein corona could form on the surface of extracellular vesicles, which might have a big impact on their ability to be used as a drug delivery vehicle. In this section, we aimed to compare the protein corona of liposomes to the protein corona of extracellular vesicles and assess the ability of the protein corona to increase the uptake of extracellular vesicles into phagocytic

immune cells. The formation of an opsonizing protein corona on the surface of extracellular vesicles would have implications for their usage as drug delivery systems such as the necessity of stealth modifications of the extracellular vesicle surface.

Contribution:

I performed the production, size-exclusion chromatography isolation, and fluorescent labeling of the EVs. Further, I performed the physicochemical characterization of the EVs (DLS, NTA, and zeta potential). NTA measurements were assisted by [redacted]. [redacted] prepared the liposomes and characterized them (DLS and zeta potential). I prepared the protein corona of EVs and liposomes and performed the THP-1 and HCT116 cell uptake experiments (flow cytometry and cLSM). [redacted] performed the moDC cell uptake. [redacted] performed the protein corona analysis (LC-MS) and Fc receptor blocking. [redacted] prepared the cryo-TEM image of EVs. I prepared all figures, except for the MS-related parts of **Figure 3.4.9** and **Figure 3.4.10**, which were prepared by [redacted]. The manuscript preparation was done by [redacted] and me. The Revision process was conducted by [redacted] and me. The Project was supervised by [redacted], [redacted], and [redacted].

3.4.1 Abstract

The influence of a protein corona on the uptake of nanoparticles in cells has been demonstrated in various publications over the last years. Extracellular vesicles can be seen as natural nanoparticles. However, extracellular vesicles are produced under different cell culture conditions and little is known about the protein corona forming on extracellular vesicles and its influence on their uptake by target cells. Here, we use a proteomic approach to analyze the protein composition of the extracellular vesicles themselves and the protein composition of a human blood plasma protein corona around extracellular vesicles. Moreover, we analyze the influence of the protein corona on extracellular vesicle uptake into human monocytes and compare it with the influence on the uptake of engineered liposomes. We show that the presence of a protein corona increases the uptake of extracellular vesicles in human monocytes. While for liposomes this seems to be triggered by the presence of immunoglobulins in the protein corona, for extracellular vesicles blocking the Fc receptors on monocytes did not show an influence on uptake. Therefore, other mechanisms of docking to the cell membrane and uptake are most like involved, demonstrating a clear difference between extracellular vesicles and liposomes as technically produced nanocarriers.

3.4.2 Introduction

Since extracellular vesicles (EVs) are attracting more and more attention as therapeutic agents and drug delivery vehicles, investigating the interaction with blood components becomes increasingly important. Liposomes, which have already entered clinical use as drug delivery vehicles, are the class of synthetic NPs closest to EVs and their protein corona is well investigated. Therefore, we have chosen liposomes for comparison with EVs in this study.

The concept of protein corona formation around synthetic NPs upon blood contact is well established. Numerous studies investigated the composition of proteins forming around synthetic NPs and their influence on biodistribution and cell uptake.[36,38] For EVs, which can be considered biological NPs similar to liposomes, the protein corona is poorly understood. However, EVs are of interest as therapeutic agents and drug delivery platforms. This raises the need for understanding interactions between EVs and blood components, which ultimately determines cellular uptake and biodistribution [131,282] also in comparison to liposomes which can be considered as possible synthetic

analogues to EVs. In this study, we investigate the influence of a protein corona on HCT116 cell-derived tumor EVs on their uptake in phagocytes and the cell line of EV origin in comparison to two types of liposomes.

EVs attracted a lot of interest as drug delivery platforms as they function as communication systems by transporting biologically active cargoes, such as proteins and RNA molecules, even to distant target cells.[117,131] Therefore, the payload is contained in a double-membrane vesicle that is equipped with transmembrane proteins capable of navigating biological environments including cell targeting and entry. EVs describe a group of vesicles ranging in diameter from 30-300 nm that can be subdivided into exosomes, microvesicles, and larger apoptotic bodies. For long-distance information transport, exosomes and microvesicles are of interest as vehicles. Exosomes are derived from endosomal compartments named multivesicular bodies (MVBs), whereas microvesicles directly bud from plasma membranes.[283,284] During long-distance transport, EVs encounter biological fluids, such as blood, and proteins likely adsorb to their surface. This is referred to as protein corona formation. The adsorbed protein corona can ultimately alter the EV functionality as observed for many NPs. This has been largely neglected in the field of EV research. The formation of an EV protein corona was first described by Tóth et al. who revealed the protein composition as well as demonstrated the influence of a protein corona on EV functionality.[212] Shortly after, this was confirmed by Wolf et al. who demonstrated that a protein corona is necessary for EVs to reach their full potential in angiogenesis and wound healing assays.[214] These findings started a paradigm shift from viewing plasma-derived proteins as contaminants of EV preparations towards considering them as additional EV components.

Presumably, the insights of the protein corona formed on NPs also will benefit the functional understanding of the EV corona. NPs quickly adsorb proteins upon contact with biological fluids. This changes their chemical identity to a biological identity and ultimately alters their biodistribution and cell uptake.[36] Distinct proteins regulate the uptake of NPs. Apolipoproteins, a class of lipid-binding proteins abundant in human blood, are known to promote a prolonged blood circulation time by avoiding uptake in phagocytic monocytes of the mononuclear phagocytic system (MPS).[217] This has also been referred to as the stealth effect. In contrast, so-called opsonins, such as immunoglobulins mark NPs for uptake in phagocytes.[285] The protein corona on liposomes and lipid NPs is well studied as this is one of the most commonly used drug carrier

systems in clinical use.[286] A major drawback for the clinical application of liposomes still is the formation of an opsonizing protein corona and uptake by phagocytes. Therefore, modifications like attachment of polyethylene glycol (PEG) are used to prolong the liposomes' blood circulation time.[287,288]

EVs are a special type of NP with a biological origin. Hence, they carry integrated and partially integrated proteins by themselves but can also acquire a protein corona from the blood plasma, as just recently demonstrated empirically.[212,214] In the previous EV protein corona studies, stem cell and stromal cell-derived EVs, which are of interest for regenerative and immunomodulatory therapies, were investigated. Here, we investigate the protein corona of tumor-derived exosomes (TEXs) as drug delivery vehicles analogous to synthetic drug carriers.

TEXs exert various functions in tumor progression and regulation leading to a multitude of possible treatment options using TEX. They are capable of reprogramming the tumor microenvironment by altering the function of neighboring tumor cells, infiltrating immune cells, and stromal cells.[190] Additionally, TEXs confer signaling in a long-distance manner addressing metastases. By this mechanism, chemoresistance and oncogenes are horizontally transferred to other cancer cells and distant metastases.[289-291] This finding also suggests that TEXs have a certain targeting capacity for tumor cells they originated from. This principle was utilized as a targeting strategy to deliver anti-cancer drugs.[84,292] As another treatment option, TEXs play a crucial role in tumor immunity, which is highly dependent on the specific context. There is evidence, that TEX mediates immunosuppression via inhibition of macrophages, dendritic cells (DC), lymphocytes, and other immune cells in the tumor microenvironment.[190,293] On the other side, isolated TEX were successfully used as tumor antigens for DC-loading and *in vivo* tumor vaccination.[294-298]

Here, we analyzed the protein corona of HCT116 EVs and its influence on vesicle uptake in comparison to liposomes as model drug carriers. EVs as well as liposomes showed an increased uptake into phagocytic THP-1 cells and monocyte-derived DCs (moDCs) upon protein corona formation. The advantage of proteomics studies of the protein corona is that specific proteins can be determined to explain these effects. Here

we demonstrate that enhanced uptake into these cells can be attributed to immunoglobulins and complement protein enrichment in the protein corona. However, uptake via Fc receptors was not the major route for EV uptake upon protein corona adsorption.

EVs and liposomes showed increased uptake also in HCT116 cells. Our data demonstrates the importance of the protein corona for cell uptake and suggests it represents a critical factor for the application of EVs as drug delivery vehicles. Further, we propose that enhanced uptake of EVs by phagocytes in the presence of a protein corona can be a benefit for the application of EVs in immunotherapy.

3.4.3 Results and Discussion

Here, we used human colorectal tumor (HCT) 116-derived tumor EVs and compared them to similar-sized liposomes as synthetic analog. The EVs were collected under serum-free conditions to avoid a pre-formed serum protein corona. EVs were isolated by size exclusion chromatography (SEC) to separate EVs from ECM components and other proteins secreted by the producing cell. This separation method isolates vesicles based on size. Therefore, the resulting sample contained a heterogeneous mixture of exosomes, microvesicles, and other vesicles. In addition, SEC is considered to be minimally damaging to the EVs' surface which preserves EV functionality.[151,299] Subsequently, EVs were labeled by reacting N-hydroxysuccinimide ester (NHS)-cyanine 5 (Cy5) to primary amines of EV surface proteins (**Figure 3.4.1**).

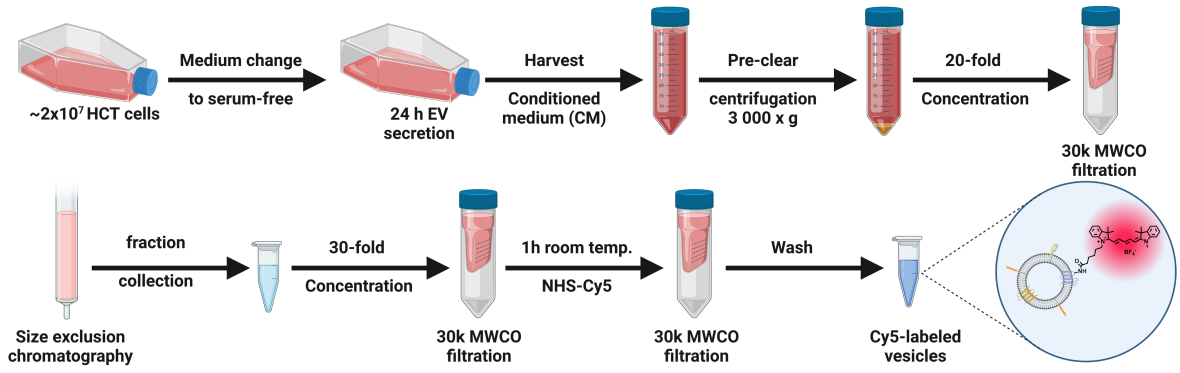

Figure 3.4.1: Production of HCT116 EVs and Cy5-labeling. EVs were collected under serum-free conditions for 24 h and subsequently purified via SEC. After concentration, EVs were labeled by reacting NHS-coupled Cy5 with primary amine groups of EV surface proteins in an aqueous solution. Access dye is removed by washing with 30 kDa MWCO centrifugal filters. This graphic was created with BioRender.com. The EV production and fluorescent labeling were done by me.

Figure 3.4.3 depicts the molecular differences between EVs (**Figure 3.4.3 A-D**) and liposomes (**Figure 3.4.3 E-F**). As shown in **Figure 3.4.3 A**, EVs contain transmembrane proteins, which are inserted into the lipid bilayer and together with the glycocalyx alter the EV surface. Additionally, they contain soluble proteins and metabolites in the aqueous lumen.[117] The cryo-TEM image of the EV preparation depicted in **Figure 3.4.3 B** showed round vesicular structures with a diameter between 50 nm and 100 nm, which fits well with typical EV sizes. The characteristic lipid bilayer of the EVs is even visible in this cryo-TEM image. Proteomic analysis of nascent EVs depicted in **Figure 3.4.3 C** demonstrated the presence of common EV markers according to MISEV guidelines.[283] The EV markers were found with low abundancies and were therefore not found among the TOP 20 identified proteins which are depicted in **Figure 3.4.3 D**. The tetraspanins CD81 and CD9 were identified. Furthermore, integrins α and β, different annexins, caveolin, ADP-ribosylation factor 6 (ARF6), HSP90-β (HSP90AB1), and ALIX (Programmed cell death 6-interacting protein) were detected in the isolated EVs. Calnexin which is a marker for endoplasmatic reticulum contamination was not detected (**Figure 3.4.3 C**). We further analyzed the EV diameter with differential light scattering (DLS) and nanoparticle tracking analysis (NTA) and determined the size distribution of vesicles imaged with cryo-TEM. Additionally, we measured the zeta potential of an EV sample (**Table 3.4.1**). The mean hydrodynamic diameter determined by NTA was 113 nm, which was in good accordance with the mean diameter observed in cryo-TEM images, 91 nm. As visible by cryo-TEM, the EV sample is a polydisperse vesicle solution and there were small vesicles observed between 30 and 60 nm in diameter. Larger vesicles were also captured by the NTA measurement as the histogram showed a shoulder reaching towards diameters of 500 nm (**Figure 3.4.2**). DLS values were not given for the EVs, as the sample was too polydisperse for this measurement technique.[300] The zeta potential in the absence of a protein corona was near neutral, which is in line with previous reports.[214]

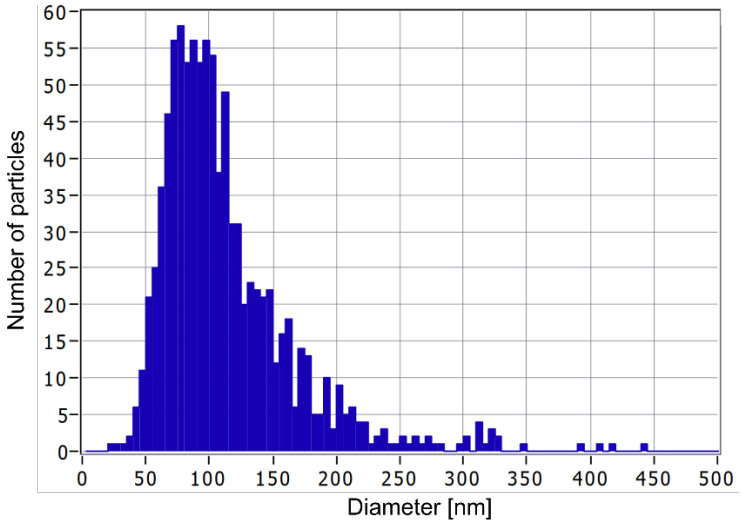

Figure 3.4.2: Histogram of particle size distribution measured by NTA. The measurement was done by me under the supervision of [redacted].

In contrast to EVs, liposomes are composed of a lipid bilayer that encloses an aqueous lumen but does not contain any additional proteins or metabolites (**Figure 3.4.3 E**). Here, we used liposomes prepared with phosphatidylcholine, cholesterol, and varying amounts of DOPE to vary the zeta potential (**Figure 3.4.3 F**). The liposomes were prepared by thin film hydration followed by extrusion to have a diameter of around 200 nm as previously reported.[301] The DLS measurement of the liposomes gave a diameter of 189 nm and 206 nm for the 33% and 5% DOPE liposomes (**Table 3.4.1**) and a narrow size distribution was observed. Depending on the DOPE amount, liposomes had a negative zeta potential of -20.6 and -11.8 for high and low DOPE liposomes, respectively (**Table 3.4.1**). In neutral pH, DOPE carries a negatively charged head group. Therefore, the more DOPE is incorporated into the lipid membrane the more negative the zeta potential will be. Additionally, DOPE carries an NH_2 group which is used for fluorescent labeling. At a DOPE content of 5%, the fluorescence labeling is weak. At a DOPE content of 33% a higher fluorescence is achieved as more coupling moieties are available. Reducing the DOPE content further would shift the zeta potential towards an even more neutral zeta potential which would be more like that of EVs. However, this would reduce the fluorescence intensity too much. Therefore, we decided to use one liposome that was highly fluorescence but had a more negative zeta potential than EVs and one liposome that was weekly fluorescence but had a more similar zeta potential compared to EVs.

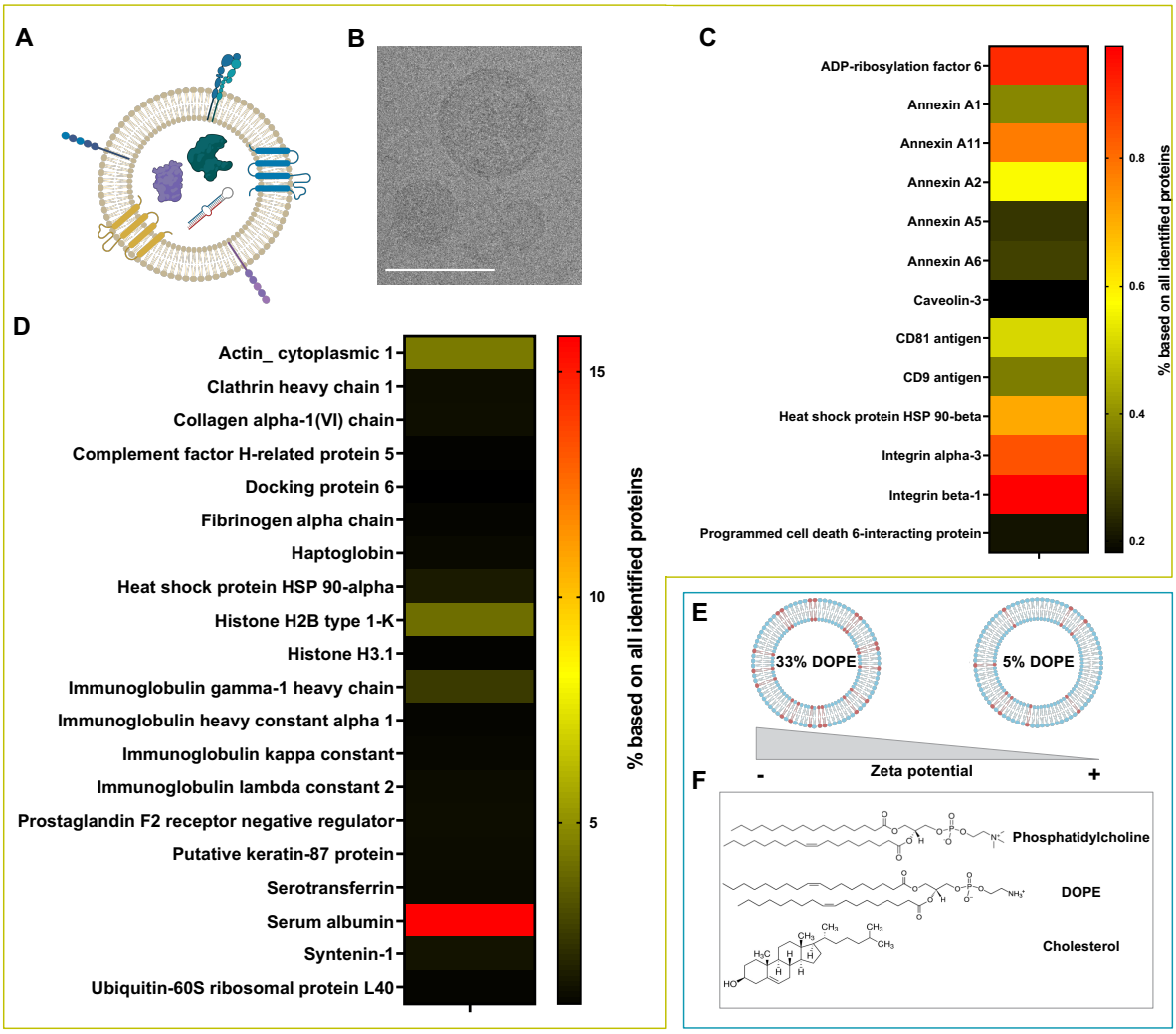

Figure 3.4.3: Characterization of liposomes and HCT116-derived EVs. A. Schematic depiction of EV. This graphic was created with BioRender.com. B. Cryo-TEM image of EV preparation. Scale bar: 100 nm. C. EV marker proteins in EV preparation identified by MS analysis. Accession numbers of the proteins are found in SI table 1. D. TOP 20 proteins of proteomic analysis of EV preparation. Accession numbers of the proteins are found in the SI Excel Sheet "AccessionNumber_20MostAbundantProteins.xlsx". E. Schematic depiction of the relation of liposomal DOPE content and zeta potential. This graphic was partly created with BioRender.com. F. Lipid components of liposomes. The EV sample was prepared by me. Cryo-TEM images were obtained by [redacted] and mass spectrometry was done by [redacted].

Table 3.4.1: Physical characterization of EVs and liposomes. The hydrodynamic diameter was determined by DLS and NTA, both measured in phosphate buffered saline (PBS) at 25°C. For HCT116 EVs, no DLS and PDI measurements were given as the population is too polydisperse. Additionally, the physical diameter was determined by analyzing cryo-TEM images. Means and standard deviations are shown. The zeta potential was measured at 20°C in 1 mM KCl. Means and standard deviations are shown. The DLS and zeta potential of the liposome samples were obtained by [redacted]. The NTA of the EV sample was measured by me and the cryo-TEM images were analyzed by me.

	D_{DLS} [nm]	PDI_{DLS}	D_{NTA} [nm]	D_{TEM} [nm]	ζ-potential [mV]
HCT116 EVs	-	-	113±54	91±109	-3±0.4
33%DOPE	189±1	0.125±0.04	-	-	-21±0.2
5%DOPE	206±4	0.153±0.03	-	-	-12±0.3

As it is well known for synthetic NPs that a protein corona can alter cell uptake, we investigated the influence of a protein corona on the uptake of EVs.[270,302,303] Depending on the particle surface and cell type, pre-adsorption of a protein corona can result in a reduced or enhanced uptake of NPs by the recipient cells.[273] Here, we tested the influence on the uptake of EVs that expose on their surface a protein corona or not in human phagocytes (THP-1, moDCs) and as a non-phagocytic cell type, the cells the EVs were derived from (HCT116), thus simulating the uptake by neighboring or distant tumor cells (e.g. metastases). To this end, we incubated 10 µg/mL of Cy5-labeled liposomes or EVs with human blood plasma at 37°C for 1 h and subsequently isolated them by centrifugation. The last pellet resulting from centrifugation was re-suspended in serum-free cell culture medium to perform the cell uptake under serum-free conditions for samples with and without pre-adsorbed protein corona. This was done to avoid the formation of a serum protein corona on plain EVs or the exchange of proteins from the pre-formed human plasma protein corona with serum proteins from fetal calf serum (FCS). In our study, we focus on the difference between particles with and without a pre-formed protein corona. Thus, our results inform about the contribution of corona proteins and neglect the eventual effect of additional free plasma proteins. However, Yang et al. demonstrate that free serum proteins can also contribute to the differential

uptake in the presence of a protein corona as they for example compete with particles for receptor binding. This effect might also play a role in EV uptake in the presence of a human plasma protein corona. The uptake of EVs and liposomes with and without a protein corona was analyzed by flow cytometry (**Figure 3.4.7**). As shown in **Figure 3.4.4** the vesicles differed in fluorescence intensity due to inequalities during the labelling process which is inherent to the amounts of possibly reactive side groups.

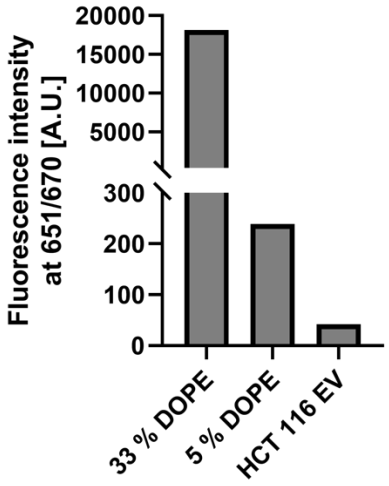

Figure 3.4.4: Cy5 fluorescence intensity of liposomes and EVs after staining. The fluorophore was excited at 651 nm±5 nm and detected at 670 nm±5 nm. The measurement was done by me.

Therefore, mean fluorescence intensity (MFI) values cannot be directly compared between vesicle types. In addition, the recovery efficiencies of vesicles after incubation with plasma (+PC) and PBS (-PC) differ. To account for particle loss after protein adsorption in plasma, MFI values were calibrated according to the fluorescence intensity of + and -PC samples. In contrast to many publications before on NPs where the protein corona had an anti-uptake effect, pre-adsorption of a protein corona increased MFI values of high DOPE liposomes (33% DOPE) and EVs in all tested cell types (**Figure 3.4.7 A**). For 5% DOPE liposomes no major differences were detected with or without PC. For all cell lines, the percentage of positive cells was near 100% when incubated with high DOPE liposomes suggesting that all cells have taken up particles (**Figure 3.4.5**). Differences between different NP formulations could be observed when analyzing the median fluorescence intensities indicating the amounts of nanocarriers taken up by cells. For 5% DOPE liposomes, the vesicles without protein corona showed near 100% uptake in THP-1 and HCT116 cells, but almost no uptake in moDCs. In contrast, the 5% DOPE liposomes with protein corona showed uptake in around 25% of THP-1 and HCT116 cells (**Figure 3.4.5**).

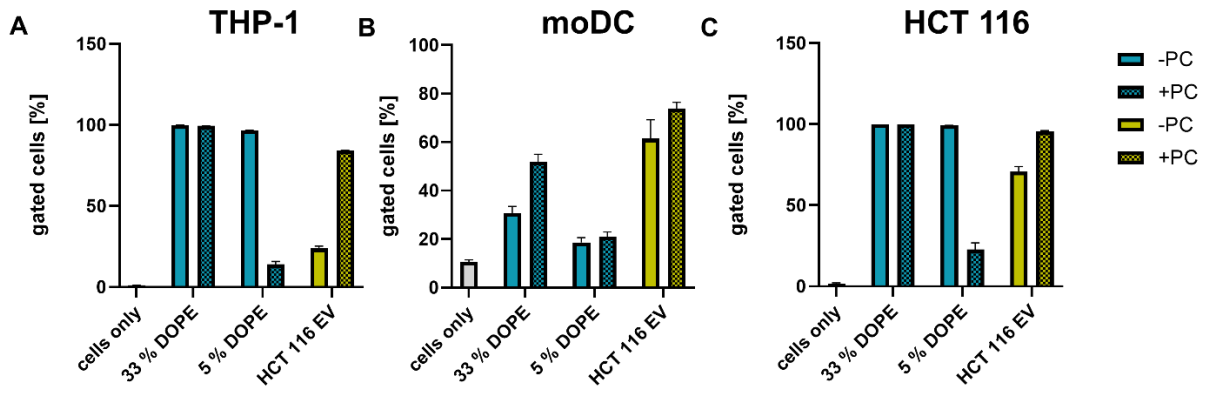

Figure 3.4.5: Uptake of liposomes and EVs with and without protein corona. Flow cytometric analyses of particle uptake into THP-1 (A), moDC (B), and HCT116 (C) cells after 16 h. Means and standard deviations of % gated cells are shown (n = 3). The protein corona adsorption and cell uptake were done by me.

Due to the loss of liposomes and EVs during protein corona formation, we adjusted the MFI values according to the different fluorescence intensities. Thereby, the inverted trend in MFI values in comparison to the percentage of particle-positive cells can be explained. This shows that the reduced percentage of particle-positive cells is due to the loss of liposomes during protein corona formation and not due to reduced uptake in the presence of a protein corona. For EV samples, the increased MFI values in the presence of a protein corona were reflected by the percentage of positive cells in THP-1 and HCT116 cells. In moDCs + and -PC showed near 100% uptake.

To validate vesicle uptake in THP-1 cells, we additionally obtained cLSM images of cells incubated with Cy5-labeled liposomes or EVs (**Figure 3.4.7 B**). To account for differences in fluorescence intensity of + and -PC samples, we used fluorescence calibration to determine the number of vesicles added to the cells. The microscopy images are in good accordance with the results from flow cytometry studies. For all vesicles, a higher uptake is observed after the adsorption of a protein corona. Furthermore, vesicle signals were detected intracellularly confirming uptake into the cell.

The ATP measurements were done in serum-free conditions. This was done to match the cell uptake conditions. After 16 h of serum-free cultivation, the cells may have entered starvation mode which can reduce the cell viability and thus ATP content. That makes them potentially more susceptible to additional stresses like particle uptake.

Uptake of vesicles independent of pre-adsorption of plasma proteins decreased ATP levels of THP-1 cells to 60-70% of untreated cells (**Figure 3.4.6**). The metabolic activity

of the cells was decreased by the interplay of serum starvation and particle uptake. However, no cells with abnormal morphology were observed under the microscope. Therefore, the cells possibly decrease metabolic activity upon particle uptake but do not enter cell death. HCT116 cells seemed to be less affected by the serum-free condition. Here, no decrease in ATP levels was observed after incubation with the liposomes or EVs.

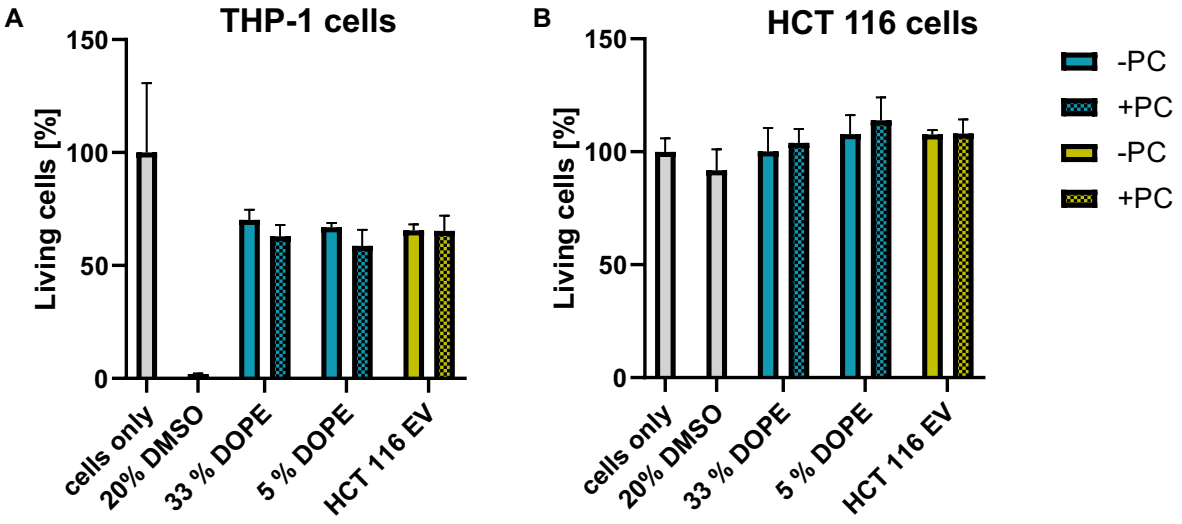

Figure 3.4.6: ATP content of cells treated with liposomes or EVs with and without protein corona. THP1 (A) or HCT116 (B) cells were incubated with particles or 20% DMSO (positive control) for 16 h. Means and standard deviations are shown (n = 3). The ATP content was measured by me.

EVs were taken up by the phagocytic THP-1 cells and moDCs, as well as by the non-phagocytic HCT116 cell line. This might also reflect the fact that TEX exert functional changes in many different cell types ranging from metastatic tumor cells to immune and stromal cells in the tumor environment.[190] Furthermore, EV uptake was increased upon protein corona adsorption by the two phagocytic cell types. This suggests that an opsonin-rich protein corona was formed probably resulting in rapid blood clearance if these would be used *in vivo*. Additionally, EV uptake in HCT116 cells was also enhanced upon protein corona adsorption. In contrast to the phagocytic uptake of EVs, this would be advantageous for a delivery strategy that utilizes the tumor-homing of EVs to the cells they originated from. In the context of tumor progression, uptake of TEX by tumor cells of origin is a mechanism to distribute chemoresistance and oncogenic traits even to distant tumor metastases.[290,304,305] Here, enhanced uptake of TEX by the tumor cells in the presence of a protein corona can be a mechanism to enhance uptake by metastatic tumor cells in contrast to neighboring tumor cells.

Previous studies have demonstrated adsorption of a protein corona on EVs increases their functionality. EVs with a protein corona showed a pronounced effect on target cells, e.g., resulting in increased interferon secretion, angiogenesis, or T-cell inhibition.[212,214] Facilitating an increased uptake of EVs could explain the enhanced biological activity in the presence of a protein corona. Moreover, the fact that we observed an enhanced uptake of EVs with protein corona in primary moDCs concurs with the finding that EVs with protein corona facilitate enhanced interferon secretion in monocyte-derived dendritic cells.[212] The increased uptake could be the mode of action to enhance EV functionality.

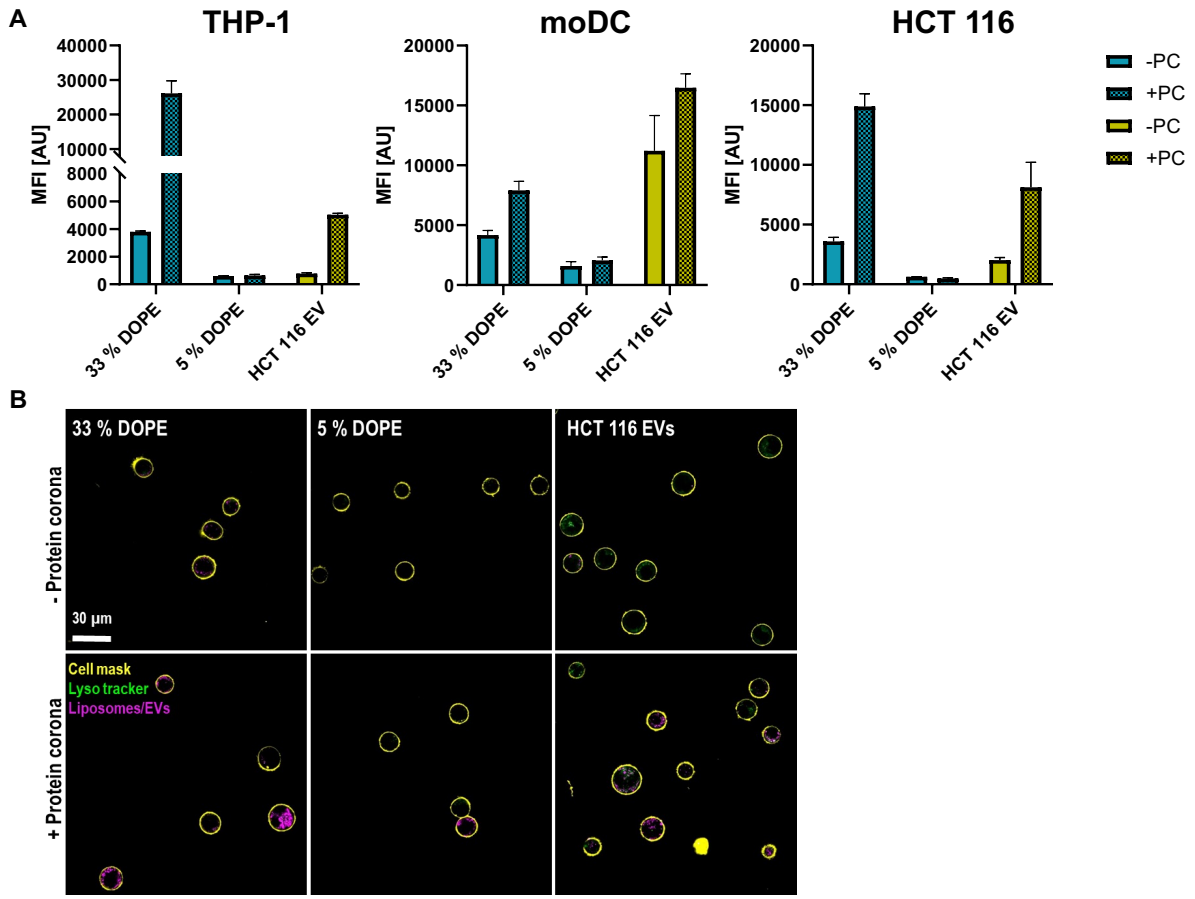

Figure 3.4.7: Uptake of liposomes and EVs with and without protein corona. A. Flow cytometric analyses of particle uptake into THP-1 cells, moDCs, and HCT116 cells after 16 h. The MFI values of untreated cells were 182±2.9 AU for THP-1 cells, 5243.3±110 AU for moDCs, and 238±11.6 AU for HCT116 cells. The MFI values of untreated were subtracted as background signal from all other values. Means and standard deviations of median fluorescence intensities are shown (n = 3). B. Confocal laser scanning microscopy images of THP-1 cells incubated with liposomes or EVs in the presence (lower) and absence (upper) of a protein corona for 16 h. The cell membrane is colored in yellow, the lysosome is pseudocolored in green, and liposomes/EVs are pseudocolored in magenta. Scale bar: 30 µm. The protein corona adsorption and cell uptake were done by me. The cLSM image was obtained by me.

To understand the enhanced uptake of liposomes and EVs in the presence of a protein corona, we used LC-MS to identify the protein corona composition. The isolation protocol applied in this study separates vesicles based on their size regardless of displayed surface markers. Therefore, the resulting samples contain a mixture of different EV subtypes such as exosomes, microvesicles, and apoptotic bodies that are within a size range of approximately 50 to 200 nm. In conclusion, the corona studied here was a mixture of different coronas forming on these different vesicles. However, the mixed population examined here is of relevance for research and clinical application as SEC is among the most popular EV isolation methods.

Since the fluorescent Cy5-labeling is necessary for cell uptake analysis and alters liposomes' and EVs' surfaces, it could influence the protein corona formation around the vesicles. The zeta potential of liposomes and EVs after adsorption of a protein corona ranged between -26.2 and -17.4 mV as depicted in **Figure 3.4.8**, which is within the expected range and suggests adsorption of a protein corona.[214]

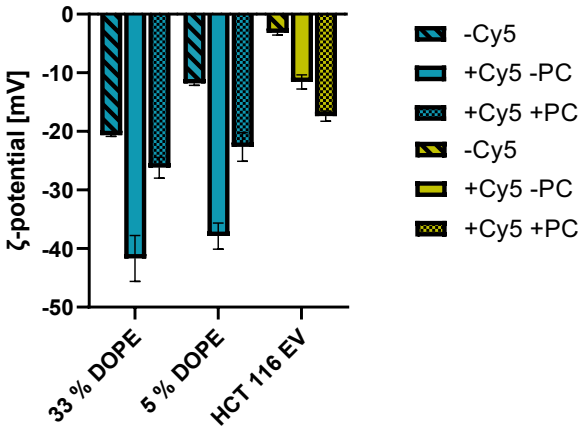

Figure 3.4.8: Zeta potential of vesicles without Cy5-labeling and with Cy5-labeling in the absence or presence of a protein corona. Measurement was performed at 20°C in 1 mM KCL. Means and standard deviations are shown (n = 3). The zeta potential was measured by me.

Analyzing the corona composition of unlabeled and Cy5-labeled EVs and liposomes did not show major differences (**Figure 3.4.9** and **Figure 3.4.10**).

Before MS analyses, the protein corona of liposomes was detached as this is the standard protocol for the preparation of a liposome protein corona and ensures comparability to former publications. This was not the case for EVs, where we analyzed a sample with and without previous adsorption of a protein corona in parallel as this also gives us the functional proteins of the EVs. Also, the separation of adhered proteins

from the protein corona and adhering or partially integrated proteins into the EV membrane could not be easily separated by a physical process like washing and centrifugation. Proteins that were only enriched in the sample with adsorbed protein corona were accounted as corona proteins from the blood plasma. All identified proteins and their relative amounts are listed in a separate file (see Supporting Information). Unlike previous studies, we used untreated plasma that was not depleted from plasma-derived EVs or lipid particles before protein corona formation. That was done to ensure that the plasma has a more original composition but also bears the risk of contamination of the MS results with plasma-derived EV and lipid particle proteins. To estimate the degree of contamination by plasma-derived EVs and lipid particles in our EV protein corona, we prepared process controls. That is a sample that undergoes the complete protein corona adsorption and isolation protocol but does not contain additional EVs. The plasma process control had a protein concentration of 0.0022 mg/mL and the LC-MS analysis revealed only 8 proteins in total (**SI table 2**). This is close to the background of an empty sample. In comparison, the EV protein corona sample had a protein concentration of 0.195 mg/mL and 225 proteins could be identified (see SI Excel Sheet “LC_MS_data_EVCorona.xlsx”). Therefore, we considered the contribution of plasma-derived EVs and lipid particles as neglectable. The EV protein corona was mainly enriched with immunoglobulins and complement system proteins (**Figure 3.4.9 A** and **B**). The biofunctional class of tissue leakage proteins, as well as serum albumin, were decreased upon adsorption of a protein corona (**Figure 3.4.9 B**). In particular, complement C3 and C4 were found. For immunoglobulins, immunoglobulin heavy constant μ and κ constant were the most abundant proteins and we also identified immunoglobulin heavy constant γ 2 (**Figure 3.4.9 C**). One of the most enriched proteins was immunoglobulin heavy constant μ which increased from approximately 0.3% to 24% of all identified proteins after adsorption of a protein corona. A similar trend was observed for complement C3 and C4-A, which increased from 0.1% to 4% and 0.1% to 2% of all identified proteins, respectively (**Figure 3.4.9 D**). A strong increase was also detected for immunoglobulin κ constant and complement C4-B. Next, we compared the most abundant protein corona proteins identified by us to major EV protein corona components identified by Toth et al.[212] Immunoglobulin heavy constant γ 2, complement C3 and C4-B, and fibrinogen α-chain identified by us are also proposed as major EV protein corona proteins by Toth et al. Additionally, they proposed ApoA1, ApoB, ApoC3,

ApoE, and immunoglobulin heavy constant γ 4. ApoA1 and ApoE were also found with lower abundancies in our samples. Furthermore, we identified clusterin among the top EV corona proteins representing a member of the apolipoprotein family (**Figure 3.4.9 C**). Comparing the protein corona of unlabeled and Cy5-labeled EVs showed a similar protein composition. The only difference for the Cy5-labeled EV's protein corona was the higher prevalence of serum albumin and less immunoglobulin heavy constant μ, but still, these proteins were in the top 20 list of proteins found. This is well within the differences of the semi-quantitative assessment of protein quantification in an unlabeled liquid chromatography-mass spectrometry (LC-MS) setup.

We also compared the most abundant EV corona proteins to liposome corona proteins (**Figure 3.4.10**). Despite the difference in zeta potential, the protein corona of high- and low-DOPE liposomes showed very similar trends as both protein coronas were enriched with apolipoproteins, immunoglobulins, and serum albumin. In contrast to the EV protein corona, complement proteins were not highly abundant. The EV protein corona was generally more complex but was less enriched for apolipoproteins and serum albumin. Comparing the protein corona of unlabeled and Cy5-labeled liposomes showed minor differences for the 5% DOPE liposomes. In the protein corona of the labeled liposomes less serum albumin, but more tissue leakage proteins and lipoproteins were found compared to the unlabeled 5% DOPE liposomes. Also this we would consider to be within the limit of assessment in a proteomics LC-MS setup. The liposomes used here, have a more negative zeta potential compared to the EVs. This could raise the question if the difference in protein corona observed between liposomes and EVs is due to the difference in zeta potential. However, the protein corona of the two differently charged liposomes was almost identical. Therefore, we conclude that the zeta potential of the liposomes plays a minor role in their protein corona composition and the difference in protein corona composition between EVs and liposomes is not mainly caused by the difference in zeta potential.

As observed for liposomes before, the EVs used in this study showed an enhanced uptake in phagocytic cell types after protein corona adsorption. We, therefore, investigated if the high amount of immunoglobulins representing known opsonins would explain the higher uptake. In the 33% DOPE liposome protein corona, we also found immunoglobulins but fewer complement proteins. Instead, apolipoproteins and serum

albumin were enriched, which are known as dysopsonins. However, the dysopsonizing proteins could not ameliorate the opsonizing effect of immunoglobulins. Overall, the protein coronas of 33% DOPE liposomes and EVs had opsonizing properties as cell uptake into phagocytes was increased upon protein corona adsorption.

Comparing our results to Mateos-Maroto et al. also stresses the importance of investigating human plasma-derived protein coronas for targeting human cell lines when developing drug delivery vehicles.[306] In contrast to our results, they found that an FBS-derived protein corona decreased the uptake of liposomes in murine macrophage cells. For liposomes, it has been known for decades that rapid blood clearance is a major problem for clinical applicability, and surface modifications are used to prolong blood circulation times.[220] This is in good accordance with our finding, that the protein corona on non-functionalized liposomes enhances uptake in monocytes. Furthermore, this raises the question if EVs would also need stealth modifications to reach their full delivery potential.

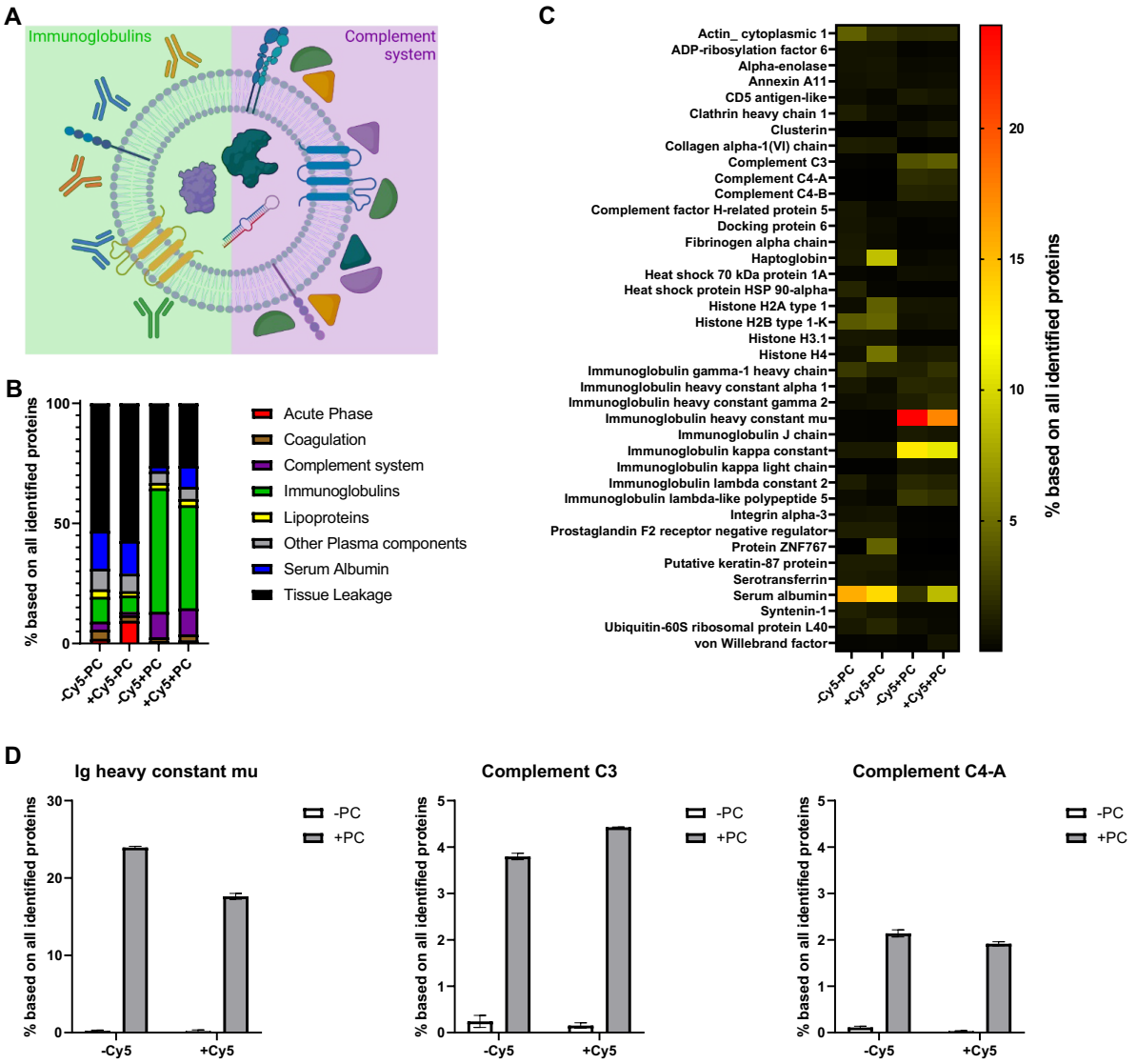

Figure 3.4.9: Proteomic analysis of EV and protein corona composition. This graphic was created with BioRender.com. A. Graphic depiction of enrichment of immunoglobulins and complement system proteins in EV protein corona. B. Assignment of proteins to different biofunctional classes. C. LC-MS revealed the top 20 hard protein corona proteins of EVs with and without Cy5-labeling. Accession numbers of the proteins are in the SI Excel Sheet "AccessionNumber_20MostAbundantProteins.xlsx". D. Enrichment of Ig heavy constant mu, complement C3, and complement C3 in protein corona on EVs with and without Cy5-labeling. The mean and standard deviation of three technical replicates are shown. The EV sample and protein corona preparation were done by me. The LC-MS measurement and analysis was done by [redacted].

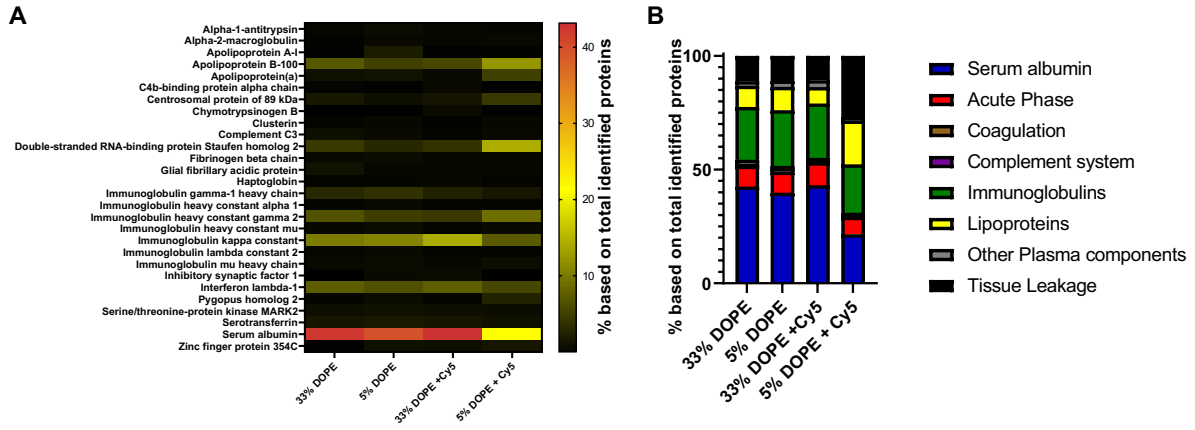

Figure 3.4.10: Analysis of proteins found in liposome hard protein corona. A. LC-MS revealed the top 20 hard protein corona proteins of 33% and 5% DOPE liposomes with and without Cy5-labeling. Accession numbers of the proteins are in the SI Excel Sheet "AccessionNumber_20MostAbundantProteins.xlsx". B. Assignment of proteins to different biofunctional classes. The protein corona preparation was done by me. The LC-MS measurement and analysis was done by [redacted].

As we found immunoglobulins enriched in liposome and EV protein coronas, we intended to test if the enhanced uptake into THP-1 cells is Fc receptor-mediated. Fc receptors are expressed on monocytes and macrophages and are one of the main receptors responsible for the clearance of NPs.[217] The receptor recognizes the Fc region of immunoglobulin G (IgG). Therefore, adsorption of IgGs on NPs can lead to adherence to the cell and ultimately phagocytosis.[307] We therefore blocked cell surface Fc receptors. Subsequently, THP-1 cells were incubated with vesicles at 4°C to avoid turnover of Fc receptors or internalization of vesicles (**Figure 3.4.11**). Interestingly, the mere cell surface binding of liposomes and EVs was higher in the absence of a protein corona. In contrast, internalization of 33% DOPE liposome and EVs was higher in the presence of a protein corona (compare **Figure 3.4.7** and **Figure 3.4.11**). This suggests that binding to the cell surface (at 4°C) and uptake into the cells (at 37°C) is influenced by the presence of proteins differently. This can be explained as binding to the cell surface is determined by the amount of receptors on the cell surface, while uptake is a distinct process and a highly abundant or strongly binding receptor may only be sluggishly taken up while a receptor expressed in low numbers may be rapidly taken up. This also gives a hint that two different uptake mechanisms are responsible for the internalization of liposomes and EVs in the presence and absence of a protein corona. Indeed, it has been previously reported that the presence and composition of the protein corona can influence the uptake mechanisms of NPs at 37°C.[308,309] When Fc receptors were blocked in the absence of a protein corona, we did not observe differences in the binding of vesicles (at 4°C) as expected. In the presence of a protein

corona, we observed a decreased binding of 33% DOPE liposomes when Fc receptors were blocked, determining that for liposomes immunoglobulins in the protein corona contribute to enhanced uptake. In contrast to this, for EVs, we did not observe a reduction of binding in the presence of the Fc receptor block. Therefore, we conclude, that for EVs, Fc receptors seemed not to be prominently involved in cell binding despite the presence of IgGs in the protein corona. This is also a clear difference from the findings for the liposomes. This is an interesting finding as it hints towards a hitherto undetermined receptor responsible for the uptake of protein-coated EVs. For this effect, a wide range of additional receptors could be responsible. In addition to Fc receptors, monocytes exhibit mannose receptors, scavenger receptors, and complement receptors that are capable of recognizing foreign materials.[217,310] They can also recognize phosphatidylserine in the outer leaflet as found in apoptotic cells.[307] This could also be a possible mechanism for the recognition of EVs as they often expose phosphatidylserine on their surface.[311]

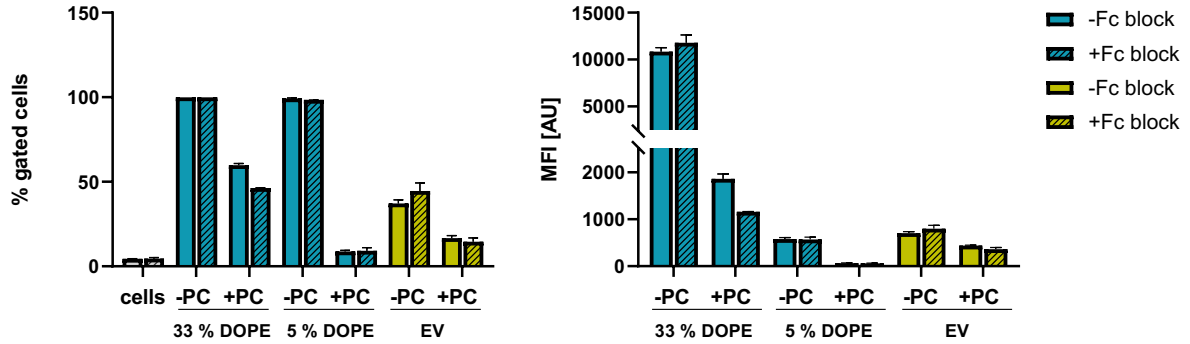

Figure 3.4.11: Binding of liposomes and EVs in the absence and presence of Fc receptor blocking. Flow cytometric analysis of vesicle binding to THP-1 cells after 40 min incubation at 4°C. The MFI value of untreated cells was 234±2.1 AU. This value was subtracted as a background signal from all other values. Means and standard deviations of % gated cells and MFI are shown (n = 3). The EV sample preparation and protein corona preparation was done by me and the Fc blocking experiment was done by [redacted].

3.4.4 Conclusion

The rising field of tumor vaccination also brings tumor-derived exosomes into focus as a vaccination agent. Here, a strong uptake into immune cells such as monocytes is rather favorable as it is expected to facilitate immune response. Enhanced uptake into monocytes, a dendritic cell precursor, could be an advantage for the development of effective anti-tumor vaccines. Therefore, our observations provide important insides into the role of a protein corona for successful uptake in moDCs in the context of immune modulation and tumor vaccination.

In this study, we demonstrate that liposome and EV uptake into phagocytic cells is enhanced in the presence of a protein corona. For 33% DOPE liposomes immunoglobulins were found in the corona as well, presumably mediating at least partially the opsonizing effect by enhanced surface binding. For EVs, this cannot be explained by the enrichment of immunoglobulins as opsonizing proteins, but rather other protein corona components would need to take up this function or the depletion of dysopsonizing proteins like apolipoproteins is responsible for this effect. Our data provide valuable insights into the mode of action of enhanced EV functionality in the presence of a protein corona. Furthermore, our results suggest that for successful vaccination using tumor-derived EVs, the protein corona plays an enhancing role. Generally, this supports the paradigm shift towards corona proteins being an integral part of EV functionality, which is an important step not only for EV research but also for the development of EVs as a drug delivery platform.

4 Conclusion

In vivo targeting of drug nanocarriers remains a major challenge in the field of nanomedicine. This is due to the complexity and highly dynamic nature of the physiological environment a nanocarrier must face during its delivery to the target site. In brief, nanocarriers are exposed to various biofluids that cause the formation of a protein corona, which critically influences its biological behavior. Moreover, this influences the biodistribution of the nanocarrier, which eventually results in unwanted side effects and determines the amount of nanocarrier reaching its target cells. Finally, nanocarriers need to overcome several biological barriers including tissue barriers, the cellular membrane, and intracellular barriers for successful drug delivery. EVs, which are small vesicles secreted by almost all cell types, function as a natural cargo transport system in the human body and are currently being explored as novel drug delivery system.

In the studies presented in this thesis, we addressed different aspects of the usage of EVs as a drug delivery system. In **sections 3.1** and **3.2**, we developed the coating of synthetic NPs with EV membranes as a novel surface functionalization strategy that is capable of meeting the complex requirements of *in vivo* targeting. In **section 3.3**, we investigated the influence of a human plasma protein corona on the exocytosis of synthetic NPs. When aiming to use the cellular EV biogenesis pathway the exocytosis of NPs is a prerequisite for harvesting packaged NPs from cell culture supernatants. In **section 3.4**, we compared the protein corona of EVs to the protein corona of liposomes to investigate the role of the EV protein corona in unwanted uptake by immune cells which can impair the delivery process.

The development of a protocol for coating synthetic SiNC with EV membranes by hijacking the cellular EV biogenesis pathway forms the core of this thesis. Before attempting to coat ultrasmall, weekly-fluorescent SiNC we used larger and highly fluorescent PS-NPs as model NPs to develop a protocol blueprint as reported in **section 3.1**. The packaging of PS-NPs was successfully confirmed by single-particle cLSM. However, this method was not quantitative and had a low resolution. Furthermore, we established the production of pristine EVs from cell culture, which was later used for the production of EVs for studying their protein corona in **section 3.4**. Based on the protocol established in **section 3.1,** we established a protocol for successfully coating SiNCs with an EV membrane as reported in **section 3.2**. To confirm packaging, we

used FCCS instead of cLSM to determine packaging rates. Furthermore, this method is more sensitive and suitable for analyzing the interaction of the binding partners in the nm range. The calculated packaging rates ranged from 3% and 7% for the 5-SiNC PEG and 25-SiNC PEG, respectively. However, as EVs were reported to be highly efficient in the delivery of RNA these packaging rates might be sufficient for a successful treatment. The presented study is a proof-of-principle study that demonstrates the feasibility of this packaging strategy and quantifies packaging for the first time. If proven necessary by functional studies in the future, increasing the packaging rates can be addressed by optimizing the parameters of the cell culture protocol. Another approach would be to use additional purification methods like density gradient ultracentrifugation to select filled from empty EVs or immunoprecipitation to select coated from uncoated SiNC. As a next step, a thorough assessment of *in vitro* and *in vivo* delivery is needed.

To identify further parameters that influence the exocytosis of NPs and hence their exocytosis in EVs, we investigated the influence of the NP protein corona on exocytosis in **section 3.3**. Interestingly, the protein corona increased the exocytosis of SiNP from HCT116 cells in an NP size-dependent manner. Larger SiNPs with a diameter of 100 nm were almost completely exocytosed in the presence of a protein corona, whereas smaller SiNPs were hardly exocytosed in the presence and absence of a protein corona. We even identified that enhanced exocytosis in the presence of a protein corona was accompanied by a decrease of the apolipoproteins E, A1, and B-100. Until now it was only known that the protein corona influences cell uptake. The findings presented here give an insight into the so far unknown relation between protein corona and exocytosis which is of relevance for fundamental research on the protein corona on NPs. This finding has implications for drug delivery as the net drug delivery is determined by endocytosis and exocytosis of the NPs. Furthermore, we identified the protein corona as a parameter influencing the exocytosis of NPs. Thus, the protein corona can be a parameter relevant for the optimization of a packaging protocol as developed in **sections 3.1** and **3.2**. Here, it would be of interest to test, if the protein corona influences exocytosis in general or, if it also influences the specific exocytosis of NPs inside of EVs.

In **section 3.4** we investigated the influence of a human plasma-derived protein corona on EV uptake in immune cells compared to liposomes. We found that the protein corona enhanced the uptake of EVs and liposomes in immune cells. While this may be

beneficial for the use of tumor-derived EVs as a vaccination agent, it impairs the usage of EVs for drug delivery. Our finding is also in good accordance with studies that reported the enrichment of EVs in the liver and spleen, which mainly accommodate immune cells responsible for rapid blood clearance.[222] Our result suggests that additional stealth modifications, as used for liposomes, might also be necessary to improve the drug delivery capability of tumor-derived EVs. This is also emphasized by a study that reported that the PEGylation of EVs increased their blood circulation time.[202] The insights on the influence of the EV protein corona on immune cell uptake and possible blood clearance also have implications on the coating of NPs with EVs as reported in **sections 3.1** and **3.2**. Aside from tumor-specific targeting, the EV membrane coating should improve the overall *in vivo* performance of the hybrid nanocarrier. However, the results presented in this section suggest that NPs coated with HCT116-derived EVs might still be prone to rapid blood clearance and need further modifications. An alternative strategy would be to assess the immune cell uptake of EVs from other cellular sources. Mesenchymal stem cell-derived EVs are eventually less immunogenic as they are derived from a primary cell source and not from a cancer cell line. However, exogenously administered EVs are likely going to be more immunogenic compared to intrinsic EVs in general. Aside from all implications for the usage of EVs as a drug delivery system, the findings presented in this section are highly relevant for fundamental EV biology. The concept of protein corona formation on EVs was introduced to EV research by Tóth et al. in 2021 [212] and since then EV protein corona has been recognized as an integral component mediating important biological functionalities. Our study delivers another set of evidence supporting this paradigm shift.

5 Abbreviations

AF4	asymmetric flow field-flow fractionation
ALIX	ALG-2 interacting protein X
BBB	blood-brain barrier
BSA	bovine serum albumin
CM	conditioned medium
CME	clathrin-mediated endocytosis
COVID-19	corona virus disease 2019
Cy5	cyanine 5
DLS	differential light scattering
DMEM	dulbecco’s Modified Eagle’s Medium
DNA	desoxyribonucleic acid
DOPE	1,2-Dioleoyl-sn-glycero-3-phosphoethanolamine
EDTA	ethylenediaminetetraacetic acid
EPR	enhanced permeation and retention
ESCRT	endosomal sorting complex required for transport
EV	extracellular vesicles
FBS	fetal bovine serum
FCCS	Fluorescence cross-correlative spectroscopy
FDA	Food and Drug Administration
GAPDH	glycolytic enzyme glyceraldehyde-3-phosphate dehydrogenase
GPC1	glypican 1

GPI	glycosylphosphatidylinositol
HCT116	human colorectal tumor 116
HDL	high density lipoprotein
HSP	heat shock proteins
HSV-1	herpes simplex virus type 1
Ig	immunoglobulin
IgG	immunoglobulin G
LNP	lipid nanoparticle
MFI	median fluorescence intensity
miRNAs	microRNAs
moDC	monocyte-derived dendritic cells
MPS	mononuclear phagocyte system
MSC	mesenchymal stem cells
MVB	multivesicular bodies
NC	nanocapsules
NHS	N-hydroxysuccinimide ester
NP	nanoparticle
PEEP	polyethylethylene phosphate
PEG	polyethylene glycol
PLGA	poly lactic-co-glycolic acid
RBC	red blood cell

RBC	red blood cell
RNA	ribonucleic acid
RSV	respiratory syncytial virus
SEC	size exclusion chromatography
SiNC	silica nanocapsules
SiNP	silica nanoparticles
SR-B1	scavenger receptor class B type1
TEM	transmission electron microscopy
TEX	tumor-derived exosomes
TSG101	tumor susceptibility gene 101 protein
UC	ultracentrifugation
VLDL	very low-density lipoprotein

6 References

1. Halwani, A.A. (2022). Development of Pharmaceutical Nanomedicines: From the Bench to the Market. Pharmaceutics *14*. 10.3390/pharmaceutics14010106.
2. Barenholz, Y. (2012). Doxil®--the first FDA-approved nano-drug: lessons learned. J Control Release *160*, 117-134. 10.1016/j.jconrel.2012.03.020.
3. Yadav, T., Kumar, S., Mishra, G., and Saxena, S.K. (2023). Tracking the COVID-19 vaccines: The global landscape. Hum Vaccin Immunother *19*, 2191577. 10.1080/21645515.2023.2191577.
4. Pelaz, B., Alexiou, C., Alvarez-Puebla, R.A., Alves, F., Andrews, A.M., Ashraf, S., Balogh, L.P., Ballerini, L., Bestetti, A., Brendel, C., et al. (2017). Diverse Applications of Nanomedicine. ACS Nano *11*, 2313-2381. 10.1021/acsnano.6b06040.
5. Guan, S., and Rosenecker, J. (2017). Nanotechnologies in delivery of mRNA therapeutics using nonviral vector-based delivery systems. Gene Ther *24*, 133-143. 10.1038/gt.2017.5.
6. Hou, X., Zaks, T., Langer, R., and Dong, Y. (2021). Lipid nanoparticles for mRNA delivery. Nature Reviews Materials *6*, 1078-1094. 10.1038/s41578-021-00358-0.
7. Wu, J. (2021). The Enhanced Permeability and Retention (EPR) Effect: The Significance of the Concept and Methods to Enhance Its Application. J Pers Med *11*. 10.3390/jpm11080771.
8. Gabizon, A., Catane, R., Uziely, B., Kaufman, B., Safra, T., Cohen, R., Martin, F., Huang, A., and Barenholz, Y. (1994). Prolonged Circulation Time and Enhanced Accumulation in Malignant Exudates of Doxorubicin Encapsulated in Polyethylene-glycol Coated Liposomes1. Cancer Research *54*, 987-992.
9. Kranz, L.M., Diken, M., Haas, H., Kreiter, S., Loquai, C., Reuter, K.C., Meng, M., Fritz, D., Vascotto, F., Hefesha, H., et al. (2016). Systemic RNA delivery to dendritic cells exploits antiviral defence for cancer immunotherapy. Nature *534*, 396-401. 10.1038/nature18300.
10. Mitchell, M.J., Billingsley, M.M., Haley, R.M., Wechsler, M.E., Peppas, N.A., and Langer, R. (2021). Engineering precision nanoparticles for drug delivery. Nature Reviews Drug Discovery *20*, 101-124. 10.1038/s41573-020-0090-8.
11. Dong, Y., and Shannon, C. (2000). Heterogeneous Immunosensing Using Antigen and Antibody Monolayers on Gold Surfaces with Electrochemical and Scanning Probe Detection. Analytical Chemistry *72*, 2371-2376. 10.1021/ac991450g.

12. Khan, Y.S., and Farhana, A. (2024). Histology, Cell. In StatPearls, (StatPearls Publishing

Copyright © 2024, StatPearls Publishing LLC.).

13. Nolte-'t Hoen, E., Cremer, T., Gallo, R.C., and Margolis, L.B. (2016). Extracellular vesicles and viruses: Are they close relatives? Proceedings of the National Academy of Sciences *113*, 9155-9161. 10.1073/pnas.1605146113.

14. Sousa de Almeida, M., Susnik, E., Drasler, B., Taladriz-Blanco, P., Petri-Fink, A., and Rothen-Rutishauser, B. (2021). Understanding nanoparticle endocytosis to improve targeting strategies in nanomedicine. Chem Soc Rev *50*, 5397-5434. 10.1039/d0cs01127d.

15. Alshatwi, A.A., Subbarayan, P.V., Ramesh, E., Al-Hazzani, A.A., Alsaif, M.A., and Alwarthan, A.A. (2013). Aluminium oxide nanoparticles induce mitochondrial-mediated oxidative stress and alter the expression of antioxidant enzymes in human mesenchymal stem cells. Food Addit Contam Part A Chem Anal Control Expo Risk Assess *30*, 1-10. 10.1080/19440049.2012.729160.

16. Senapati, V.A., Kumar, A., Gupta, G.S., Pandey, A.K., and Dhawan, A. (2015). ZnO nanoparticles induced inflammatory response and genotoxicity in human blood cells: A mechanistic approach. Food Chem Toxicol *85*, 61-70. 10.1016/j.fct.2015.06.018.

17. Yuan, X., Nie, W., He, Z., Yang, J., Shao, B., Ma, X., Zhang, X., Bi, Z., Sun, L., Liang, X., et al. (2020). Carbon black nanoparticles induce cell necrosis through lysosomal membrane permeabilization and cause subsequent inflammatory response. Theranostics *10*, 4589-4605. 10.7150/thno.34065.

18. Shin, T.H., Seo, C., Lee, D.Y., Ji, M., Manavalan, B., Basith, S., Chakkarapani, S.K., Kang, S.H., Lee, G., Paik, M.J., and Park, C.B. (2019). Silica-coated magnetic nanoparticles induce glucose metabolic dysfunction in vitro via the generation of reactive oxygen species. Arch Toxicol *93*, 1201-1212. 10.1007/s00204-019-02402-z.

19. Banik, B.L., Fattahi, P., and Brown, J.L. (2016). Polymeric nanoparticles: the future of nanomedicine. WIREs Nanomedicine and Nanobiotechnology *8*, 271-299. https://doi.org/10.1002/wnan.1364.

20. Rideau, E., Dimova, R., Schwille, P., Wurm, F.R., and Landfester, K. (2018). Liposomes and polymersomes: a comparative review towards cell mimicking. Chemical Society Reviews *47*, 8572-8610. 10.1039/C8CS00162F.

21. Ahmed, F., Pakunlu, R.I., Srinivas, G., Brannan, A., Bates, F., Klein, M.L., Minko, T., and Discher, D.E. (2006). Shrinkage of a rapidly growing tumor by drug-loaded

polymersomes: pH-triggered release through copolymer degradation. Mol Pharm *3*, 340-350. 10.1021/mp050103u.

22. Bobo, D., Robinson, K.J., Islam, J., Thurecht, K.J., and Corrie, S.R. (2016). Nanoparticle-Based Medicines: A Review of FDA-Approved Materials and Clinical Trials to Date. Pharm Res *33*, 2373-2387. 10.1007/s11095-016-1958-5.
23. Janjua, T.I., Cao, Y., Yu, C., and Popat, A. (2021). Clinical translation of silica nanoparticles. Nature Reviews Materials *6*, 1072-1074. 10.1038/s41578-021-00385-x.
24. Taleghani, A.S., Nakhjiri, A.T., Khakzad, M.J., Rezayat, S.M., Ebrahimnejad, P., Heydarinasab, A., Akbarzadeh, A., and Marjani, A. (2021). Mesoporous silica nanoparticles as a versatile nanocarrier for cancer treatment: A review. Journal of Molecular Liquids *328*, 115417. https://doi.org/10.1016/j.molliq.2021.115417.
25. Janjua, T.I., Cao, Y., Kleitz, F., Linden, M., Yu, C., and Popat, A. (2023). Silica nanoparticles: A review of their safety and current strategies to overcome biological barriers. Advanced Drug Delivery Reviews *203*, 115115. https://doi.org/10.1016/j.addr.2023.115115.
26. Anselmo, A.C., and Mitragotri, S. (2019). Nanoparticles in the clinic: An update. Bioeng Transl Med *4*, e10143. 10.1002/btm2.10143.
27. Sarfraz, M., Afzal, A., Yang, T., Gai, Y., Raza, S.M., Khan, M.W., Cheng, Y., Ma, X., and Xiang, G. (2018). Development of Dual Drug Loaded Nanosized Liposomal Formulation by A Reengineered Ethanolic Injection Method and Its Pre-Clinical Pharmacokinetic Studies. Pharmaceutics *10*. 10.3390/pharmaceutics10030151.
28. Cheng, X., and Lee, R.J. (2016). The role of helper lipids in lipid nanoparticles (LNPs) designed for oligonucleotide delivery. Adv Drug Deliv Rev *99*, 129-137. 10.1016/j.addr.2016.01.022.
29. Piradashvili, K., Fichter, M., Mohr, K., Gehring, S., Wurm, F.R., and Landfester, K. (2015). Biodegradable protein nanocontainers. Biomacromolecules *16*, 815-821. 10.1021/bm5016915.
30. Brückner, M., Simon, J., Jiang, S., Landfester, K., and Mailänder, V. (2020). Preparation of the protein corona: How washing shapes the proteome and influences cellular uptake of nanocarriers. Acta Biomater *114*, 333-342. 10.1016/j.actbio.2020.07.041.
31. Simon, J., Kuhn, G., Fichter, M., Gehring, S., Landfester, K., and Mailänder, V. (2021). Unraveling the In Vivo Protein Corona. Cells *10*. 10.3390/cells10010132.

32. Vroman, L. (1962). Effect of Adsorbed Proteins on the Wettability of Hydrophilic and Hydrophobic Solids. Nature *196*, 476-477. 10.1038/196476a0.
33. Vroman, L., Adams, A.L., Fischer, G.C., and Munoz, P.C. (1980). Interaction of high molecular weight kininogen, factor XII, and fibrinogen in plasma at interfaces. Blood *55*, 156-159.
34. Casals, E., Pfaller, T., Duschl, A., Oostingh, G.J., and Puntes, V. (2010). Time evolution of the nanoparticle protein corona. ACS Nano *4*, 3623-3632. 10.1021/nn901372t.
35. Tenzer, S., Docter, D., Kuharev, J., Musyanovych, A., Fetz, V., Hecht, R., Schlenk, F., Fischer, D., Kiouptsi, K., Reinhardt, C., et al. (2013). Rapid formation of plasma protein corona critically affects nanoparticle pathophysiology. Nat Nanotechnol *8*, 772-781. 10.1038/nnano.2013.181.
36. Walczyk, D., Bombelli, F.B., Monopoli, M.P., Lynch, I., and Dawson, K.A. (2010). What the Cell "Sees" in Bionanoscience. Journal of the American Chemical Society *132*, 5761-5768. 10.1021/ja910675v.
37. Lundqvist, M., Stigler, J., Cedervall, T., Berggård, T., Flanagan, M.B., Lynch, I., Elia, G., and Dawson, K. (2011). The Evolution of the Protein Corona around Nanoparticles: A Test Study. ACS Nano *5*, 7503-7509. 10.1021/nn202458g.
38. Monopoli, M.P., Åberg, C., Salvati, A., and Dawson, K.A. (2012). Biomolecular coronas provide the biological identity of nanosized materials. Nature Nanotechnology *7*, 779-786. 10.1038/nnano.2012.207.
39. da Costa Marques, R., Hüppe, N., Speth, K.R., Oberländer, J., Lieberwirth, I., Landfester, K., and Mailänder, V. (2023). Proteomics reveals time-dependent protein corona changes in the intracellular pathway. Acta Biomater *172*, 355-368. 10.1016/j.actbio.2023.10.010.
40. Milani, S., Baldelli Bombelli, F., Pitek, A.S., Dawson, K.A., and Rädler, J. (2012). Reversible versus Irreversible Binding of Transferrin to Polystyrene Nanoparticles: Soft and Hard Corona. ACS Nano *6*, 2532-2541. 10.1021/nn204951s.
41. Ke, P.C., Lin, S., Parak, W.J., Davis, T.P., and Caruso, F. (2017). A Decade of the Protein Corona. ACS Nano *11*, 11773-11776. 10.1021/acsnano.7b08008.
42. Nel, A.E., Mädler, L., Velegol, D., Xia, T., Hoek, E.M.V., Somasundaran, P., Klaessig, F., Castranova, V., and Thompson, M. (2009). Understanding biophysicochemical interactions at the nano–bio interface. Nature Materials *8*, 543-557. 10.1038/nmat2442.

43. Hühn, D., Kantner, K., Geidel, C., Brandholt, S., De Cock, I., Soenen, S.J., Rivera Gil, P., Montenegro, J.M., Braeckmans, K., Müllen, K., et al. (2013). Polymer-coated nanoparticles interacting with proteins and cells: focusing on the sign of the net charge. ACS Nano *7*, 3253-3263. 10.1021/nn3059295.

44. Walkey, C.D., Olsen, J.B., Guo, H., Emili, A., and Chan, W.C.W. (2012). Nanoparticle Size and Surface Chemistry Determine Serum Protein Adsorption and Macrophage Uptake. Journal of the American Chemical Society *134*, 2139-2147. 10.1021/ja2084338.

45. Gagner, J.E., Lopez, M.D., Dordick, J.S., and Siegel, R.W. (2011). Effect of gold nanoparticle morphology on adsorbed protein structure and function. Biomaterials *32*, 7241-7252. 10.1016/j.biomaterials.2011.05.091.

46. Tenzer, S., Docter, D., Rosfa, S., Wlodarski, A., Kuharev, J., Rekik, A., Knauer, S.K., Bantz, C., Nawroth, T., Bier, C., et al. (2011). Nanoparticle Size Is a Critical Physicochemical Determinant of the Human Blood Plasma Corona: A Comprehensive Quantitative Proteomic Analysis. ACS Nano *5*, 7155-7167. 10.1021/nn201950e.

47. Walkey, C.D., and Chan, W.C.W. (2012). Understanding and controlling the interaction of nanomaterials with proteins in a physiological environment. Chemical Society Reviews *41*, 2780-2799. 10.1039/C1CS15233E.

48. Cedervall, T., Lynch, I., Lindman, S., Berggård, T., Thulin, E., Nilsson, H., Dawson, K.A., and Linse, S. (2007). Understanding the nanoparticle–protein corona using methods to quantify exchange rates and affinities of proteins for nanoparticles. Proceedings of the National Academy of Sciences *104*, 2050-2055. 10.1073/pnas.0608582104.

49. Ghosh, G., and Panicker, L. (2021). Protein–nanoparticle interactions and a new insight. Soft Matter *17*, 3855-3875. 10.1039/D0SM02050H.

50. Li, S.-D., and Huang, L. (2008). Pharmacokinetics and Biodistribution of Nanoparticles. Molecular Pharmaceutics *5*, 496-504. 10.1021/mp800049w.

51. Ngo, W., Ahmed, S., Blackadar, C., Bussin, B., Ji, Q., Mladjenovic, S.M., Sepahi, Z., and Chan, W.C.W. (2022). Why nanoparticles prefer liver macrophage cell uptake in vivo. Advanced Drug Delivery Reviews *185*, 114238. https://doi.org/10.1016/j.addr.2022.114238.

52. Klibanov, A.L., Maruyama, K., Torchilin, V.P., and Huang, L. (1990). Amphipathic polyethyleneglycols effectively prolong the circulation time of liposomes. FEBS Lett *268*, 235-237. 10.1016/0014-5793(90)81016-h.

53. Perrault, S.D., Walkey, C., Jennings, T., Fischer, H.C., and Chan, W.C. (2009). Mediating tumor targeting efficiency of nanoparticles through design. Nano Lett *9*, 1909-1915. 10.1021/nl900031y.

54. Gref, R., Lück, M., Quellec, P., Marchand, M., Dellacherie, E., Harnisch, S., Blunk, T., and Müller, R.H. (2000). 'Stealth' corona-core nanoparticles surface modified by polyethylene glycol (PEG): influences of the corona (PEG chain length and surface density) and of the core composition on phagocytic uptake and plasma protein adsorption. Colloids and Surfaces B: Biointerfaces *18*, 301-313. https://doi.org/10.1016/S0927-7765(99)00156-3.

55. Ma, K., Sai, H., and Wiesner, U. (2012). Ultrasmall Sub-10 nm Near-Infrared Fluorescent Mesoporous Silica Nanoparticles. Journal of the American Chemical Society *134*, 13180-13183. 10.1021/ja3049783.

56. Schöttler, S., Becker, G., Winzen, S., Steinbach, T., Mohr, K., Landfester, K., Mailänder, V., and Wurm, F.R. (2016). Protein adsorption is required for stealth effect of poly(ethylene glycol)- and poly(phosphoester)-coated nanocarriers. Nature Nanotechnology *11*, 372-377. 10.1038/nnano.2015.330.

57. Bertrand, N., and Leroux, J.C. (2012). The journey of a drug-carrier in the body: an anatomo-physiological perspective. J Control Release *161*, 152-163. 10.1016/j.jconrel.2011.09.098.

58. Ishida, T., Ichihara, M., Wang, X., Yamamoto, K., Kimura, J., Majima, E., and Kiwada, H. (2006). Injection of PEGylated liposomes in rats elicits PEG-specific IgM, which is responsible for rapid elimination of a second dose of PEGylated liposomes. J Control Release *112*, 15-25. 10.1016/j.jconrel.2006.01.005.

59. Shah, S., Prematta, T., Adkinson, N.F., and Ishmael, F.T. (2013). Hypersensitivity to polyethylene glycols. J Clin Pharmacol *53*, 352-355. 10.1177/0091270012447122.

60. Zhao, J., and Stenzel, M.H. (2018). Entry of nanoparticles into cells: the importance of nanoparticle properties. Polymer Chemistry *9*, 259-272. 10.1039/C7PY01603D.

61. Wang, T., Bai, J., Jiang, X., and Nienhaus, G.U. (2012). Cellular uptake of nanoparticles by membrane penetration: a study combining confocal microscopy with FTIR spectroelectrochemistry. ACS Nano *6*, 1251-1259. 10.1021/nn203892h.

62. Yang, N.J., and Hinner, M.J. (2015). Getting across the cell membrane: an overview for small molecules, peptides, and proteins. Methods Mol Biol *1266*, 29-53. 10.1007/978-1-4939-2272-7_3.

63. Doherty, G.J., and McMahon, H.T. (2009). Mechanisms of endocytosis. Annu Rev Biochem *78*, 857-902. 10.1146/annurev.biochem.78.081307.110540.

64. Gordon, S. (2016). Phagocytosis: An Immunobiologic Process. Immunity *44*, 463-475. 10.1016/j.immuni.2016.02.026.

65. May, R.C., and Machesky, L.M. (2001). Phagocytosis and the actin cytoskeleton. J Cell Sci *114*, 1061-1077. 10.1242/jcs.114.6.1061.

66. Levine, B., Mizushima, N., and Virgin, H.W. (2011). Autophagy in immunity and inflammation. Nature *469*, 323-335. 10.1038/nature09782.

67. Segawa, K., and Nagata, S. (2015). An Apoptotic 'Eat Me' Signal: Phosphatidylserine Exposure. Trends Cell Biol *25*, 639-650. 10.1016/j.tcb.2015.08.003.

68. Wilson, G.J., Marakalala, M.J., Hoving, J.C., van Laarhoven, A., Drummond, R.A., Kerscher, B., Keeton, R., van de Vosse, E., Ottenhoff, T.H., Plantinga, T.S., et al. (2015). The C-type lectin receptor CLECSF8/CLEC4D is a key component of anti-mycobacterial immunity. Cell Host Microbe *17*, 252-259. 10.1016/j.chom.2015.01.004.

69. Nishijima, N., Hirai, T., Misato, K., Aoyama, M., Kuroda, E., Ishii, K.J., Higashisaka, K., Yoshioka, Y., and Tsutsumi, Y. (2017). Human Scavenger Receptor A1-Mediated Inflammatory Response to Silica Particle Exposure Is Size Specific. Front Immunol *8*, 379. 10.3389/fimmu.2017.00379.

70. Song, G., Petschauer, J.S., Madden, A.J., and Zamboni, W.C. (2014). Nanoparticles and the mononuclear phagocyte system: pharmacokinetics and applications for inflammatory diseases. Curr Rheumatol Rev *10*, 22-34. 10.2174/1573403x10666140914160554.

71. Canton, I., and Battaglia, G. (2012). Endocytosis at the nanoscale. Chemical Society Reviews *41*, 2718-2739. 10.1039/C2CS15309B.

72. Swanson, J.A., and Watts, C. (1995). Macropinocytosis. Trends in Cell Biology *5*, 424-428. https://doi.org/10.1016/S0962-8924(00)89101-1.

73. Reifarth, M., Hoeppener, S., and Schubert, U.S. (2018). Uptake and Intracellular Fate of Engineered Nanoparticles in Mammalian Cells: Capabilities and Limitations of Transmission Electron Microscopy—Polymer-Based Nanoparticles. Advanced Materials *30*, 1703704. https://doi.org/10.1002/adma.201703704.

74. Gao, H., Shi, W., and Freund, L.B. (2005). Mechanics of receptor-mediated endocytosis. Proceedings of the National Academy of Sciences *102*, 9469-9474. 10.1073/pnas.0503879102.

75. McMahon, H.T., and Boucrot, E. (2011). Molecular mechanism and physiological functions of clathrin-mediated endocytosis. Nature Reviews Molecular Cell Biology *12*, 517-533. 10.1038/nrm3151.

76. Rejman, J., Oberle, V., Zuhorn, I.S., and Hoekstra, D. (2004). Size-dependent internalization of particles via the pathways of clathrin- and caveolae-mediated endocytosis. Biochem J *377*, 159-169. 10.1042/bj20031253.

77. Rennick, J.J., Johnston, A.P.R., and Parton, R.G. (2021). Key principles and methods for studying the endocytosis of biological and nanoparticle therapeutics. Nature Nanotechnology *16*, 266-276. 10.1038/s41565-021-00858-8.

78. Jovic, M., Sharma, M., Rahajeng, J., and Caplan, S. (2010). The early endosome: a busy sorting station for proteins at the crossroads. Histol Histopathol *25*, 99-112. 10.14670/hh-25.99.

79. Huotari, J., and Helenius, A. (2011). Endosome maturation. Embo j *30*, 3481-3500. 10.1038/emboj.2011.286.

80. Donahue, N.D., Acar, H., and Wilhelm, S. (2019). Concepts of nanoparticle cellular uptake, intracellular trafficking, and kinetics in nanomedicine. Adv Drug Deliv Rev *143*, 68-96. 10.1016/j.addr.2019.04.008.

81. Fullstone, G., Nyberg, S., Tian, X., and Battaglia, G. (2016). Chapter Two - From the Blood to the Central Nervous System: A Nanoparticle's Journey Through the Blood–Brain Barrier by Transcytosis. In International Review of Neurobiology, K.T. Al-Jamal, ed. (Academic Press), pp. 41-72. https://doi.org/10.1016/bs.irn.2016.06.001.

82. Lönn, P., Kacsinta, A.D., Cui, X.-S., Hamil, A.S., Kaulich, M., Gogoi, K., and Dowdy, S.F. (2016). Enhancing Endosomal Escape for Intracellular Delivery of Macromolecular Biologic Therapeutics. Scientific Reports *6*, 32301. 10.1038/srep32301.

83. Ho, L.W.C., Chan, C.K.W., Han, R., Lau, Y.F.Y., Li, H., Ho, Y.-P., Zhuang, X., and Choi, C.H.J. (2022). Mammalian Cells Exocytose Alkylated Gold Nanoparticles via Extracellular Vesicles. ACS Nano *16*, 2032-2045. 10.1021/acsnano.1c07418.

84. Yong, T., Zhang, X., Bie, N., Zhang, H., Zhang, X., Li, F., Hakeem, A., Hu, J., Gan, L., Santos, H.A., and Yang, X. (2019). Tumor exosome-based nanoparticles are efficient drug carriers for chemotherapy. Nature Communications *10*, 3838. 10.1038/s41467-019-11718-4.

85. Sahay, G., Querbes, W., Alabi, C., Eltoukhy, A., Sarkar, S., Zurenko, C., Karagiannis, E., Love, K., Chen, D., Zoncu, R., et al. (2013). Efficiency of siRNA delivery by lipid

nanoparticles is limited by endocytic recycling. Nature Biotechnology *31*, 653-658. 10.1038/nbt.2614.

86. Yanes, R.E., Tarn, D., Hwang, A.A., Ferris, D.P., Sherman, S.P., Thomas, C.R., Lu, J., Pyle, A.D., Zink, J.I., and Tamanoi, F. (2013). Involvement of Lysosomal Exocytosis in the Excretion of Mesoporous Silica Nanoparticles and Enhancement of the Drug Delivery Effect by Exocytosis Inhibition. Small *9*, 697-704. https://doi.org/10.1002/smll.201201811.
87. Li, Y., and Ju, D. (2018). The Role of Autophagy in Nanoparticles-Induced Toxicity and Its Related Cellular and Molecular Mechanisms. In Cellular and Molecular Toxicology of Nanoparticles, Q. Saquib, M. Faisal, A.A. Al-Khedhairy, and A.A. Alatar, eds. (Springer International Publishing), pp. 71-84. 10.1007/978-3-319-72041-8_5.
88. Mehrpour, M., Esclatine, A., Beau, I., and Codogno, P. (2010). Overview of macroautophagy regulation in mammalian cells. Cell Research *20*, 748-762. 10.1038/cr.2010.82.
89. Fader, C.M., and Colombo, M.I. (2009). Autophagy and multivesicular bodies: two closely related partners. Cell Death & Differentiation *16*, 70-78. 10.1038/cdd.2008.168.
90. Kaczmarek, J.C., Kauffman, K.J., Fenton, O.S., Sadtler, K., Patel, A.K., Heartlein, M.W., DeRosa, F., and Anderson, D.G. (2018). Optimization of a Degradable Polymer–Lipid Nanoparticle for Potent Systemic Delivery of mRNA to the Lung Endothelium and Immune Cells. Nano Letters *18*, 6449-6454. 10.1021/acs.nanolett.8b02917.
91. Simon, J., Müller, L.K., Kokkinopoulou, M., Lieberwirth, I., Morsbach, S., Landfester, K., and Mailänder, V. (2018). Exploiting the biomolecular corona: pre-coating of nanoparticles enables controlled cellular interactions. Nanoscale *10*, 10731-10739. 10.1039/c8nr03331e.
92. Schöttler, S., Becker, G., Winzen, S., Steinbach, T., Mohr, K., Landfester, K., Mailänder, V., and Wurm, F.R. (2016). Protein adsorption is required for stealth effect of poly(ethylene glycol)- and poly(phosphoester)-coated nanocarriers. Nat Nanotechnol *11*, 372-377. 10.1038/nnano.2015.330.
93. Tonigold, M., Simon, J., Estupiñán, D., Kokkinopoulou, M., Reinholz, J., Kintzel, U., Kaltbeitzel, A., Renz, P., Domogalla, M.P., Steinbrink, K., et al. (2018). Pre-

adsorption of antibodies enables targeting of nanocarriers despite a biomolecular corona. Nature Nanotechnology *13*, 862-869. 10.1038/s41565-018-0171-6.

94. Lin, X., O'Reilly Beringhs, A., and Lu, X. (2021). Applications of Nanoparticle-Antibody Conjugates in Immunoassays and Tumor Imaging. Aaps j *23*, 43. 10.1208/s12248-021-00561-5.
95. Brückner, M., Fichter, M., da Costa Marques, R., Landfester, K., and Mailänder, V. (2022). PEG Spacer Length Substantially Affects Antibody-Based Nanocarrier Targeting of Dendritic Cell Subsets. Pharmaceutics *14*. 10.3390/pharmaceutics14081614.
96. Lee, Y.H., Medhi, H., Liu, X., Ha, I.H., Nam, K.T., and Ploegh, H. (2023). Selective Targeting of Nanobody-Modified Gold Nanoparticles to Distinct Cell Types. ACS Applied Materials & Interfaces *15*, 59258-59268. 10.1021/acsami.3c16829.
97. Todaro, B., Ottalagana, E., Luin, S., and Santi, M. (2023). Targeting Peptides: The New Generation of Targeted Drug Delivery Systems. Pharmaceutics *15*. 10.3390/pharmaceutics15061648.
98. Miller, N.L., Clark, T., Raman, R., and Sasisekharan, R. (2021). Glycans in Virus-Host Interactions: A Structural Perspective. Front Mol Biosci *8*, 666756. 10.3389/fmolb.2021.666756.
99. Ghitman, J., Pircalabioru, G.G., Zainea, A., Marutescu, L., Iovu, H., Vasile, E., Stavarache, C., Vasile, B.S., and Stan, R. (2022). Macrophage-targeted mannose-decorated PLGA-vegetable oil hybrid nanoparticles loaded with anti-inflammatory agents. Colloids and Surfaces B: Biointerfaces *213*, 112423. https://doi.org/10.1016/j.colsurfb.2022.112423.
100. Hatami, E., Mu, Y., Shields, D.N., Chauhan, S.C., Kumar, S., Cory, T.J., and Yallapu, M.M. (2019). Mannose-decorated hybrid nanoparticles for enhanced macrophage targeting. Biochem Biophys Rep *17*, 197-207. 10.1016/j.bbrep.2019.01.007.
101. Singodia, D., Verma, A., Verma, R.K., and Mishra, P.R. (2012). Investigations into an alternate approach to target mannose receptors on macrophages using 4-sulfated N-acetyl galactosamine more efficiently in comparison with mannose-decorated liposomes: an application in drug delivery. Nanomedicine: Nanotechnology, Biology and Medicine *8*, 468-477. https://doi.org/10.1016/j.nano.2011.07.002.
102. Daniels, T.R., Bernabeu, E., Rodríguez, J.A., Patel, S., Kozman, M., Chiappetta, D.A., Holler, E., Ljubimova, J.Y., Helguera, G., and Penichet, M.L. (2012). The transferrin

receptor and the targeted delivery of therapeutic agents against cancer. Biochim Biophys Acta *1820*, 291-317. 10.1016/j.bbagen.2011.07.016.

103. Jose, S., A, C.T., Sebastian, R., H, S.M., A, A.N., Durazzo, A., Lucarini, M., Santini, A., and Souto, E.B. (2019). Transferrin-Conjugated Docetaxel-PLGA Nanoparticles for Tumor Targeting: Influence on MCF-7 Cell Cycle. Polymers (Basel) *11*. 10.3390/polym11111905.
104. Assaraf, Y.G., Leamon, C.P., and Reddy, J.A. (2014). The folate receptor as a rational therapeutic target for personalized cancer treatment. Drug Resist Updat *17*, 89-95. 10.1016/j.drup.2014.10.002.
105. Yan, Y., Dong, Y., Yue, S., Qiu, X., Sun, H., and Zhong, Z. (2019). Dually Active Targeting Nanomedicines Based on a Direct Conjugate of Two Purely Natural Ligands for Potent Chemotherapy of Ovarian Tumors. ACS Applied Materials & Interfaces *11*, 46548-46557. 10.1021/acsami.9b17223.
106. Meng, S., Su, B., Li, W., Ding, Y., Tang, L., Zhou, W., Song, Y., Li, H., and Zhou, C. (2010). Enhanced antitumor effect of novel dual-targeted paclitaxel liposomes. Nanotechnology *21*, 415103. 10.1088/0957-4484/21/41/415103.
107. Hu, C.-M.J., Zhang, L., Aryal, S., Cheung, C., Fang, R.H., and Zhang, L. (2011). Erythrocyte membrane-camouflaged polymeric nanoparticles as a biomimetic delivery platform. Proceedings of the National Academy of Sciences *108*, 10980-10985. 10.1073/pnas.1106634108.
108. Hu, C.-M.J., Fang, R.H., Luk, B.T., Chen, K.N.H., Carpenter, C., Gao, W., Zhang, K., and Zhang, L. (2013). 'Marker-of-self' functionalization of nanoscale particles through a top-down cellular membrane coating approach. Nanoscale *5*, 2664-2668. 10.1039/C3NR00015J.
109. Oldenborg, P.A., Zheleznyak, A., Fang, Y.F., Lagenaur, C.F., Gresham, H.D., and Lindberg, F.P. (2000). Role of CD47 as a marker of self on red blood cells. Science *288*, 2051-2054. 10.1126/science.288.5473.2051.
110. Parodi, A., Quattrocchi, N., van de Ven, A.L., Chiappini, C., Evangelopoulos, M., Martinez, J.O., Brown, B.S., Khaled, S.Z., Yazdi, I.K., Enzo, M.V., et al. (2013). Synthetic nanoparticles functionalized with biomimetic leukocyte membranes possess cell-like functions. Nature Nanotechnology *8*, 61-68. 10.1038/nnano.2012.212.
111. Rao, L., Bu, L.-L., Cai, B., Xu, J.-H., Li, A., Zhang, W.-F., Sun, Z.-J., Guo, S.-S., Liu, W., Wang, T.-H., and Zhao, X.-Z. (2016). Cancer Cell Membrane-Coated

Upconversion Nanoprobes for Highly Specific Tumor Imaging. Advanced Materials *28*, 3460-3466. https://doi.org/10.1002/adma.201506086.

112. Dumontel, B., Jiménez-Jiménez, C., Vallet-Regí, M., and Manzano, M. (2023). Bioinspired extracellular vesicle-coated silica nanoparticles as selective delivery systems. Materials Today Bio *23*, 100850. https://doi.org/10.1016/j.mtbio.2023.100850.
113. Colombo, M., Raposo, G., and Théry, C. (2014). Biogenesis, Secretion, and Intercellular Interactions of Exosomes and Other Extracellular Vesicles. Annual Review of Cell and Developmental Biology *30*, 255-289. 10.1146/annurev-cellbio-101512-122326.
114. Heijnen, H.F.G., Schiel, A.E., Fijnheer, R., Geuze, H.J., and Sixma, J.J. (1999). Activated Platelets Release Two Types of Membrane Vesicles: Microvesicles by Surface Shedding and Exosomes Derived From Exocytosis of Multivesicular Bodies and α-Granules. Blood *94*, 3791-3799. https://doi.org/10.1182/blood.V94.11.3791.
115. Yu, L., Zhu, G., Zhang, Z., Yu, Y., Zeng, L., Xu, Z., Weng, J., Xia, J., Li, J., and Pathak, J.L. (2023). Apoptotic bodies: bioactive treasure left behind by the dying cells with robust diagnostic and therapeutic application potentials. Journal of Nanobiotechnology *21*, 218. 10.1186/s12951-023-01969-1.
116. S, E.L.A., Mäger, I., Breakefield, X.O., and Wood, M.J. (2013). Extracellular vesicles: biology and emerging therapeutic opportunities. Nat Rev Drug Discov *12*, 347-357. 10.1038/nrd3978.
117. van Niel, G., D'Angelo, G., and Raposo, G. (2018). Shedding light on the cell biology of extracellular vesicles. Nature Reviews Molecular Cell Biology *19*, 213-228. 10.1038/nrm.2017.125.
118. Charrin, S., Jouannet, S., Boucheix, C., and Rubinstein, E. (2014). Tetraspanins at a glance. J Cell Sci *127*, 3641-3648. 10.1242/jcs.154906.
119. van Niel, G., Charrin, S., Simoes, S., Romao, M., Rochin, L., Saftig, P., Marks, M.S., Rubinstein, E., and Raposo, G. (2011). The tetraspanin CD63 regulates ESCRT-independent and -dependent endosomal sorting during melanogenesis. Dev Cell *21*, 708-721. 10.1016/j.devcel.2011.08.019.
120. Hoshino, A., Costa-Silva, B., Shen, T.-L., Rodrigues, G., Hashimoto, A., Tesic Mark, M., Molina, H., Kohsaka, S., Di Giannatale, A., Ceder, S., et al. (2015). Tumour exosome integrins determine organotropic metastasis. Nature *527*, 329-335. 10.1038/nature15756.

121. Morelli, A.E., Larregina, A.T., Shufesky, W.J., Sullivan, M.L., Stolz, D.B., Papworth, G.D., Zahorchak, A.F., Logar, A.J., Wang, Z., Watkins, S.C., et al. (2004). Endocytosis, intracellular sorting, and processing of exosomes by dendritic cells. Blood *104*, 3257-3266. 10.1182/blood-2004-03-0824.

122. Schorey, J.S., Cheng, Y., Singh, P.P., and Smith, V.L. (2015). Exosomes and other extracellular vesicles in host-pathogen interactions. EMBO Rep *16*, 24-43. 10.15252/embr.201439363.

123. Song, Y.-x., Li, X., Nie, S.-d., Hu, Z.-x., Zhou, D., Sun, D.-y., Zhou, G.-y., Wang, Y., Liu, J.-j., Song, T., and Wang, S. (2023). Extracellular vesicles released by glioma cells are decorated by Annexin A2 allowing for cellular uptake via heparan sulfate. Cancer Gene Therapy *30*, 1156-1166. 10.1038/s41417-023-00627-w.

124. Baietti, M.F., Zhang, Z., Mortier, E., Melchior, A., Degeest, G., Geeraerts, A., Ivarsson, Y., Depoortere, F., Coomans, C., Vermeiren, E., et al. (2012). Syndecan-syntenin-ALIX regulates the biogenesis of exosomes. Nat Cell Biol *14*, 677-685. 10.1038/ncb2502.

125. Dar, G.H., Mendes, C.C., Kuan, W.-L., Speciale, A.A., Conceição, M., Görgens, A., Uliyakina, I., Lobo, M.J., Lim, W.F., El Andaloussi, S., et al. (2021). GAPDH controls extracellular vesicle biogenesis and enhances the therapeutic potential of EV mediated siRNA delivery to the brain. Nature Communications *12*, 6666. 10.1038/s41467-021-27056-3.

126. Géminard, C., De Gassart, A., Blanc, L., and Vidal, M. (2004). Degradation of AP2 during reticulocyte maturation enhances binding of hsc70 and Alix to a common site on TFR for sorting into exosomes. Traffic *5*, 181-193. 10.1111/j.1600-0854.2004.0167.x.

127. Théry, C., Boussac, M., Véron, P., Ricciardi-Castagnoli, P., Raposo, G., Garin, J., and Amigorena, S. (2001). Proteomic analysis of dendritic cell-derived exosomes: a secreted subcellular compartment distinct from apoptotic vesicles. J Immunol *166*, 7309-7318. 10.4049/jimmunol.166.12.7309.

128. Valadi, H., Ekström, K., Bossios, A., Sjöstrand, M., Lee, J.J., and Lötvall, J.O. (2007). Exosome-mediated transfer of mRNAs and microRNAs is a novel mechanism of genetic exchange between cells. Nature Cell Biology *9*, 654-659. 10.1038/ncb1596.

129. Kahlert, C., Melo, S.A., Protopopov, A., Tang, J., Seth, S., Koch, M., Zhang, J., Weitz, J., Chin, L., Futreal, A., and Kalluri, R. (2014). Identification of Double-stranded Genomic DNA Spanning All Chromosomes with Mutated KRAS and p53

DNA in the Serum Exosomes of Patients with Pancreatic Cancer*. Journal of Biological Chemistry *289*, 3869-3875. https://doi.org/10.1074/jbc.C113.532267.

130. Thakur, B.K., Zhang, H., Becker, A., Matei, I., Huang, Y., Costa-Silva, B., Zheng, Y., Hoshino, A., Brazier, H., Xiang, J., et al. (2014). Double-stranded DNA in exosomes: a novel biomarker in cancer detection. Cell Res *24*, 766-769. 10.1038/cr.2014.44.
131. Herrmann, I.K., Wood, M.J.A., and Fuhrmann, G. (2021). Extracellular vesicles as a next-generation drug delivery platform. Nature Nanotechnology *16*, 748-759. 10.1038/s41565-021-00931-2.
132. Buschow, S.I., Nolte-'t Hoen, E.N., van Niel, G., Pols, M.S., ten Broeke, T., Lauwen, M., Ossendorp, F., Melief, C.J., Raposo, G., Wubbolts, R., et al. (2009). MHC II in dendritic cells is targeted to lysosomes or T cell-induced exosomes via distinct multivesicular body pathways. Traffic *10*, 1528-1542. 10.1111/j.1600-0854.2009.00963.x.
133. Costa Verdera, H., Gitz-Francois, J.J., Schiffelers, R.M., and Vader, P. (2017). Cellular uptake of extracellular vesicles is mediated by clathrin-independent endocytosis and macropinocytosis. J Control Release *266*, 100-108. 10.1016/j.jconrel.2017.09.019.
134. Tian, T., Zhu, Y.L., Zhou, Y.Y., Liang, G.F., Wang, Y.Y., Hu, F.H., and Xiao, Z.D. (2014). Exosome uptake through clathrin-mediated endocytosis and macropinocytosis and mediating miR-21 delivery. J Biol Chem *289*, 22258-22267. 10.1074/jbc.M114.588046.
135. Svensson, K.J., Christianson, H.C., Wittrup, A., Bourseau-Guilmain, E., Lindqvist, E., Svensson, L.M., Mörgelin, M., and Belting, M. (2013). Exosome Uptake Depends on ERK1/2-Heat Shock Protein 27 Signaling and Lipid Raft-mediated Endocytosis Negatively Regulated by Caveolin-1*. Journal of Biological Chemistry *288*, 17713-17724. https://doi.org/10.1074/jbc.M112.445403.
136. Kalluri, R., and LeBleu, V.S. (2020). The biology, function, and biomedical applications of exosomes. Science *367*, eaau6977. 10.1126/science.aau6977.
137. Mathieu, M., Martin-Jaular, L., Lavieu, G., and Théry, C. (2019). Specificities of secretion and uptake of exosomes and other extracellular vesicles for cell-to-cell communication. Nature Cell Biology *21*, 9-17. 10.1038/s41556-018-0250-9.
138. Murphy, D.E., de Jong, O.G., Evers, M.J.W., Nurazizah, M., Schiffelers, R.M., and Vader, P. (2021). Natural or Synthetic RNA Delivery: A Stoichiometric Comparison

of Extracellular Vesicles and Synthetic Nanoparticles. Nano Letters *21*, 1888-1895. 10.1021/acs.nanolett.1c00094.

139. Gross, J.C., Chaudhary, V., Bartscherer, K., and Boutros, M. (2012). Active Wnt proteins are secreted on exosomes. Nature Cell Biology *14*, 1036-1045. 10.1038/ncb2574.
140. Robbins, P.D., and Morelli, A.E. (2014). Regulation of immune responses by extracellular vesicles. Nat Rev Immunol *14*, 195-208. 10.1038/nri3622.
141. Raposo, G., Nijman, H.W., Stoorvogel, W., Liejendekker, R., Harding, C.V., Melief, C.J., and Geuze, H.J. (1996). B lymphocytes secrete antigen-presenting vesicles. J Exp Med *183*, 1161-1172. 10.1084/jem.183.3.1161.
142. Melo, S.A., Sugimoto, H., O'Connell, J.T., Kato, N., Villanueva, A., Vidal, A., Qiu, L., Vitkin, E., Perelman, L.T., Melo, C.A., et al. (2014). Cancer exosomes perform cell-independent microRNA biogenesis and promote tumorigenesis. Cancer Cell *26*, 707-721. 10.1016/j.ccell.2014.09.005.
143. Webber, J., Steadman, R., Mason, M.D., Tabi, Z., and Clayton, A. (2010). Cancer exosomes trigger fibroblast to myofibroblast differentiation. Cancer Res *70*, 9621-9630. 10.1158/0008-5472.Can-10-1722.
144. Aung, T., Chapuy, B., Vogel, D., Wenzel, D., Oppermann, M., Lahmann, M., Weinhage, T., Menck, K., Hupfeld, T., Koch, R., et al. (2011). Exosomal evasion of humoral immunotherapy in aggressive B-cell lymphoma modulated by ATP-binding cassette transporter A3. Proc Natl Acad Sci U S A *108*, 15336-15341. 10.1073/pnas.1102855108.
145. Théry, C., Amigorena, S., Raposo, G., and Clayton, A. (2006). Isolation and Characterization of Exosomes from Cell Culture Supernatants and Biological Fluids. Current Protocols in Cell Biology *30*, 3.22.21-23.22.29. https://doi.org/10.1002/0471143030.cb0322s30.
146. Brennan, K., Martin, K., FitzGerald, S.P., O'Sullivan, J., Wu, Y., Blanco, A., Richardson, C., and Mc Gee, M.M. (2020). A comparison of methods for the isolation and separation of extracellular vesicles from protein and lipid particles in human serum. Scientific Reports *10*, 1039. 10.1038/s41598-020-57497-7.
147. Gardiner, C., Di Vizio, D., Sahoo, S., Théry, C., Witwer, K.W., Wauben, M., and Hill, A.F. (2016). Techniques used for the isolation and characterization of extracellular vesicles: results of a worldwide survey. J Extracell Vesicles *5*, 32945. 10.3402/jev.v5.32945.

148. Bard, M.P., Hegmans, J.P., Hemmes, A., Luider, T.M., Willemsen, R., Severijnen, L.A., van Meerbeeck, J.P., Burgers, S.A., Hoogsteden, H.C., and Lambrecht, B.N. (2004). Proteomic analysis of exosomes isolated from human malignant pleural effusions. Am J Respir Cell Mol Biol *31*, 114-121. 10.1165/rcmb.2003-0238OC.

149. György, B., Módos, K., Pállinger, E., Pálóczi, K., Pásztói, M., Misják, P., Deli, M.A., Sipos, A., Szalai, A., Voszka, I., et al. (2011). Detection and isolation of cell-derived microparticles are compromised by protein complexes resulting from shared biophysical parameters. Blood *117*, e39-48. 10.1182/blood-2010-09-307595.

150. Rood, I.M., Deegens, J.K., Merchant, M.L., Tamboer, W.P., Wilkey, D.W., Wetzels, J.F., and Klein, J.B. (2010). Comparison of three methods for isolation of urinary microvesicles to identify biomarkers of nephrotic syndrome. Kidney Int *78*, 810-816. 10.1038/ki.2010.262.

151. Boing, A.N., van der Pol, E., Grootemaat, A.E., Coumans, F.A., Sturk, A., and Nieuwland, R. (2014). Single-step isolation of extracellular vesicles by size-exclusion chromatography. J Extracell Vesicles *3*. 10.3402/jev.v3.23430.

152. Brahmer, A., Neuberger, E., Esch-Heisser, L., Haller, N., Jorgensen, M.M., Baek, R., Möbius, W., Simon, P., and Krämer-Albers, E.-M. (2019). Platelets, endothelial cells and leukocytes contribute to the exercise-triggered release of extracellular vesicles into the circulation. J Extracell Vesicles *8*, 1615820. https://doi.org/10.1080/20013078.2019.1615820.

153. Corso, G., Mäger, I., Lee, Y., Görgens, A., Bultema, J., Giebel, B., Wood, M.J.A., Nordin, J.Z., and Andaloussi, S.E. (2017). Reproducible and scalable purification of extracellular vesicles using combined bind-elute and size exclusion chromatography. Sci Rep *7*, 11561. 10.1038/s41598-017-10646-x.

154. Mol, E.A., Goumans, M.J., Doevendans, P.A., Sluijter, J.P.G., and Vader, P. (2017). Higher functionality of extracellular vesicles isolated using size-exclusion chromatography compared to ultracentrifugation. Nanomedicine *13*, 2061-2065. 10.1016/j.nano.2017.03.011.

155. Benedikter, B.J., Bouwman, F.G., Vajen, T., Heinzmann, A.C.A., Grauls, G., Mariman, E.C., Wouters, E.F.M., Savelkoul, P.H., Lopez-Iglesias, C., Koenen, R.R., et al. (2017). Ultrafiltration combined with size exclusion chromatography efficiently isolates extracellular vesicles from cell culture media for compositional and functional studies. Scientific Reports *7*, 15297. 10.1038/s41598-017-15717-7.

156. Nordin, J.Z., Lee, Y., Vader, P., Mäger, I., Johansson, H.J., Heusermann, W., Wiklander, O.P., Hällbrink, M., Seow, Y., Bultema, J.J., et al. (2015). Ultrafiltration with size-exclusion liquid chromatography for high yield isolation of extracellular vesicles preserving intact biophysical and functional properties. Nanomedicine *11*, 879-883. 10.1016/j.nano.2015.01.003.

157. Lobb, R.J., Becker, M., Wen, S.W., Wong, C.S., Wiegmans, A.P., Leimgruber, A., and Möller, A. (2015). Optimized exosome isolation protocol for cell culture supernatant and human plasma. J Extracell Vesicles *4*, 27031. 10.3402/jev.v4.27031.

158. Balaj, L., Atai, N.A., Chen, W., Mu, D., Tannous, B.A., Breakefield, X.O., Skog, J., and Maguire, C.A. (2015). Heparin affinity purification of extracellular vesicles. Sci Rep *5*, 10266. 10.1038/srep10266.

159. Brett, S.I., Lucien, F., Guo, C., Williams, K.C., Kim, Y., Durfee, P.N., Brinker, C.J., Chin, J.I., Yang, J., and Leong, H.S. (2017). Immunoaffinity based methods are superior to kits for purification of prostate derived extracellular vesicles from plasma samples. Prostate *77*, 1335-1343. 10.1002/pros.23393.

160. Nakai, W., Yoshida, T., Diez, D., Miyatake, Y., Nishibu, T., Imawaka, N., Naruse, K., Sadamura, Y., and Hanayama, R. (2016). A novel affinity-based method for the isolation of highly purified extracellular vesicles. Sci Rep *6*, 33935. 10.1038/srep33935.

161. Sharma, P., Ludwig, S., Muller, L., Hong, C.S., Kirkwood, J.M., Ferrone, S., and Whiteside, T.L. (2018). Immunoaffinity-based isolation of melanoma cell-derived exosomes from plasma of patients with melanoma. J Extracell Vesicles *7*, 1435138. 10.1080/20013078.2018.1435138.

162. Roda, B., Zattoni, A., Reschiglian, P., Moon, M.H., Mirasoli, M., Michelini, E., and Roda, A. (2009). Field-flow fractionation in bioanalysis: A review of recent trends. Anal Chim Acta *635*, 132-143. 10.1016/j.aca.2009.01.015.

163. Yang, J.S., Lee, J.C., Byeon, S.K., Rha, K.H., and Moon, M.H. (2017). Size Dependent Lipidomic Analysis of Urinary Exosomes from Patients with Prostate Cancer by Flow Field-Flow Fractionation and Nanoflow Liquid Chromatography-Tandem Mass Spectrometry. Anal Chem *89*, 2488-2496. 10.1021/acs.analchem.6b04634.

164. Zhang, H., Freitas, D., Kim, H.S., Fabijanic, K., Li, Z., Chen, H., Mark, M.T., Molina, H., Martin, A.B., Bojmar, L., et al. (2018). Identification of distinct nanoparticles and

subsets of extracellular vesicles by asymmetric flow field-flow fractionation. Nat Cell Biol *20*, 332-343. 10.1038/s41556-018-0040-4.

165. Frampton, A.E., Prado, M.M., López-Jiménez, E., Fajardo-Puerta, A.B., Jawad, Z.A.R., Lawton, P., Giovannetti, E., Habib, N.A., Castellano, L., Stebbing, J., et al. (2018). Glypican-1 is enriched in circulating-exosomes in pancreatic cancer and correlates with tumor burden. Oncotarget *9*, 19006-19013. 10.18632/oncotarget.24873.
166. Etayash, H., McGee, A.R., Kaur, K., and Thundat, T. (2016). Nanomechanical sandwich assay for multiple cancer biomarkers in breast cancer cell-derived exosomes. Nanoscale *8*, 15137-15141. 10.1039/c6nr03478k.
167. Li, J., Chen, Y., Guo, X., Zhou, L., Jia, Z., Peng, Z., Tang, Y., Liu, W., Zhu, B., Wang, L., and Ren, C. (2017). GPC1 exosome and its regulatory miRNAs are specific markers for the detection and target therapy of colorectal cancer. J Cell Mol Med *21*, 838-847. 10.1111/jcmm.12941.
168. Han, Y., Li, X., Zhang, Y., Han, Y., Chang, F., and Ding, J. (2019). Mesenchymal Stem Cells for Regenerative Medicine. Cells *8*. 10.3390/cells8080886.
169. Hosseini, S., Shamekhi, M.A., Jahangir, S., Bagheri, F., and Eslaminejad, M.B. (2019). The Robust Potential of Mesenchymal Stem Cell-Loaded Constructs for Hard Tissue Regeneration After Cancer Removal. held in Cham, 2019//. P.V. Pham, ed. (Springer International Publishing), pp. 17-43.
170. Jafarinia, M., Alsahebfosoul, F., Salehi, H., Eskandari, N., and Ganjalikhani-Hakemi, M. (2020). Mesenchymal Stem Cell-Derived Extracellular Vesicles: A Novel Cell-Free Therapy. Immunol Invest *49*, 758-780. 10.1080/08820139.2020.1712416.
171. Liang, X., Ding, Y., Zhang, Y., Tse, H.-F., and Lian, Q. (2014). Paracrine Mechanisms of Mesenchymal Stem Cell-Based Therapy: Current Status and Perspectives. Cell Transplantation *23*, 1045-1059. 10.3727/096368913X667709.
172. Kordelas, L., Rebmann, V., Ludwig, A.K., Radtke, S., Ruesing, J., Doeppner, T.R., Epple, M., Horn, P.A., Beelen, D.W., and Giebel, B. (2014). MSC-derived exosomes: a novel tool to treat therapy-refractory graft-versus-host disease. Leukemia *28*, 970-973. 10.1038/leu.2014.41.
173. Kou, M., Huang, L., Yang, J., Chiang, Z., Chen, S., Liu, J., Guo, L., Zhang, X., Zhou, X., Xu, X., et al. (2022). Mesenchymal stem cell-derived extracellular vesicles for immunomodulation and regeneration: a next generation therapeutic tool? Cell Death & Disease *13*, 580. 10.1038/s41419-022-05034-x.

174. Sun, D., Zhuang, X., Xiang, X., Liu, Y., Zhang, S., Liu, C., Barnes, S., Grizzle, W., Miller, D., and Zhang, H.G. (2010). A novel nanoparticle drug delivery system: the anti-inflammatory activity of curcumin is enhanced when encapsulated in exosomes. Mol Ther *18*, 1606-1614. 10.1038/mt.2010.105.

175. Alexander, M., Hu, R., Runtsch, M.C., Kagele, D.A., Mosbruger, T.L., Tolmachova, T., Seabra, M.C., Round, J.L., Ward, D.M., and O'Connell, R.M. (2015). Exosome-delivered microRNAs modulate the inflammatory response to endotoxin. Nature Communications *6*, 7321. 10.1038/ncomms8321.

176. Fuhrmann, G., Serio, A., Mazo, M., Nair, R., and Stevens, M.M. (2015). Active loading into extracellular vesicles significantly improves the cellular uptake and photodynamic effect of porphyrins. Journal of Controlled Release *205*, 35-44. https://doi.org/10.1016/j.jconrel.2014.11.029.

177. Mahati, S., Fu, X., Ma, X., Zhang, H., and Xiao, L. (2021). Delivery of miR-26a Using an Exosomes-Based Nanosystem Inhibited Proliferation of Hepatocellular Carcinoma. Frontiers in Molecular Biosciences *8*. 10.3389/fmolb.2021.738219.

178. Lara, P., Palma-Florez, S., Salas-Huenuleo, E., Polakovicova, I., Guerrero, S., Lobos-Gonzalez, L., Campos, A., Muñoz, L., Jorquera-Cordero, C., Varas-Godoy, M., et al. (2020). Gold nanoparticle based double-labeling of melanoma extracellular vesicles to determine the specificity of uptake by cells and preferential accumulation in small metastatic lung tumors. Journal of Nanobiotechnology *18*, 20. 10.1186/s12951-020-0573-0.

179. Sancho-Albero, M., Martín-Pardillos, A., Lujan, L., Sebastian, V., Santamaria, J., and Martín-Duque, P. (2022). Exosomes loaded with ultrasmall Pt nanoparticles: a novel low-toxicity alternative to cisplatin. Journal of Nanobiotechnology *20*, 473. 10.1186/s12951-022-01675-4.

180. Wu, D., Chen, Q., Chen, X., Han, F., Chen, Z., and Wang, Y. (2023). The blood–brain barrier: structure, regulation, and drug delivery. Signal Transduction and Targeted Therapy *8*, 217. 10.1038/s41392-023-01481-w.

181. Betzer, O., Perets, N., Angel, A., Motiei, M., Sadan, T., Yadid, G., Offen, D., and Popovtzer, R. (2017). In Vivo Neuroimaging of Exosomes Using Gold Nanoparticles. ACS Nano *11*, 10883-10893. 10.1021/acsnano.7b04495.

182. Yang, T., Martin, P., Fogarty, B., Brown, A., Schurman, K., Phipps, R., Yin, V.P., Lockman, P., and Bai, S. (2015). Exosome delivered anticancer drugs across the

blood-brain barrier for brain cancer therapy in Danio rerio. Pharm Res *32*, 2003-2014. 10.1007/s11095-014-1593-y.

183. Morad, G., Carman, C.V., Hagedorn, E.J., Perlin, J.R., Zon, L.I., Mustafaoglu, N., Park, T.-E., Ingber, D.E., Daisy, C.C., and Moses, M.A. (2019). Tumor-Derived Extracellular Vesicles Breach the Intact Blood–Brain Barrier via Transcytosis. ACS Nano *13*, 13853-13865. 10.1021/acsnano.9b04397.

184. Zhuang, X., Xiang, X., Grizzle, W., Sun, D., Zhang, S., Axtell, R.C., Ju, S., Mu, J., Zhang, L., Steinman, L., et al. (2011). Treatment of brain inflammatory diseases by delivering exosome encapsulated anti-inflammatory drugs from the nasal region to the brain. Mol Ther *19*, 1769-1779. 10.1038/mt.2011.164.

185. Banks, W.A., Sharma, P., Bullock, K.M., Hansen, K.M., Ludwig, N., and Whiteside, T.L. (2020). Transport of Extracellular Vesicles across the Blood-Brain Barrier: Brain Pharmacokinetics and Effects of Inflammation. Int J Mol Sci *21*. 10.3390/ijms21124407.

186. Lenzini, S., Bargi, R., Chung, G., and Shin, J.-W. (2020). Matrix mechanics and water permeation regulate extracellular vesicle transport. Nature Nanotechnology *15*, 217-223. 10.1038/s41565-020-0636-2.

187. Schindler, C., Collinson, A., Matthews, C., Pointon, A., Jenkinson, L., Minter, R.R., Vaughan, T.J., and Tigue, N.J. (2019). Exosomal delivery of doxorubicin enables rapid cell entry and enhanced in vitro potency. PLoS One *14*, e0214545. 10.1371/journal.pone.0214545.

188. van Dongen Helena, M., Masoumi, N., Witwer Kenneth, W., and Pegtel, D.M. (2016). Extracellular Vesicles Exploit Viral Entry Routes for Cargo Delivery. Microbiology and Molecular Biology Reviews *80*, 369-386. 10.1128/mmbr.00063-15.

189. Lener, T., Gimona, M., Aigner, L., Börger, V., Buzas, E., Camussi, G., Chaput, N., Chatterjee, D., Court, F.A., del Portillo, H.A., et al. (2015). Applying extracellular vesicles based therapeutics in clinical trials – an ISEV position paper. J Extracell Vesicles *4*, 30087. https://doi.org/10.3402/jev.v4.30087.

190. Dai, J., Su, Y., Zhong, S., Cong, L., Liu, B., Yang, J., Tao, Y., He, Z., Chen, C., and Jiang, Y. (2020). Exosomes: key players in cancer and potential therapeutic strategy. Signal Transduction and Targeted Therapy *5*, 145. 10.1038/s41392-020-00261-0.

191. Almeria, C., Kreß, S., Weber, V., Egger, D., and Kasper, C. (2022). Heterogeneity of mesenchymal stem cell-derived extracellular vesicles is highly impacted by the

tissue/cell source and culture conditions. Cell & Bioscience *12*, 51. 10.1186/s13578-022-00786-7.

192. Patel, D.B., Gray, K.M., Santharam, Y., Lamichhane, T.N., Stroka, K.M., and Jay, S.M. (2017). Impact of cell culture parameters on production and vascularization bioactivity of mesenchymal stem cell-derived extracellular vesicles. Bioeng Transl Med *2*, 170-179. 10.1002/btm2.10065.

193. Rohde, E., Pachler, K., and Gimona, M. (2019). Manufacturing and characterization of extracellular vesicles from umbilical cord–derived mesenchymal stromal cells for clinical testing. Cytotherapy *21*, 581-592. https://doi.org/10.1016/j.jcyt.2018.12.006.

194. Alvarez-Erviti, L., Seow, Y., Yin, H., Betts, C., Lakhal, S., and Wood, M.J.A. (2011). Delivery of siRNA to the mouse brain by systemic injection of targeted exosomes. Nature Biotechnology *29*, 341-345. 10.1038/nbt.1807.

195. Kooijmans, S.A.A., Stremersch, S., Braeckmans, K., de Smedt, S.C., Hendrix, A., Wood, M.J.A., Schiffelers, R.M., Raemdonck, K., and Vader, P. (2013). Electroporation-induced siRNA precipitation obscures the efficiency of siRNA loading into extracellular vesicles. J Control Release *172*, 229-238. 10.1016/j.jconrel.2013.08.014.

196. Momen-Heravi, F., Bala, S., Bukong, T., and Szabo, G. (2014). Exosome-mediated delivery of functionally active miRNA-155 inhibitor to macrophages. Nanomedicine *10*, 1517-1527. 10.1016/j.nano.2014.03.014.

197. Fuhrmann, G., Serio, A., Mazo, M., Nair, R., and Stevens, M.M. (2015). Active loading into extracellular vesicles significantly improves the cellular uptake and photodynamic effect of porphyrins. J Control Release *205*, 35-44. 10.1016/j.jconrel.2014.11.029.

198. Khongkow, M., Yata, T., Boonrungsiman, S., Ruktanonchai, U.R., Graham, D., and Namdee, K. (2019). Surface modification of gold nanoparticles with neuron-targeted exosome for enhanced blood–brain barrier penetration. Scientific Reports *9*, 8278. 10.1038/s41598-019-44569-6.

199. Hettich, B.F., Bader, J.J., and Leroux, J.-C. (2022). Encapsulation of Hydrophilic Compounds in Small Extracellular Vesicles: Loading Capacity and Impact on Vesicle Functions. Advanced Healthcare Materials *11*, 2100047. https://doi.org/10.1002/adhm.202100047.

200. Haney, M.J., Klyachko, N.L., Zhao, Y., Gupta, R., Plotnikova, E.G., He, Z., Patel, T., Piroyan, A., Sokolsky, M., Kabanov, A.V., and Batrakova, E.V. (2015). Exosomes as

drug delivery vehicles for Parkinson's disease therapy. Journal of Controlled Release *207*, 18-30. https://doi.org/10.1016/j.jconrel.2015.03.033.

201. Srivastava, A., Amreddy, N., Babu, A., Panneerselvam, J., Mehta, M., Muralidharan, R., Chen, A., Zhao, Y.D., Razaq, M., Riedinger, N., et al. (2016). Nanosomes carrying doxorubicin exhibit potent anticancer activity against human lung cancer cells. Sci Rep *6*, 38541. 10.1038/srep38541.
202. Kooijmans, S.A., Aleza, C.G., Roffler, S.R., van Solinge, W.W., Vader, P., and Schiffelers, R.M. (2016). Display of GPI-anchored anti-EGFR nanobodies on extracellular vesicles promotes tumour cell targeting. J Extracell Vesicles *5*, 31053. 10.3402/jev.v5.31053.
203. Choi, H., Kim, Y., Mirzaaghasi, A., Heo, J., Kim, Y.N., Shin, J.H., Kim, S., Kim, N.H., Cho, E.S., In Yook, J., et al. (2020). Exosome-based delivery of super-repressor IκBα relieves sepsis-associated organ damage and mortality. Science Advances *6*, eaaz6980. doi:10.1126/sciadv.aaz6980.
204. Ran, N., Gao, X., Dong, X., Li, J., Lin, C., Geng, M., and Yin, H. (2020). Effects of exosome-mediated delivery of myostatin propeptide on functional recovery of mdx mice. Biomaterials *236*, 119826. 10.1016/j.biomaterials.2020.119826.
205. Pascucci, L., Coccè, V., Bonomi, A., Ami, D., Ceccarelli, P., Ciusani, E., Viganò, L., Locatelli, A., Sisto, F., Doglia, S.M., et al. (2014). Paclitaxel is incorporated by mesenchymal stromal cells and released in exosomes that inhibit in vitro tumor growth: a new approach for drug delivery. J Control Release *192*, 262-270. 10.1016/j.jconrel.2014.07.042.
206. Kauscher, U., Penders, J., Nagelkerke, A., Holme, M.N., Nele, V., Massi, L., Gopal, S., Whittaker, T.E., and Stevens, M.M. (2020). Gold Nanocluster Extracellular Vesicle Supraparticles: Self-Assembled Nanostructures for Three-Dimensional Uptake Visualization. Langmuir *36*, 3912-3923. 10.1021/acs.langmuir.9b03479.
207. Illes, B., Hirschle, P., Barnert, S., Cauda, V., Wuttke, S., and Engelke, H. (2017). Exosome-Coated Metal–Organic Framework Nanoparticles: An Efficient Drug Delivery Platform. Chemistry of Materials *29*, 8042-8046. 10.1021/acs.chemmater.7b02358.
208. Cheng, G., Li, W., Ha, L., Han, X., Hao, S., Wan, Y., Wang, Z., Dong, F., Zou, X., Mao, Y., and Zheng, S.-Y. (2018). Self-Assembly of Extracellular Vesicle-like Metal–Organic Framework Nanoparticles for Protection and Intracellular Delivery of

Biofunctional Proteins. Journal of the American Chemical Society *140*, 7282-7291. 10.1021/jacs.8b03584.

209. Zhu, D., Liu, Z., Li, Y., Huang, Q., Xia, L., and Li, K. (2021). Delivery of manganese carbonyl to the tumor microenvironment using Tumor-Derived exosomes for cancer gas therapy and low dose radiotherapy. Biomaterials *274*, 120894. https://doi.org/10.1016/j.biomaterials.2021.120894.
210. Lin, Y., Wu, J., Gu, W., Huang, Y., Tong, Z., Huang, L., and Tan, J. (2018). Exosome-Liposome Hybrid Nanoparticles Deliver CRISPR/Cas9 System in MSCs. Adv Sci (Weinh) *5*, 1700611. 10.1002/advs.201700611.
211. Ezzat, K., Pernemalm, M., Pålsson, S., Roberts, T.C., Järver, P., Dondalska, A., Bestas, B., Sobkowiak, M.J., Levänen, B., Sköld, M., et al. (2019). The viral protein corona directs viral pathogenesis and amyloid aggregation. Nature Communications *10*, 2331. 10.1038/s41467-019-10192-2.
212. Tóth, E.Á., Turiák, L., Visnovitz, T., Cserép, C., Mázló, A., Sódar, B.W., Försönits, A.I., Petővári, G., Sebestyén, A., Komlósi, Z., et al. (2021). Formation of a protein corona on the surface of extracellular vesicles in blood plasma. J Extracell Vesicles *10*, e12140. https://doi.org/10.1002/jev2.12140.
213. Cedervall, T., Lynch, I., Lindman, S., Berggård, T., Thulin, E., Nilsson, H., Dawson, K.A., and Linse, S. (2007). Understanding the nanoparticle-protein corona using methods to quantify exchange rates and affinities of proteins for nanoparticles. Proc Natl Acad Sci U S A *104*, 2050-2055. 10.1073/pnas.0608582104.
214. Wolf, M., Poupardin, R.W., Ebner-Peking, P., Andrade, A.C., Blöchl, C., Obermayer, A., Gomes, F.G., Vari, B., Maeding, N., Eminger, E., et al. (2022). A functional corona around extracellular vesicles enhances angiogenesis, skin regeneration and immunomodulation. J Extracell Vesicles *11*, e12207. https://doi.org/10.1002/jev2.12207.
215. Smolarz, M., Pietrowska, M., Matysiak, N., Mielańczyk, Ł., and Widłak, P. (2019). Proteome Profiling of Exosomes Purified from a Small Amount of Human Serum: The Problem of Co-Purified Serum Components. Proteomes *7*. 10.3390/proteomes7020018.
216. Théry, C., Witwer, K.W., Aikawa, E., Alcaraz, M.J., Anderson, J.D., Andriantsitohaina, R., Antoniou, A., Arab, T., Archer, F., Atkin-Smith, G.K., et al. (2018). Minimal information for studies of extracellular vesicles 2018 (MISEV2018): a position statement of the International Society for Extracellular Vesicles and update

of the MISEV2014 guidelines. J Extracell Vesicles *7*, 1535750. 10.1080/20013078.2018.1535750.

217. Gustafson, H.H., Holt-Casper, D., Grainger, D.W., and Ghandehari, H. (2015). Nanoparticle uptake: The phagocyte problem. Nano Today *10*, 487-510. https://doi.org/10.1016/j.nantod.2015.06.006.
218. Moein Moghimi, S., and Patel, H.M. (1989). Serum opsonins and phagocytosis of saturated and unsaturated phospholipid liposomes. Biochimica et Biophysica Acta (BBA) - Biomembranes *984*, 384-387. https://doi.org/10.1016/0005-2736(89)90307-6.
219. Schöttler, S., Landfester, K., and Mailänder, V. (2016). Controlling the Stealth Effect of Nanocarriers through Understanding the Protein Corona. Angew Chem Int Ed Engl *55*, 8806-8815. 10.1002/anie.201602233.
220. Shen, Z., Fisher, A., Liu, W.K., and Li, Y. (2018). 1 - PEGylated “stealth” nanoparticles and liposomes. In Engineering of Biomaterials for Drug Delivery Systems, A. Parambath, ed. (Woodhead Publishing), pp. 1-26. https://doi.org/10.1016/B978-0-08-101750-0.00001-5.
221. Torchilin, V.P., Omelyanenko, V.G., Papisov, M.I., Bogdanov, A.A., Trubetskoy, V.S., Herron, J.N., and Gentry, C.A. (1994). Poly(ethylene glycol) on the liposome surface: on the mechanism of polymer-coated liposome longevity. Biochimica et Biophysica Acta (BBA) - Biomembranes *1195*, 11-20. https://doi.org/10.1016/0005-2736(94)90003-5.
222. Wiklander, O.P.B., Nordin, J.Z., O'Loughlin, A., Gustafsson, Y., Corso, G., Mäger, I., Vader, P., Lee, Y., Sork, H., Seow, Y., et al. (2015). Extracellular vesicle in vivo biodistribution is determined by cell source, route of administration and targeting. J Extracell Vesicles *4*, 26316. https://doi.org/10.3402/jev.v4.26316.
223. Dietz, L., Oberländer, J., Mateos-Maroto, A., Schunke, J., Fichter, M., Krämer-Albers, E.M., Landfester, K., and Mailänder, V. (2023). Uptake of extracellular vesicles into immune cells is enhanced by the protein corona. J Extracell Vesicles *12*, e12399. 10.1002/jev2.12399.
224. Hecht, L.L., Schoth, A., Munoz-Espí, R., Javadi, A., Köhler, K., Miller, R., Landfester, K., and Schuchmann, H.P. (2013). Determination of the ideal surfactant concentration in miniemulsion polymerization. Macromolecular chemistry and physics *214*, 812-823. 10.1002/macp.201200583.

225. Landfester, K. (2003). Miniemulsions for Nanoparticle Synthesis. In Colloid Chemistry II, M. Antonietti, ed. (Springer Berlin Heidelberg), pp. 75-123. 10.1007/3-540-36412-9_4.

226. Brahmer, A., Neuberger, E., Esch-Heisser, L., Haller, N., Jorgensen, M.M., Baek, R., Möbius, W., Simon, P., and Krämer-Albers, E.M. (2019). Platelets, endothelial cells and leukocytes contribute to the exercise-triggered release of extracellular vesicles into the circulation. J Extracell Vesicles *8*, 1615820. 10.1080/20013078.2019.1615820.

227. Doan-Nguyen, T.P., Jiang, S., Koynov, K., Landfester, K., and Crespy, D. (2021). Ultrasmall Nanocapsules Obtained by Controlling Ostwald Ripening. Angew. Chem. *133*, 18242-18250.

228. Rigler, R., and Elson, E.S. (2012). Fluorescence correlation spectroscopy: theory and applications (Springer Science & Business Media).

229. Thurmond, C.D. (1952). Control of dust in solution for turbidimetry. Journal of Polymer Science *8*, 607-609. https://doi.org/10.1002/pol.1952.120080605.

230. Rausch, K., Reuter, A., Fischer, K., and Schmidt, M. (2010). Evaluation of Nanoparticle Aggregation in Human Blood Serum. Biomacromolecules *11*, 2836-2839. 10.1021/bm100971q.

231. Stöber, W., Fink, A., and Bohn, E. (1968). Controlled growth of monodisperse silica spheres in the micron size range. Journal of Colloid and Interface Science *26*, 62-69. https://doi.org/10.1016/0021-9797(68)90272-5.

232. Kokkinopoulou, M., Simon, J., Landfester, K., Mailänder, V., and Lieberwirth, I. (2017). Visualization of the protein corona: towards a biomolecular understanding of nanoparticle-cell-interactions. Nanoscale *9*, 8858-8870. 10.1039/c7nr02977b.

233. Simon, J., Wolf, T., Klein, K., Landfester, K., Wurm, F.R., and Mailänder, V. (2018). Hydrophilicity Regulates the Stealth Properties of Polyphosphoester-Coated Nanocarriers. Angewandte Chemie International Edition *57*, 5548-5553. https://doi.org/10.1002/anie.201800272.

234. Simon, J., Wolf, T., Klein, K., Landfester, K., Wurm, F.R., and Mailänder, V. (2018). Hydrophilicity Regulates the Stealth Properties of Polyphosphoester-Coated Nanocarriers. Angew Chem Int Ed Engl *57*, 5548-5553. 10.1002/anie.201800272.

235. Silva, J.C., Gorenstein, M.V., Li, G.Z., Vissers, J.P., and Geromanos, S.J. (2006). Absolute quantification of proteins by LCMSE: a virtue of parallel MS acquisition. Mol Cell Proteomics *5*, 144-156. 10.1074/mcp.M500230-MCP200.

236. Fichter, M., Dedters, M., Pietrzak-Nguyen, A., Pretsch, L., Meyer, C.U., Strand, S., Zepp, F., Baier, G., Landfester, K., and Gehring, S. (2015). Monophosphoryl lipid A coating of hydroxyethyl starch nanocapsules drastically increases uptake and maturation by dendritic cells while minimizing the adjuvant dosage. Vaccine *33*, 838-846. 10.1016/j.vaccine.2014.12.072.

237. Silva, J.C., Gorenstein, M.V., Li, G.Z., Vissers, J.P., and Geromanos, S.J. (2006). Absolute quantification of proteins by LCMSE: a virtue of parallel MS acquisition. Mol. Cell. Proteomics *5*, 144-156. 10.1074/mcp.M500230-MCP200.

238. Suk, J.S., Xu, Q., Kim, N., Hanes, J., and Ensign, L.M. (2016). PEGylation as a strategy for improving nanoparticle-based drug and gene delivery. Advanced Drug Delivery Reviews *99*, 28-51. https://doi.org/10.1016/j.addr.2015.09.012.

239. Brückner, M., Simon, J., Landfester, K., and Mailänder, V. (2021). The conjugation strategy affects antibody orientation and targeting properties of nanocarriers. Nanoscale *13*, 9816-9824. 10.1039/D0NR08191D.

240. Pant, K., Neuber, C., Zarschler, K., Wodtke, J., Meister, S., Haag, R., Pietzsch, J., and Stephan, H. (2020). Active Targeting of Dendritic Polyglycerols for Diagnostic Cancer Imaging. Small *16*, 1905013. https://doi.org/10.1002/smll.201905013.

241. Tonigold, M., Simon, J., Estupiñán, D., Kokkinopoulou, M., Reinholz, J., Kintzel, U., Kaltbeitzel, A., Renz, P., Domogalla, M.P., Steinbrink, K., et al. (2018). Pre-adsorption of antibodies enables targeting of nanocarriers despite a biomolecular corona. Nat Nanotechnol *13*, 862-869. 10.1038/s41565-018-0171-6.

242. Zhao, Y.Z., Lin, Q., Wong, H.L., Shen, X.T., Yang, W., Xu, H.L., Mao, K.L., Tian, F.R., Yang, J.J., Xu, J., et al. (2016). Glioma-targeted therapy using Cilengitide nanoparticles combined with UTMD enhanced delivery. J Control Release *224*, 112-125. 10.1016/j.jconrel.2016.01.015.

243. Jiang, X., Xin, H., Ren, Q., Gu, J., Zhu, L., Du, F., Feng, C., Xie, Y., Sha, X., and Fang, X. (2014). Nanoparticles of 2-deoxy-D-glucose functionalized poly(ethylene glycol)-co-poly(trimethylene carbonate) for dual-targeted drug delivery in glioma treatment. Biomaterials *35*, 518-529. 10.1016/j.biomaterials.2013.09.094.

244. Venturelli, L., Nappini, S., Bulfoni, M., Gianfranceschi, G., Dal Zilio, S., Coceano, G., Del Ben, F., Turetta, M., Scoles, G., Vaccari, L., et al. (2016). Glucose is a key driver for GLUT1-mediated nanoparticles internalization in breast cancer cells. Scientific Reports *6*, 21629. 10.1038/srep21629.

245. Li, R., He, Y., Zhang, S., Qin, J., and Wang, J. (2018). Cell membrane-based nanoparticles: a new biomimetic platform for tumor diagnosis and treatment. Acta Pharmaceutica Sinica B *8*, 14-22. https://doi.org/10.1016/j.apsb.2017.11.009.

246. Loos, C., Syrovets, T., Musyanovych, A., Mailänder, V., Landfester, K., Nienhaus, G.U., and Simmet, T. (2014). Functionalized polystyrene nanoparticles as a platform for studying bio–nano interactions. Beilstein Journal of Nanotechnology *5*, 2403-2412. 10.3762/bjnano.5.250.

247. Böing, A.N., van der Pol, E., Grootemaat, A.E., Coumans, F.A., Sturk, A., and Nieuwland, R. (2014). Single-step isolation of extracellular vesicles by size-exclusion chromatography. J Extracell Vesicles *3*. 10.3402/jev.v3.23430.

248. Tominaga, N., Hagiwara, K., Kosaka, N., Honma, K., Nakagama, H., and Ochiya, T. (2014). RPN2-mediated glycosylation of tetraspanin CD63 regulates breast cancer cell malignancy. Mol Cancer *13*, 134. 10.1186/1476-4598-13-134.

249. Hirn, S., Semmler-Behnke, M., Schleh, C., Wenk, A., Lipka, J., Schäffler, M., Takenaka, S., Möller, W., Schmid, G., Simon, U., and Kreyling, W.G. (2011). Particle size-dependent and surface charge-dependent biodistribution of gold nanoparticles after intravenous administration. European Journal of Pharmaceutics and Biopharmaceutics *77*, 407-416. https://doi.org/10.1016/j.ejpb.2010.12.029.

250. Slowing, I.I., Vivero-Escoto, J.L., Zhao, Y., Kandel, K., Peeraphatdit, C., Trewyn, B.G., and Lin, V.S.-Y. (2011). Exocytosis of Mesoporous Silica Nanoparticles from Mammalian Cells: From Asymmetric Cell-to-Cell Transfer to Protein Harvesting. Small *7*, 1526-1532. https://doi.org/10.1002/smll.201002077.

251. Eskelinen, E.L. (2005). Maturation of autophagic vacuoles in Mammalian cells. Autophagy *1*, 1-10. 10.4161/auto.1.1.1270.

252. Dunn, W.A., Jr. (1994). Autophagy and related mechanisms of lysosome-mediated protein degradation. Trends Cell Biol *4*, 139-143. 10.1016/0962-8924(94)90069-8.

253. Schwille, P., Meyer-Almes, F.J., and Rigler, R. (1997). Dual-color fluorescence cross-correlation spectroscopy for multicomponent diffusional analysis in solution. Biophys J *72*, 1878-1886. 10.1016/s0006-3495(97)78833-7.

254. Schmitt, S., Nuhn, L., Barz, M., Butt, H.-J., and Koynov, K. (2022). Shining Light on Polymeric Drug Nanocarriers with Fluorescence Correlation Spectroscopy. Macromolecular Rapid Communications *43*, 2100892. https://doi.org/10.1002/marc.202100892.

255. Schaeffel, D., Staff, R.H., Butt, H.J., Landfester, K., Crespy, D., and Koynov, K. (2012). Fluorescence correlation spectroscopy directly monitors coalescence during nanoparticle preparation. Nano Lett *12*, 6012-6017. 10.1021/nl303581q.

256. Hess, S.T., Huang, S., Heikal, A.A., and Webb, W.W. (2002). Biological and chemical applications of fluorescence correlation spectroscopy: a review. Biochemistry *41*, 697-705. 10.1021/bi0118512.

257. Nuhn, L., Hirsch, M., Krieg, B., Koynov, K., Fischer, K., Schmidt, M., Helm, M., and Zentel, R. (2012). Cationic Nanohydrogel Particles as Potential siRNA Carriers for Cellular Delivery. ACS Nano *6*, 2198-2214. 10.1021/nn204116u.

258. Bantly, A.D., Gray, B.D., Breslin, E., Weinstein, E.G., Muirhead, K.A., Ohlsson-Wilhelm, B.M., and Moore, J.S. (2007). CellVue Claret, a new far-red dye, facilitates polychromatic assessment of immune cell proliferation. Immunol Invest *36*, 581-605. 10.1080/08820130701712461.

259. Polack, F.P., Thomas, S.J., Kitchin, N., Absalon, J., Gurtman, A., Lockhart, S., Perez, J.L., Marc, G.P., Moreira, E.D., Zerbini, C., et al. (2020). Safety and Efficacy of the BNT162b2 mRNA Covid-19 Vaccine. New England Journal of Medicine *383*, 2603-2615. doi:10.1056/NEJMoa2034577.

260. Sousa de Almeida, M., Susnik, E., Drasler, B., Taladriz-Blanco, P., Petri-Fink, A., and Rothen-Rutishauser, B. (2021). Understanding nanoparticle endocytosis to improve targeting strategies in nanomedicine. Chemical Society Reviews *50*, 5397-5434. 10.1039/D0CS01127D.

261. Sakhtianchi, R., Minchin, R.F., Lee, K.-B., Alkilany, A.M., Serpooshan, V., and Mahmoudi, M. (2013). Exocytosis of nanoparticles from cells: Role in cellular retention and toxicity. Advances in Colloid and Interface Science *201-202*, 18-29. https://doi.org/10.1016/j.cis.2013.10.013.

262. Krol, S., Macrez, R., Docagne, F., Defer, G., Laurent, S., Rahman, M., Hajipour, M.J., Kehoe, P.G., and Mahmoudi, M. (2013). Therapeutic Benefits from Nanoparticles: The Potential Significance of Nanoscience in Diseases with Compromise to the Blood Brain Barrier. Chemical Reviews *113*, 1877-1903. 10.1021/cr200472g.

263. Hu, Y.-B., Dammer, E.B., Ren, R.-J., and Wang, G. (2015). The endosomal-lysosomal system: from acidification and cargo sorting to neurodegeneration. Translational Neurodegeneration *4*, 18. 10.1186/s40035-015-0041-1.

264. Kim, C.S., Le, N.D.B., Xing, Y., Yan, B., Tonga, G.Y., Kim, C., Vachet, R.W., and Rotello, V.M. (2014). The Role of Surface Functionality in Nanoparticle Exocytosis.

Advanced Healthcare Materials *3*, 1200-1202. https://doi.org/10.1002/adhm.201400001.

265. Oh, N., and Park, J.-H. (2014). Surface Chemistry of Gold Nanoparticles Mediates Their Exocytosis in Macrophages. ACS Nano *8*, 6232-6241. 10.1021/nn501668a.
266. Chithrani, B.D., and Chan, W.C.W. (2007). Elucidating the Mechanism of Cellular Uptake and Removal of Protein-Coated Gold Nanoparticles of Different Sizes and Shapes. Nano Letters *7*, 1542-1550. 10.1021/nl070363y.
267. da Costa Marques, R., Hüppe, N., Speth, K.R., Oberländer, J., Lieberwirth, I., Landfester, K., and Mailänder, V. (2023). Proteomics reveals time-dependent protein corona changes in the intracellular pathway. Acta Biomaterialia. https://doi.org/10.1016/j.actbio.2023.10.010.
268. Lundqvist, M., Stigler, J., Elia, G., Lynch, I., Cedervall, T., and Dawson, K.A. (2008). Nanoparticle size and surface properties determine the protein corona with possible implications for biological impacts. Proceedings of the National Academy of Sciences *105*, 14265-14270. 10.1073/pnas.0805135105.
269. Tenzer, S., Docter, D., Rosfa, S., Wlodarski, A., Kuharev, J., Rekik, A., Knauer, S.K., Bantz, C., Nawroth, T., Bier, C., et al. (2011). Nanoparticle size is a critical physicochemical determinant of the human blood plasma corona: a comprehensive quantitative proteomic analysis. ACS Nano *5*, 7155-7167. 10.1021/nn201950e.
270. Schöttler, S., Landfester, K., and Mailänder, V. (2016). Controlling the Stealth Effect of Nanocarriers through Understanding the Protein Corona. Angewandte Chemie International Edition *55*, 8806-8815. https://doi.org/10.1002/anie.201602233.
271. Lesniak, A., Fenaroli, F., Monopoli, M.P., Åberg, C., Dawson, K.A., and Salvati, A. (2012). Effects of the presence or absence of a protein corona on silica nanoparticle uptake and impact on cells. ACS Nano *6*, 5845-5857. 10.1021/nn300223w.
272. Panyam, J., and Labhasetwar, V. (2003). Dynamics of endocytosis and exocytosis of poly(D,L-lactide-co-glycolide) nanoparticles in vascular smooth muscle cells. Pharm Res *20*, 212-220. 10.1023/a:1022219003551.
273. Berrecoso, G., Crecente-Campo, J., and Alonso, M.J. (2020). Unveiling the pitfalls of the protein corona of polymeric drug nanocarriers. Drug Delivery and Translational Research *10*, 730-750. 10.1007/s13346-020-00745-0.
274. Monopoli, M.P., Walczyk, D., Campbell, A., Elia, G., Lynch, I., Baldelli Bombelli, F., and Dawson, K.A. (2011). Physical−Chemical Aspects of Protein Corona: Relevance

to in Vitro and in Vivo Biological Impacts of Nanoparticles. Journal of the American Chemical Society *133*, 2525-2534. 10.1021/ja107583h.

275. Zhang, M., Charles, R., Tong, H., Zhang, L., Patel, M., Wang, F., Rames, M.J., Ren, A., Rye, K.-A., Qiu, X., et al. (2015). HDL surface lipids mediate CETP binding as revealed by electron microscopy and molecular dynamics simulation. Scientific Reports *5*, 8741. 10.1038/srep08741.
276. Barrán-Berdón, A.L., Pozzi, D., Caracciolo, G., Capriotti, A.L., Caruso, G., Cavaliere, C., Riccioli, A., Palchetti, S., and Laganà, A. (2013). Time evolution of nanoparticle-protein corona in human plasma: relevance for targeted drug delivery. Langmuir *29*, 6485-6494. 10.1021/la401192x.
277. Sun, B., Eckhardt, E.R., Shetty, S., van der Westhuyzen, D.R., and Webb, N.R. (2006). Quantitative analysis of SR-BI-dependent HDL retroendocytosis in hepatocytes and fibroblasts. J Lipid Res *47*, 1700-1713. 10.1194/jlr.M500450-JLR200.
278. Wüstner, D., Mondal, M., Huang, A., and Maxfield, F.R. (2004). Different transport routes for high density lipoprotein and its associated free sterol in polarized hepatic cells. J Lipid Res *45*, 427-437. 10.1194/jlr.M300440-JLR200.
279. German, J.B., Smilowitz, J.T., and Zivkovic, A.M. (2006). Lipoproteins: When size really matters. Curr Opin Colloid Interface Sci *11*, 171-183. 10.1016/j.cocis.2005.11.006.
280. Panyam, J., and Labhasetwar, V. (2003). Dynamics of Endocytosis and Exocytosis of Poly(D,L-Lactide-co-Glycolide) Nanoparticles in Vascular Smooth Muscle Cells. Pharmaceutical Research *20*, 212-220. 10.1023/A:1022219003551.
281. Serda, R.E., Mack, A., van de Ven, A.L., Ferrati, S., Dunner Jr., K., Godin, B., Chiappini, C., Landry, M., Brousseau, L., Liu, X., et al. (2010). Logic-Embedded Vectors for Intracellular Partitioning, Endosomal Escape, and Exocytosis of Nanoparticles. Small *6*, 2691-2700. https://doi.org/10.1002/smll.201000727.
282. Murphy, D.E., de Jong, O.G., Brouwer, M., Wood, M.J., Lavieu, G., Schiffelers, R.M., and Vader, P. (2019). Extracellular vesicle-based therapeutics: natural versus engineered targeting and trafficking. Experimental & Molecular Medicine *51*, 1-12. 10.1038/s12276-019-0223-5.
283. Théry, C., Witwer, K.W., Aikawa, E., Alcaraz, M.J., Anderson, J.D., Andriantsitohaina, R., Antoniou, A., Arab, T., Archer, F., Atkin-Smith, G.K., et al. (2018). Minimal information for studies of extracellular vesicles 2018 (MISEV2018):

a position statement of the International Society for Extracellular Vesicles and update of the MISEV2014 guidelines. J Extracell Vesicles *7*, 1535750. 10.1080/20013078.2018.1535750.

284. Théry, C., Zitvogel, L., and Amigorena, S. (2002). Exosomes: composition, biogenesis and function. Nature Reviews Immunology *2*, 569-579. 10.1038/nri855.
285. Yang, S.-T., Liu, Y., Wang, Y.-W., and Cao, A. (2013). Biosafety and Bioapplication of Nanomaterials by Designing Protein–Nanoparticle Interactions. Small *9*, 1635-1653. https://doi.org/10.1002/smll.201201492.
286. Onishchenko, N., Tretiakova, D., and Vodovozova, E. (2021). Spotlight on the protein corona of liposomes. Acta Biomater *134*, 57-78. 10.1016/j.actbio.2021.07.074.
287. Torchilin, V.P. (2005). Recent advances with liposomes as pharmaceutical carriers. Nature Reviews Drug Discovery *4*, 145-160. 10.1038/nrd1632.
288. Blanco, E., Shen, H., and Ferrari, M. (2015). Principles of nanoparticle design for overcoming biological barriers to drug delivery. Nature Biotechnology *33*, 941-951. 10.1038/nbt.3330.
289. Al-Nedawi, K., Meehan, B., Micallef, J., Lhotak, V., May, L., Guha, A., and Rak, J. (2008). Intercellular transfer of the oncogenic receptor EGFRvIII by microvesicles derived from tumour cells. Nature Cell Biology *10*, 619-624. 10.1038/ncb1725.
290. Asare-Werehene, M., Nakka, K., Reunov, A., Chiu, C.-T., Lee, W.-T., Abedini, M.R., Wang, P.-W., Shieh, D.-B., Dilworth, F.J., Carmona, E., et al. (2020). The exosome-mediated autocrine and paracrine actions of plasma gelsolin in ovarian cancer chemoresistance. Oncogene *39*, 1600-1616. 10.1038/s41388-019-1087-9.
291. Chen, W.X., Liu, X.M., Lv, M.M., Chen, L., Zhao, J.H., Zhong, S.L., Ji, M.H., Hu, Q., Luo, Z., Wu, J.Z., and Tang, J.H. (2014). Exosomes from drug-resistant breast cancer cells transmit chemoresistance by a horizontal transfer of microRNAs. PLoS One *9*, e95240. 10.1371/journal.pone.0095240.
292. Qiao, L., Hu, S., Huang, K., Su, T., Li, Z., Vandergriff, A., Cores, J., Dinh, P.U., Allen, T., Shen, D., et al. (2020). Tumor cell-derived exosomes home to their cells of origin and can be used as Trojan horses to deliver cancer drugs. Theranostics *10*, 3474-3487. 10.7150/thno.39434.
293. Naseri, M., Bozorgmehr, M., Zöller, M., Ranaei Pirmardan, E., and Madjd, Z. (2020). Tumor-derived exosomes: the next generation of promising cell-free vaccines in cancer immunotherapy. Oncoimmunology *9*, 1779991-1779991. 10.1080/2162402X.2020.1779991.

294. Bu, N., Li, Q.-L., Feng, Q., and Sun, B.-Z. (2006). Immune protection effect of exosomes against attack of L1210 tumor cells. Leukemia & Lymphoma *47*, 913-918. 10.1080/10428190500376191.

295. Gu, X., Erb, U., Büchler, M.W., and Zöller, M. (2015). Improved vaccine efficacy of tumor exosome compared to tumor lysate loaded dendritic cells in mice. International Journal of Cancer *136*, E74-E84. https://doi.org/10.1002/ijc.29100.

296. Lee, E.-Y., Park, K.-S., Yoon, Y.J., Lee, J., Moon, H.-G., Jang, S.C., Choi, K.-H., Kim, Y.-K., and Gho, Y.S. (2012). Therapeutic Effects of Autologous Tumor-Derived Nanovesicles on Melanoma Growth and Metastasis. PLOS ONE *7*, e33330. 10.1371/journal.pone.0033330.

297. Liu, H., Chen, L., Peng, Y., Yu, S., Liu, J., Wu, L., Zhang, L., Wu, Q., Chang, X., Yu, X., and Liu, T. (2017). Dendritic cells loaded with tumor derived exosomes for cancer immunotherapy. Oncotarget *9*.

298. Wolfers, J., Lozier, A., Raposo, G., Regnault, A., Théry, C., Masurier, C., Flament, C., Pouzieux, S., Faure, F., Tursz, T., et al. (2001). Tumor-derived exosomes are a source of shared tumor rejection antigens for CTL cross-priming. Nature Medicine *7*, 297-303. 10.1038/85438.

299. Sidhom, K., Obi, P.O., and Saleem, A. (2020). A Review of Exosomal Isolation Methods: Is Size Exclusion Chromatography the Best Option? Int J Mol Sci *21*, 6466. 10.3390/ijms21186466.

300. Caputo, F., Vogel, R., Savage, J., Vella, G., Law, A., Della Camera, G., Hannon, G., Peacock, B., Mehn, D., Ponti, J., et al. (2021). Measuring particle size distribution and mass concentration of nanoplastics and microplastics: addressing some analytical challenges in the sub-micron size range. Journal of Colloid and Interface Science *588*, 401-417. https://doi.org/10.1016/j.jcis.2020.12.039.

301. Gai, M., Simon, J., Lieberwirth, I., Mailänder, V., Morsbach, S., and Landfester, K. (2020). A bio-orthogonal functionalization strategy for site-specific coupling of antibodies on vesicle surfaces after self-assembly. Polymer Chemistry *11*, 527-540. 10.1039/C9PY01136F.

302. Prawatborisut, M., Oberländer, J., Jiang, S., Graf, R., Avlasevich, Y., Morsbach, S., Crespy, D., Mailänder, V., and Landfester, K. (2022). Temperature-Responsive Nanoparticles Enable Specific Binding of Apolipoproteins from Human Plasma. Small *18*, e2103138. 10.1002/smll.202103138.

303. Ritz, S., Schöttler, S., Kotman, N., Baier, G., Musyanovych, A., Kuharev, J., Landfester, K., Schild, H., Jahn, O., Tenzer, S., and Mailänder, V. (2015). Protein Corona of Nanoparticles: Distinct Proteins Regulate the Cellular Uptake. Biomacromolecules *16*, 1311-1321. 10.1021/acs.biomac.5b00108.

304. Crow, J., Atay, S., Banskota, S., Artale, B., Schmitt, S., and Godwin, A.K. (2017). Exosomes as mediators of platinum resistance in ovarian cancer. Oncotarget *8*.

305. Paskeh, M.D.A., Entezari, M., Mirzaei, S., Zabolian, A., Saleki, H., Naghdi, M.J., Sabet, S., Khoshbakht, M.A., Hashemi, M., Hushmandi, K., et al. (2022). Emerging role of exosomes in cancer progression and tumor microenvironment remodeling. Journal of Hematology & Oncology *15*, 83. 10.1186/s13045-022-01305-4.

306. Mateos-Maroto, A., Gai, M., Brückner, M., da Costa Marques, R., Harley, I., Simon, J., Mailänder, V., Morsbach, S., and Landfester, K. (2023). Systematic modulation of the lipid composition enables the tuning of liposome cellular uptake. Acta Biomaterialia *158*, 463-474. https://doi.org/10.1016/j.actbio.2022.12.058.

307. Aderem, A., and Underhill, D.M. (1999). MECHANISMS OF PHAGOCYTOSIS IN MACROPHAGES. Annual Review of Immunology *17*, 593-623. 10.1146/annurev.immunol.17.1.593.

308. Digiacomo, L., Cardarelli, F., Pozzi, D., Palchetti, S., Digman, M.A., Gratton, E., Capriotti, A.L., Mahmoudi, M., and Caracciolo, G. (2017). An apolipoprotein-enriched biomolecular corona switches the cellular uptake mechanism and trafficking pathway of lipid nanoparticles. Nanoscale *9*, 17254-17262. 10.1039/C7NR06437C.

309. Francia, V., Yang, K., Deville, S., Reker-Smit, C., Nelissen, I., and Salvati, A. (2019). Corona Composition Can Affect the Mechanisms Cells Use to Internalize Nanoparticles. ACS Nano *13*, 11107-11121. 10.1021/acsnano.9b03824.

310. and, A.A., and Underhill, D.M. (1999). MECHANISMS OF PHAGOCYTOSIS IN MACROPHAGES. Annual Review of Immunology *17*, 593-623. 10.1146/annurev.immunol.17.1.593.

311. Sharma, R., Huang, X., Brekken, R.A., and Schroit, A.J. (2017). Detection of phosphatidylserine-positive exosomes for the diagnosis of early-stage malignancies. Br J Cancer *117*, 545-552. 10.1038/bjc.2017.183.

7 Curriculum Vitae

8 Acknowledgements